



Bachelor Thesis

**Recent cryogenic processes at Samoylov Island, North Siberia for
calibrating a stable-isotope thermometer for ice wedges**

Bachelor Earth Science
University of Potsdam
Institute of Earth and Environmental Science
Potsdam, 25th February 2014

Supervisors:
Dr. Hanno Meyer
Prof. Dr. Hans-Wolfgang Hubberten

Clara Kleine
Student Nr: 755040
ckleine@uni-potsdam.de

Table of Contents

Index of Figures	III
Index of Tables	III
List of abbreviations	IV
Abstract	1
Zusammenfassung	2
1. Introduction	3
2. Study area and study objects	5
2.1. Study area	5
2.2. Study objects	6
3. Methodological background	8
3.1. Stable isotope geochemistry principles of H and O isotopes	8
3.2. Isotope measurement	12
3.2.1. Finnigan MAT Delta-S mass spectrometer	12
3.2.2. Picarro L2120-i Isotopic H ₂ O	14
4. Methods	16
4.1. Field work	16
4.1.1. Selection of an ice-wedge polygon	16
4.1.2. Spore (tracer) experiment	17
4.1.3. Sampling (Ice wedge drilling)	18
4.1.4. Frost cracking experiment	18
4.2. Laboratory work	19
4.2.1. Subsampling of the ice cores in the cold-laboratory	19
4.2.2. High-resolution experiment	20
4.2.3. Spore analysis	20
4.2.4. Temperature data	22
5. Results	23
5.1. Comparison of Picarro and mass spectrometer measurements	23
5.2. High resolution experiment	24
5.3. Frost-cracking experiment	25
5.4. Comparison of temperature data of Samoylov to other measuring stations	28
5.5. Spore (tracer) experiment	29
5.5.1. Discovered spores	29

5.5.2. Statistical classification of the samples	30
5.5.3. Isotope variations over the years	31
5.5.4. Comparison of isotope compositions and temperatures	32
5.5.4.1. Correlation of isotope and temperature data over all eight years	33
5.5.4.2. Differentiation between ice-vein and no-ice-vein samples	34
5.5.4.3. Correlation of isotope and temperature data over different time periods	34
5.5.5. Calibration of a stable-isotope thermometer for ice wedges	36
6. Discussion	37
6.1. Methodical aspects	37
6.2. Interpretation of temperature differences between measuring stations	37
6.3. Evaluation of fractionation effects during refreezing	38
6.4. Assessment of the spore experiment	38
6.5. Appraisal of the spore experiment	40
6.6. Comparison of the statistical methods	41
6.7. Evaluation of the ice-wedge isotope thermometer calibration	42
7. Conclusions	45
8. Outlook	47
References	V
Index of Appendices	VIII
Appendix	X
Acknowledgments	XXXIII
Affidavit	XXXIV

Index of Figures

Figure 1:	Investigation area	3
Figure 2:	Investigated ice-wedge polygon on Samoylov Island	7
Figure 3:	Model of isotopic effects	9
Figure 4:	Schematic illustration of the ring-down measurement with a Picarro CRDS analyzer	14
Figure 5:	Lycopodium spore tracers	16
Figure 6:	Scheme of the tracer experiment	17
Figure 7:	Scheme of frost cracking experimental set up.	17
Figure 8:	Comparison of $\delta^{18}\text{O}$ results of Finnigan MAT Delta-S mass spectrometer and Picarro L2120-i.	17 22
Figure 9:	$\delta^{18}\text{O}$ and d-excess measurement results of the High resolution experiment	23
Figure 10:	Number of detected frost-cracking events	24
Figure 11:	Comparison of snow depth and number of frost-cracking events.	25
Figure 12:	Ice-wedge-polygon-soil temperatures.	26
Figure 13:	Comparison of average temperatures from Samoylov Island, Stolb and Tiksi.	27
Figure 14:	Quantitative results of the spore investigation tests 1 (A) and 2 (B)	28
Figure 15:	$\delta^{18}\text{O}$ values of the samples assigned to the respective year	28
Figure 16:	Box plot of $\delta^{18}\text{O}$ values of the samples assigned to the respective year	29
Figure 18:	Comparison of $\delta^{18}\text{O}$ data and Samoylov temperatures	31
Figure 19:	Linear regression between $T_{\text{cold season}}$ and average $\delta^{18}\text{O}$	31

Index of Tables

Table I:	Snow free periods of the years 2003 till 2008 (Boike et al., 2013)	5
Table II:	Stable hydrogen and oxygen isotopes and their relative abundance in nature	9
Table III:	Overview of cracking experiments	27
Table IV:	Correlation matrix of Stolb and Samoylov temperatures and $\delta^{18}\text{O}$ data over all eight years	33
Table V:	Correlation matrix of Samoylov temperatures and $\delta^{18}\text{O}$ data in four year steps	34
Table VI:	Correlation matrix of Samoylov temperatures and $\delta^{18}\text{O}$ data from 2004 to 2010	35

List of abbreviations

AL	Active layer
a.s.l.	Above sea level
BH	Borehole
d-excess	Deuterium excess
GMWL	Global Meteoric Water Line
HDW2	Mixed water from the Potsdam region
IQR	Interquartile range
KARA	Kara Sea Water
LD10	Lena Delta 2010
min.	Minimum
max.	Maximum
NGT	North, Greenland Traverse
PC	Principal Component
PCA	Principal Component Analysis
R	Ratio
r	Correlation coefficient
r ²	Coefficient of determination
SD	Standard deviation
SEZ	Severnaja Zemlja water
SLAP	Standard Light Antarctic Precipitation
T _{April}	Average April temperatures
T _{cold season}	Average temperatures of the cold season (Nov to May)
T _{December}	Average December temperatures
T _{February}	Average February temperatures
T _{January}	Average January temperatures
T _{March}	Average March temperatures
T _{May}	Average May temperatures
T _{November}	Average November temperatures
T _{spring}	Average spring temperatures (Mar to May)
T _{winter}	Average winter temperatures (Dec to Feb)
VSMOW	Vienna Standard Mean Ocean Water
WS-CRDS	Wavelength-Scanned Cavity Ringdown Spectroscopy
α	Fractionation factor
δ	Delta value
1 σ	Standard deviation

Abstract

Permafrost regions cover approximately 24 % of the northern hemisphere land surface and are very sensitive to climate changes. Therefore they are important to better understand the climate of the past. Unfortunately, established climate archives like ice caps, deep lakes and marine deposits are rare in such regions. But permafrost regions contain ground ice potentially providing palaeo-climate information, the most appropriate ground ice type for palaeo-climatic reconstruction are ice wedges. Ice wedges are vertical structures in permafrost ground, that grow by snow melt water penetrating into frost cracks. Their isotope composition can provide temperature data of ten thousands of years. So far temperature reconstructions from ice wedges are restricted by the missing correlation between isotope data and corresponding temperatures. This study deals with the calibration of a stable isotope thermometer for ice wedges by a tracer experiment. The experiment was carried out on a recent ice-wedge polygon on Samoylov Island, located in the largest river delta in northern Asia, the Lena Delta in northern Siberia. The tracers (colored *Lycopodium* spores) allowed to assign ice-wedge ice to the year of its formation. Therefore the isotope data of the ice could be measured and correlated with measured temperature data for a particular year. For a correlation like this it is important to understand different factors which might influence the isotope composition of the ice wedge. One such factor is isotope fractionation during refreezing, which was studied using a high-resolution experiment and turned out to be negligible. Additionally environmental conditions like temperature and snow-depth influence frost cracking and therefore determine the time period of ice wedge growth. These conditions were investigated by frost-cracking experiments, which identified December as the main season for thermal-contraction cracking at Samoylov Island. Two main seasons for penetration of snow and melt water into frost cracks were found: the first one in December when frost cracking takes place and the second one at snow melt in spring. Therefore the isotope signal of an ice wedge represents spring and winter temperatures. A shift in seasonality between the first two years and the later years was observed in the isotope signal. For the years 2004 to 2010 a isotope-temperature equation was obtained.

Recent ground ice from an ice-wedge was successfully attributed to the year of its formation and showed that the isotope signal from ice-wedge samples is influenced by both, spring and winter temperatures.

Zusammenfassung

Permafrostgebiete bedecken etwa 24 % der Landoberfläche der nördlichen Hemisphäre und reagieren empfindlich auf Klimaänderungen. Deshalb können sie dazu beitragen das Klima der Vergangenheit besser zu verstehen. Leider sind etablierte Klimaarchive wie Eiskappen, tiefe Seen und marine Ablagerungen in diesen Regionen selten. Dafür weisen sie Grundeis auf, wie z.B. Eiskeile. Diese können Informationen über das Klima der Vergangenheit liefern. Eiskeile sind vertikale Strukturen im Permafrost die durch Wasser, welches in Frostrisse eindringt wachsen. Ihre Isotopenzusammensetzung kann Temperaturinformationen über zehntausende Jahre liefern. Bisher werden solche Temperaturrekonstruktionen jedoch durch die fehlende Korrelation zwischen Isotopenzusammensetzungen und zugehörigen Temperaturen eingeschränkt. Diese Arbeit befasst sich mit der Kalibrierung eines stabilen Isotopen Thermometers für Eiskeile mit Hilfe eines Tracerexperiments, welches an einem rezenten Eiskeilpolygon auf Samoylov Island im Lenadelta durchgeführt wurde. Die Tracer (eingefärbte *Lycopodiumsporen*) ermöglichten es, Eissegmente aus den Eiskeilen dem Jahr ihrer Entstehung zuzuordnen. Auf diese Weise konnte die gemessene Isotopenzusammensetzung dieser Segmente mit den Temperaturdaten aus dem entsprechenden Jahr korreliert werden. Für solch eine Korrelation ist es wichtig die verschiedenen Faktoren, die die Isotopenzusammensetzung in Eiskeilen beeinflussen können, einzubeziehen. Dazu gehören z.B. Fraktionierungsprozesse beim Gefrieren. Diese wurden durch die feine Beprobung einer Eisader untersucht und erwiesen sich als vernachlässigbar. Andere Faktoren sind Umweltbedingungen wie Temperatur und Schneetiefe die Frostsprengungsprozesse beeinflussen können und damit den Zeitraum für Eiskeilwachstums festlegen. Diese Bedingungen wurden durch Frostsprengungsexperimente untersucht und zeigten, dass die Hauptsaison für Frostsprengung auf Samoylov Island im Dezember liegt. Zwei Zeitfenster für das Eindringen von Schnee und Schmelzwasser in Frostrisse konnten beobachtet werden: das Erste im Dezember wenn es zu Frostsprengung kommt und das Zweite im Frühjahr. Daher enthalten Isotopendaten aus Eiskeilen sowohl Frühjahrs- als auch Wintertemperaturen. Zwischen den ersten beiden und den folgenden Jahren wurde eine Saisonalitätsverschiebung von Dezember- zu Frühjahrstemperaturen im Isotopensignal festgestellt. Für die Jahre 2004 bis 2010 konnte eine Funktion zwischen Temperatur- und Isotopendaten ermittelt werden. Rezente Eiskeilproben konnten mit Hilfe der Tracer erfolgreich dem Jahr ihrer Entstehung zugeordnet werden und zeigen das sowohl Frühjahrs- als auch Wintertemperaturen einen Einfluss auf das Isotopenverhältnis in Eiskeilproben haben.

1. Introduction

To better understand the recent changes of the climate system it is important to recognize the development of the climate in the past. However, direct meteorological observations mostly go back to the 19th century only, especially in the Arctic (e.g. Polyakov et al., 2003). To get information about past climate variations climatic archives are needed.

Established climate archives are ice caps, deep lakes and marine deposits (Opel et al., 2010). However such archives are not available in permafrost regions which, constitute 24 % of the northern hemisphere land surface (Boike et al., 2012) and are very sensitive to climate changes (Osterkamp, 2005; Lemke et al., 2007; Romanovsky et al., 2007). Permafrost areas are characterized by cold continental climate with little precipitation and contain ground ice (Zhang et al., 1999). Ground ice includes all types of ice contained in frozen ground (International Permafrost Association, 1998) and can provide palaeo climate information (Meyer et al., 2002, b). The most appropriate ground ice type for palaeo-climatic reconstruction are ice wedges (e.g. Vaikmäe, 1989; Vasil'chuk, 1991, 1992). These are vertically-foliated structures in the permafrost which grow by water that trickles into frost cracks and refreezes there to ice (French, 1996). Therefore ice wedges consisting of massive ground ice (French, 1996).

In ice bodies hydrogen and oxygen isotopes of ice are useful tools to reconstruct palaeo temperatures due to their isotopes dependency on condensation temperatures (Dansgaard, 1964). Stable isotopes in ice cores are widely used for climate reconstructions (e.g. North Greenland Ice Core Project Members, 2004) and show isotope variations of 0.695 ‰ per 1 ° C (Dansgaard, 1964). Paleoclimate reconstruction from ground ice especially from ice wedges is also possible using stable isotopes. Nonetheless ice wedges were little used for palaeoclimate studies in the past 30 years. Mainly scientists from north America, Russia and Germany dealt with this issue (Mackay, Vaikmäe, Michel, Vasil'chuk, Nikolaev, Mikhalev, Meyer, Opel, Lacelle, Lachniet, Fritz).

The main source for the growth of ice wedges is melting snow (Mackay, 1983; Vaikmäe 1989). Therefore Michel (1982), Mackay (1983), Vaikmäe (1989) and Vasil'chuk (1991) consider oxygen isotope variations in ice wedges as an indicator for winter temperature changes. Vasil'chuk (1992), Nikolaev and Mikhalev (1995), Meyer (2002, 2010) and Opel (2010) showed that climate reconstruction with ice wedges is possible. Even long time palaeoclimate record of 10. 000-s of years can be achieved when ice wedges of different generations are available (Meyer et al., 2002, b). The temporal assessment with ¹⁴C dating can provide an up to centennial-scale resolution for stable isotopes in ice wedges (Meyer et al., 2010). Different factors that influence the isotope

composition of ice wedges include various processes from the formation to the deposition of air humidity and changing moisture sources (Jouzel et al., 1997), seasonality of precipitation and ice-wedge formation (Jouzel et al., 1997) and alteration processes (Meyer et al., 2002, b) were studied. So far the missing correlations of single ice veins forming ice wedges to the year of their formation restrict the temperature reconstruction with ice wedges (Meyer, 2002, a). Therefore a tracer experiment was carried out on a ice-wedge polygon at Samoylov Island. Samoylov Island is located in a zone of continuous permafrost (Boike et al., 2008) in the north of Siberia characterized by mainly low-center ice-wedge polygons and therefore well suited for the experiment. Colored *Lycopodium* spores were used as tracers expected to penetrate into the ice wedge with the melt water to enable a relation of the ice to the respective year of its formation. Afterwards the $\delta^{18}\text{O}$ values of the ice formed in a discrete year can be correlated with temperature data from a climate station. That way a correlation might be found and a stable isotope thermometer for ice wedges can be calibrate (Meyer, 2002, a). Such a calibration study is subject of this bachelor thesis. Furthermore, this experiment could help to understand processes related to ice-wedge growth better.

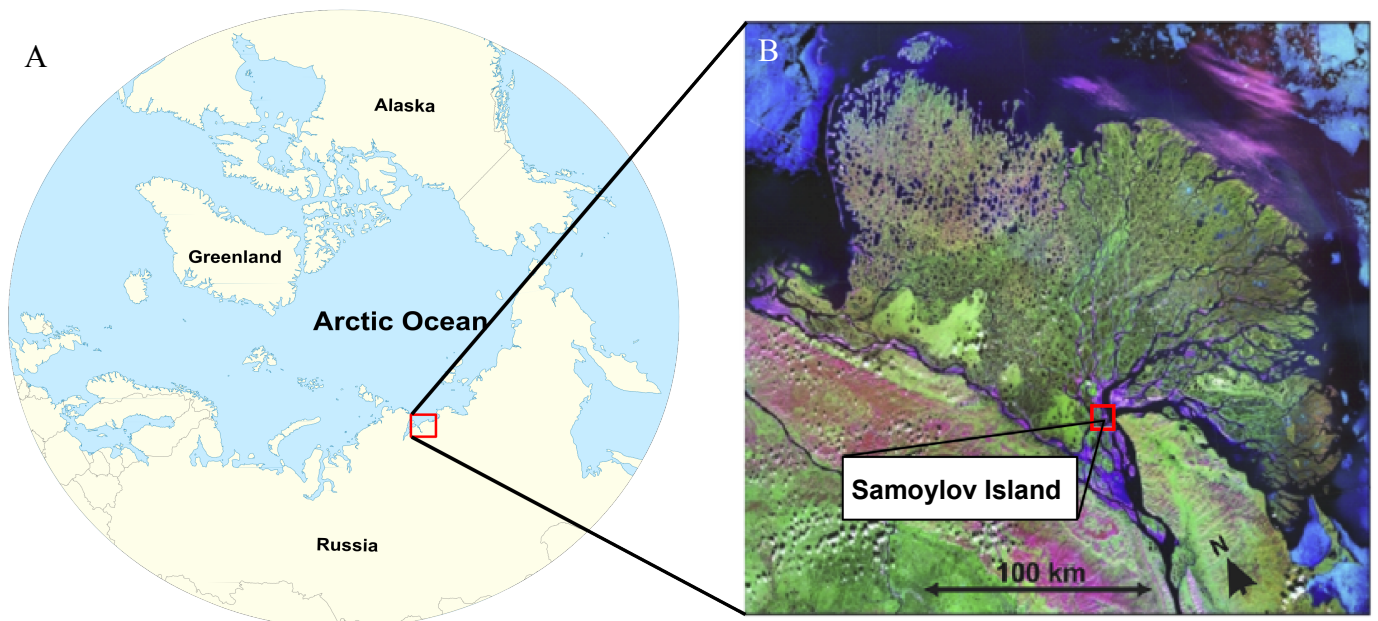


Fig. 1: Investigation area

A - Location of the Lena River Delta (red square) on global scale, **B** - Map of the Lena River Delta in Siberia., with Samoylov Island (red square) (Satellite image provided by Statens Kartverk, UNEP/GRID-Arendal and Landsat)

2. Study area and study objects

2.1. Study area

The study area is located on Samoylov Island (72220 N, 126300 E). It is one of 1500 islands within the Lena River Delta in northern Siberia close to the Laptev Sea (Fig. 1). The delta is the largest river delta in northern Asia (Gilg et al., 2000) and one of the most important regions for the research of permafrost processes (Rachold & Grigoriev, 1999). To make scientific investigation projects possible a research base was built on Samoylov Island. This station is equipped with an automatic climate and soil station which records hourly data since 1998, though several gaps exist due to technical problems (Boike et al., 2008). Furthermore, there are official meteorological stations at Tiksi located 120 km to the south-east and at Stolb located 6 km to the north-east of Samoylov Island.

The region is dominated by dry continental arctic climate. Rapid changes of cold, moist, arctic air masses from the north and warm, dry, continental air masses from the south characterize the weather from spring to autumn (Boike et al., 2008). The mean annual air temperature from 2002 to 2010 was -12.11 °C. The main rainfall season is from the middle of June to the middle of September (Boike et al., 2008). The snow season normally starts between middle of September and middle of October and ends between middle of May and middle of June (Boike et al., 2013, Tab. I). The precipitation in winter is far less than in summer (Boike et al., 2013). Less than a third of the annual precipitation is snow. Commonly snow melt starts in middle of May and the snow cover normally disappears by early June (Boike et al., 2013).

Samoylov Island is located in the south of the Lena Delta in a zone of continuous permafrost (Boike et al., 2008). The island is dominated by wet polygon tundra (Boike et al., 2008). The permafrost thaws maximally 0.5 m deep during summer (Sachs et al., 2008). This soil layer that thaws in summer and refreezes in winter is called active layer (AL).

Tab. I: Snow free periods of the years 2003 till 2008 (Boike et al., 2013)

	2003	2004	2005	2006	2007	2008
End of snow melt	12 May	16 June	12 June	-	31 May	26 May
Beginning of snow coverage	16 Oct	7 Oct	-	-	8 Sep	-

The island is subdivided into four geomorphological areas (Akhmadeeva et al., 1999): a lower and a middle flood plain which are annually flooded and a high flood plain, which is located in the western part and only flooded during high floods. These flood plains belong to the 1st Lena river terrace, which is the active Lena Delta (dark green in Fig.1). This terrace is characterized by polygonal-patterned ground (Meyer, 2002, a). The flood plains are separated by a cliff from an old river terrace which is the fourth geomorphological area (Meyer, 2002, a).

2.2. Study objects

As introduced above ice wedges are vertical structures in permafrost composed of massive ice (French, 1996) and widespread in non-glacial high latitude areas (Meyer et al., 2010). They form by the periodic occurrence of frost cracking and freezing processes. Rapid cooling in winter leads to thermal contraction, which can result in frost cracking in the upper permafrost (Lachenbruch, 1962). The snow melt in spring provides water that can trickle into these cracks and refreeze there as narrow, subvertical ice veins (Lachenbruch, 1962). It is assumed that the water penetrating into the frost crack is mainly melt water of the previous winter precipitation (Meyer et al., 2002, c).

The frequency of frost cracking is highly variable (Mackay, 1992). Frost cracks are most likely to occur near the ice wedge center, often at the same location due to the weakness of the zone created by previous ice veins (Mackay, 1974). This leads ideally to gradual ice-wedge growth with younger ice in the middle and older ice towards the rim (Mackay, 1974, 1992).

Whether an ice vein will form or not depends on the occurrence of thermal-contraction cracking and on the availability of melt water (French, 1996). Best conditions for frost cracking are air temperature drops of 1.8°C/day over four days (French, 1996). Also low heat insulation above the ice wedge caused by soil, vegetation or snow cover is conducive for cracking (Mackay, 1974). In general, ice wedges only form in areas with mean annual air temperatures below -6°C (Péwé, 1966). After Mackay (1974), frost cracking mostly occurs between mid January and mid March at North Kanada. Christiansen (2005) detected the main cracking season at Spitsbergen between February and June after ground temperatures drop below -15°C .

Since it is assumed that the main source for ice-wedge growth is melt water, the stable isotope composition of ice veins can be related to the mean winter temperature of the year of formation (Vasil'chuk, 1992; Nikolayev & Mikhalev, 1995; Vasil'chuk & Vasil'chuk, 1998). Michel (1982) concludes from experiments that water, which rivulets into a frost crack of an ice wedge, forming

ice veins, refreezes to rapidly for isotope fractionation (see chapter 3.1) due to the cold soil temperatures.

Several processes influencing the isotope composition need to be considered when using isotopes for climate reconstruction. Changing moisture sources (Jouzel et al., 1997) and seasonality of precipitation may have great impact on the isotope composition of ice wedges (Jouzel et al., 1997). In addition isotope fractionation during snow melt has to be taken into account: with the first melt water having lighter δD and $\delta^{18}\text{O}$ values than the last (Meyer et al., 2002, b). Furthermore, it was found that alteration processes of old ice wedges due to the migration of water from the enclosing ice, can modify the isotope signal (Meyer et al., 2002, b). In summer, the AL above the ice wedge contains water which can not drain into the soil due to the ice below. Ice segregation can lead to a transition horizon between active layer and ice wedge. Therefore approximately the upper 10 cm of an ice wedge are not usable for climate reconstruction (Shur et al., 2005; Meyer et al., 2010).

At the surface the frost cracks generate linear structures. Several frost cracks next to each other form ice-wedge polygon patterns (French, 1996) (Fig.2). When ice wedges become inactive and permafrost starts to thaw water accumulates in the trough above the ice wedge (French, 1996). The latent heat of the water in the trough in turn may support the degradation of the ice wedge below (Greene, 1966). The ice-wedge polygons on Samoylov Island can be divided in different polygon types by their stage of development (Meyer, 2002, a). The appropriate polygon types for this study are the juvenile and the mature type. The polygons are usually still in growth and show recent, clearly visible frost cracks (Meyer, 2002, a). They contain no water in their troughs above the ice wedge and show no signs of degradation (Meyer, 2002, a). The juvenile type is characterized by a low relief with little elevation differences from the polygon center to the polygon wall and it is still quite small. The mature type is already well developed and shows a relatively high relief with elevation differences in the polygon of about 0.5 m. This leads to a clearly defined catchment area for the penetrating snow (Meyer, 2002, a).

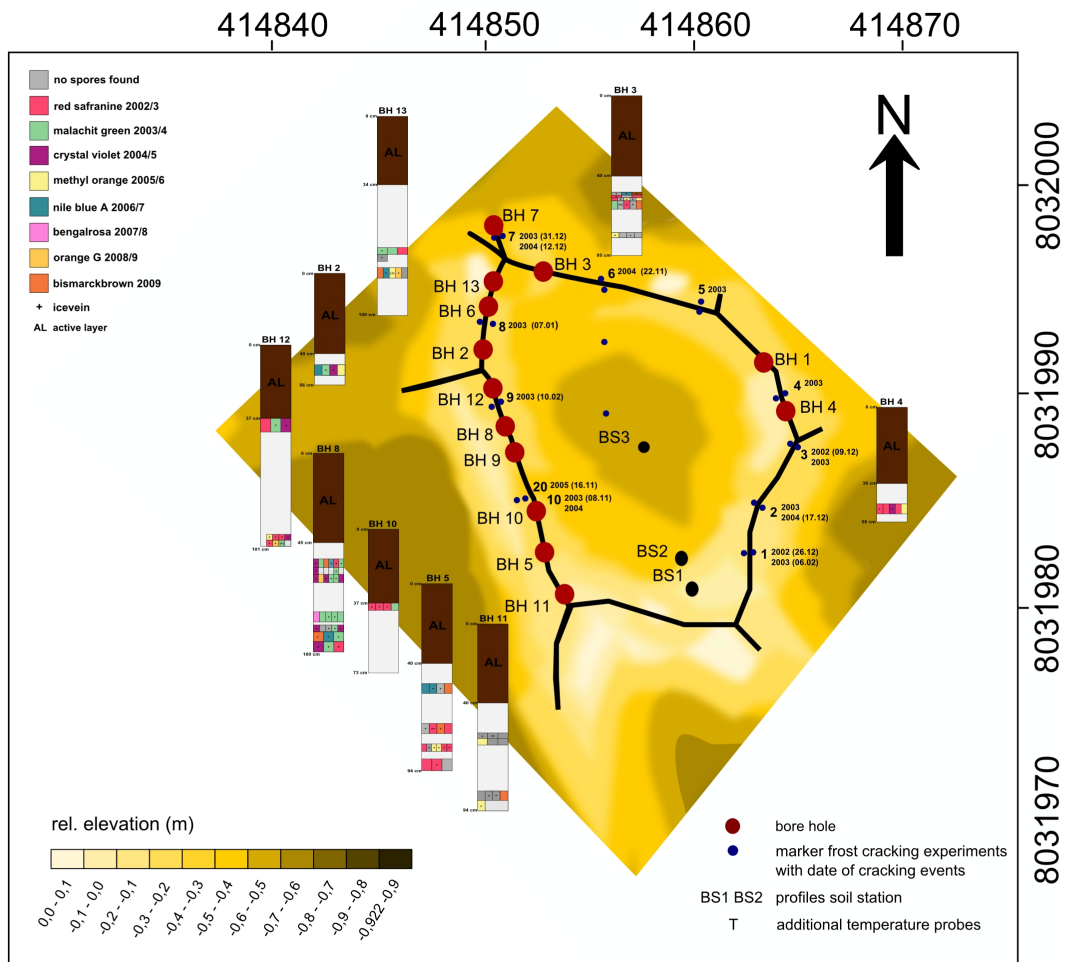


Fig. 2: Investigated ice-wedge polygon on Samoylov Island
 The figure is displayed in relative elevation and includes location of cracking experiments and bore holes. Ice cores with position of all detected spores are schematically illustrated next to their bore hole.

3. Methodological background

3.1. Stable isotope geochemistry principles of H and O isotopes

Isotopes are atoms which contain the same number of protons but a different number of neutrons and they therefore differ in their mass (Hoefs, 1997). The isotopes of hydrogen and oxygen considered in this study are stable. Hydrogen has two and oxygen has three stable isotopes (Tab. II).

The light isotopes (H, ^{16}O) are the most abundant ones (Tab. II). The isotope composition of a substance is generally given as ratio of the two considered isotopes of an element normalized to the more prevalent isotope e.g. $^2\text{D}/^1\text{H}$ or $^{18}\text{O}/^{16}\text{O}$ (Clark & Fritz, 1997). Isotope compositions are related to a known reference because determining variations in stable isotope concentrations is less complicated than measuring total abundances and it is, thus, difficult to measure an absolute isotope ratio (Clark & Fritz, 1997). For hydrogen and oxygen isotope compositions in water the standard is in general *Vienna Standard Mean Ocean Water* (VSMOW). For samples from cold regions the *Standard Light Antarctic Precipitation* (SLAP) can also be used. The well mixed water of the ocean, as the biggest reservoir for water, is defined as 0 ‰ by VSMOW. The difference between the sample and the standard is used, expressed by delta values in permil [Eq. 1] (Hoefs, 1997):

$$\delta_{\text{sample}} = ((R_{\text{sample}}/R_{\text{ST}})-1) * 10^3 (\text{‰}) \quad [\text{Eq. 1}]$$

where R_{sample} is the considered isotope ratio of a sample and R_{ST} is the defined isotope ratio of a standard sample (Hoefs, 1997). Substances with relatively more heavy isotopes compared to the standard have positive δ -values, substances with less heavy isotopes have negative ones.

Tab. II: Stable hydrogen and oxygen isotopes and their relative environmental abundance

Element	Isotope mass	Abundance	Isotope mass	Abundance	Isotope mass	Abundance
Hydrogen	^1H	99.9844	^2D	0.0156		
	^{16}O	99.7630	^{17}O	0.0375	^{18}O	0.1995

The different atomic mass induce different physical properties of the isotopes (Hoefs, 1997). Due to the same number of electrons the chemical properties are similar but by reason of mass difference they differ in reaction rate (Urey, 1947). These differences in properties are called isotope effects (Hoefs, 1997) and lead to isotope fractionation (Urey, 1947). Isotope fractionation describes the exchange of isotopes between two reservoirs (Hoefs, 1997).

In Fig. 3 the energy of a diatomic molecule is shown as a function of the distance between the two atoms (Clark & Fritz, 1997). The upper horizontal line represents the dissociation energy of the molecule with light isotopes and the lower line the counterpart of the molecule with heavy isotopes. This implicates that light isotopes containing molecules has a weaker bond and requires less energy to dissociate than heavy ones (Clark & Fritz, 1997). Hence light isotopes react faster than heavy ones (Hoefs, 1997).

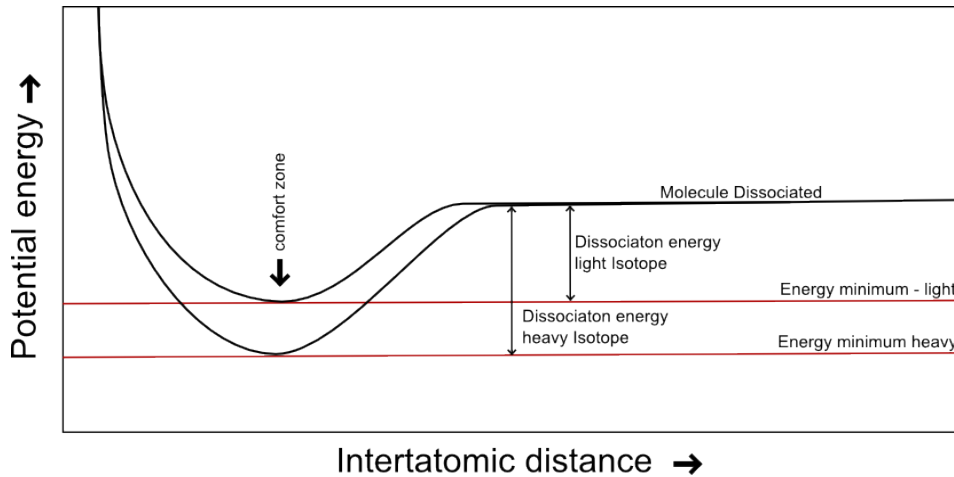


Fig. 3: Model of isotopic effects

Potential energy as a function of interatomic distance for a diatomic molecule with light or heavy isotopes (Clark & Fritz, 1997).

In general the fractionation is higher the lower the temperature is. Two main fractionation processes are distinguished: isotope exchange reactions and kinetic processes (Hoefs, 1997).

Isotope exchange includes all processes which changes the isotope distribution among different reservoirs (Hoefs, 1997). These reactions are a special case of a chemical equilibrium and can be expressed as [Eq. 2]:



where the subscript indicate that the species A and B contain either the light (1) or heavy isotope (2) (Hoefs, 1997). For this formula it is necessary that forward and backward reaction rates are equal, that there is enough mixing time and that product and reactant reservoirs are well mixed (Clark & Fritz, 1997).

Isotope exchange reactions are characterized by the fractionation factor (α) [Eq. 3]. The fractionation factor is stated by the ratio (R) of two isotopes in one chemical compound (A) divided by the corresponding ratio for an other chemical compound (B) (Hoefs, 1997):

$$\alpha_{A-B} = R_A/R_B \quad [\text{Eq. 3}]$$

The δ -value and the fractionation factor are related by [Eq. 4] (Hoefs, 1997):

$$\delta_A - \delta_B = \delta_{A-B} \approx 10^3 \ln \alpha_{A-B} \quad [\text{Eq. 4}]$$

For the water isotopes, differences in the vapor pressure during evaporation and condensation processes lead to significant isotope fractionation (Hoefs, 1997). While lighter molecules enrich in the vapor, heavy molecules remain in the liquid (Hoefs, 1997). Here, the extent of fractionation depends on the temperature (Hoefs, 1997).

The kinetic effects are primarily dependent from differences in reaction rates of isotopic molecules (Hoefs, 1997). They occur when the equilibrium is unbalanced by incomplete or unidirectional processes. These are substantial in evaporation, dissociation, biologically mediated reactions, and diffusion and can provide information on reaction pathways. (Hoefs, 1997)

On a global scale, δD and $\delta^{18}O$ of fresh surface waters generally correlate linearly between the various reservoirs (ocean, vapour, rain, runoff, groundwater, snow and ice), due to temperature-dependent fractionation at the phase transitions of water in the hydrological cycle (Clark & Fritz, 1997). This relationship can be represented graphically in a co-isotope plot, where δD is plotted against $\delta^{18}O$ and is described by the "Global Meteoric Water Line" (GMWL) [Eq. 5] (Craig, 1961).

$$\delta D = 8.0 * \delta^{18}O + 10 \text{ ‰} \quad [\text{Eq. 5}]$$

The position relative to the GMWL in a δD - $\delta^{18}O$ diagram is given by the deuterium excess (d) [Eq. 6] (Dansgaard, 1964).

$$d = \delta D - 8 * \delta^{18}O \quad [\text{Eq. 6}]$$

The deuterium excess (d-excess) reflects the sensitivity of oxygen and hydrogen isotopes to evaporation conditions in the moisture source region and kinetic fractionation processes. It depends on relative humidity, sea surface temperature and wind speed in the moisture source region (Merlivat & Jouzel, 1979) and therefore can be used to identify precipitation sources.

Due to isotope fractionation, atmospheric water vapour is isotopically lighter than the source water and has, thus, a lower δ -value. Towards higher latitudes, altitudes or distance from the ocean the isotope composition of an air mass becomes progressively lighter due to the fact that with every precipitation event, the air mass loses proportional more heavy than light isotopes (Meyer et al., 2002, c), again with the rate of the fractionation depending on temperature. The lowest $\delta^{18}O$ and δD

values are attributed to the coldest temperatures (Meyer et al., 2000, c). For this reason it is possible to use the isotope composition accumulated in glacier and permafrost ice for temperature reconstructions.

3.2. Isotope measurement

There are different methods to measure isotope ratios of a given water sample. An approved method at the Alfred Wegener Institute in Potsdam are measurements with *Finnigan MAT Delta-S mass spectrometers*. A second possible technique is the measurement with a laser-optical device (*Picarro L2120-i*) which offers the opportunity to measure very small sample volumes. Therefore all water samples in this thesis were measured with the *Picarro L2120-i* and for comparison some samples were also measured with the mass spectrometer.

3.2.1. Finnigan MAT Delta-S mass spectrometer

The *Finnigan MAT Delta-isotopes mass spectrometer* is a gas mass spectrometer which divides isotopes by their mass-to-charge ratio.

It provides two equilibration units with a capacity of 24 sample bottles each. Overall, 48 samples could be measured per auto sampler in one measuring sequence. The sample bottles are ~25 ml glass bottles in which 1 ml to 5 ml sample water are filled for isotopic analysis. The bottles are evacuated with a two-stage rotary pump (Meyer et al., 2000). The remaining bottle volume is filled with hydrogen gas for δD measurements. After finishing the complete sequence the hydrogen gas is evacuated and replaced by carbon dioxide for $\delta^{18}\text{O}$ measurements.

The H_2O sample and the gas (CO_2 , H_2) exchange isotopes until an equilibrium is reached. The equilibrium should be reached for hydrogen after approximately 45 min and for oxygen after 200 min. To ensure that the equilibrium is fully achieved, an exchange time of 180 min for hydrogen and 400 min for oxygen isotopes is used (Meyer et al., 2000). Due to the temperature-dependency of the fractionation the units are placed into a water-shaking bath which covers the bottles to two thirds and keeps them at a constant temperature of 18 ± 0.01 °C. For best temperature homogenization the water baths are shaken with a frequency of 90 min^{-1} (Meyer et al., 2000). The temperature should not vary more than ± 0.05 °C due to the temperature coefficient of the fractionation factor of deuterium between H_2O and H_2 of $-5.4 \text{ ‰} / \text{°C}$ (Meyer et al., 2000).

Catalysts are needed for the hydrogen isotope exchange. For this purpose hydrophobic sticks with activated platinum are used (Meyer et al., 2000).

The equilibrated sample gas is transferred into the so called sample bellow. To remove water vapor the gas passes a cooling trap with dry ice and ethanol of $-78\text{ }^{\circ}\text{C}$ (Meyer et al., 2000). As a reference the standard NGT (North, Greenland Traverse) is used. The first bottle of each unit contains NGT which is equilibrated with hydrogen or carbon dioxide gas like the samples. The equilibrated gas is subsequently transmitted into the standard bellow of the inlet system and is measured versus every sample of the equilibration unit (Meyer et al., 2000). The pressure in the standard bellow is higher than in the sample bellow to provide sufficient gas for the whole measuring sequence (Meyer et al., 2000).

Alternately sample and reference gas are injected from sample and standard bellows into the mass spectrometer. This procedure is repeated ten times for each sample in order to allow statistical evaluation. The 1σ error is generally less than $\pm 0.8\text{ }‰$ for δD and $\pm 0.1\text{ }‰$ for $\delta^{18}\text{O}$ otherwise the measurement has to be repeated (Meyer et al., 2000).

In the mass spectrometer the gas molecules are impact ionized at a heated tungsten filament and accelerated in a magnetic field. An electro magnet deflects the ions differently and divides them by their mass and their charge. The intensity of the different isotopes is detected in so called Faraday cups and the isotope ratio is calculated. For δD the measurements are carried out at 5 nA H_2 and for $\delta^{18}\text{O}$ at 10 nA mass 44 intensity (Meyer et al., 2000).

For isotope composition calculation the ISODAT software was applied. δD and $\delta^{18}\text{O}$ values are displayed as permil differences relative to VSMOW (Meyer et al., 2000). Six bottles per unit contain standards for quality control and linear corrections. The selection of the standards depends up on the expected isotope composition of the samples (Meyer et al., 2000). Here NGT, KARA (Kara See Water), HDW2 (mixed water from the Potsdam region) and SEZ (Severnaja Zemlja water) were selected.

Advantage of mass spectrometry is the long-term experience with this method of about 50 years. However mass spectrometers need a larger sample volume than Picarro.

3.2.2. Picarro L2120-i Isotopic H₂O

The *Picarro L2120-i Isotopic H₂O* allows simultaneous measurement of D/H and ¹⁸O/¹⁶O ratios (Gkinis et al., 2010). It operates with Wavelength-Scanned Cavity Ringdown Spectroscopy (WS-CRDS). This is an optical spectroscopic method, which enables to measure small sample volumes. Only 1.8 µl water are necessary for one single stable isotope measurement (IAES, 2009).

An autosampler (PAR HTC-Xt) allows for the measurement of sample sequences (56*2 samples). The samples are taken with a syringe from a 2 ml glass vial through a septum cap and are then injected through another septum into the evaporation module. The syringe is purged after every sample with 1-methyl-2-pyrrolidone-liquid to reduce memory effects (IAES, 2009). In the evaporation module the water sample is evaporated and subsequently transported to the resonator. In order to prevent isotopic fractionation effects an immediate evaporation is necessary.(Gkinis et al., 2010) To avoid condensation the distance between evaporation module and resonator has to be as short as possible. The water vapor concentration arriving in the resonator should be between 18000 ppm and 22000 ppm. The amount of injected water and the dry gas flow are important for a stable water mixing ratio and therefore they are automatically controlled (Gkinis et al., 2010).

The resonator consists of three highly reflective mirrors (>99.999 %) where the sample is exposed to an infrared laser. The laser beam is repeatedly reflected by the mirrors and passes the sample vapor continuously. That way, optical path lengths of about 20 km are reached. This intensifies the measured absorption lines and a high signal-to-noise ratio is reached (IAEA, 2009).

When the detected signal reaches a steady state condition, the laser is turned off. The light intensity in the resonator slowly leaks out due to the slight reduced reflectivity of the mirrors and due to the absorption of the gas (IACE, 2009). This process called ring down is tracked by a quantitative photodetector in real-time (Fig. 4). Thus, it is possible to scan the absorption lines that are unique to H₂¹⁶O, H₂¹⁸O and HD¹⁶O and obtain δD and δ¹⁸O data simultaneously (Gkinis et al., 2010). The absorption line intensity is linearly dependent from the concentration of molecules in the resonator. The laser exciting vibrations frequency and rotation in the molecules depends on the mass of the atoms. This leads to lines at different frequencies for the different molecules (IACE, 2009). To isolate and measure these unique spectral lines, a high resolution and absolute wavelength precision is necessary. The resulting isotope ratio depends on the relative absorption line intensities. Because WS-CRDS measures decay rates, fluctuations in the laser intensity have no effect on the measurement (IACE, 2009).

For δD and δ¹⁸O a precision better than 0.5 ‰ and 0.1 ‰ is promised by the manufacturer,

respectively (Picarro, 2014, a). At the isotope laboratory of the Alfred Wegener Institute all measurements with precisions less than 0.8 ‰ for δD and 0.1 ‰ for $\delta^{18}\text{O}$ were repeated. For long sample series there is a drift of about ± 0.3 ‰ for $\delta^{18}\text{O}$ and ± 0.9 ‰ for δD (Picarro, 2014, a). Therefore within this project only short series were measured.

To ensure optimal measurements the WS-CRDS analyzer features a high-precision wavelength monitor and a thermal and pressure controlled optical cavity (Picarro, 2014, a). The temperature control and the pressure control are within 0.002 °C and 0.003 atm accurate respectively.

The Picarro is prone to a memory effect which can not be completely eliminated, even though Picarro has a temperature controlled and stabilized vaporization system (Gkinis et al., 2010). Therefore, only the last three of six consecutive measurements are used for the statistical evaluation. The same standards as for mass spectrometry are used for quality control. In general the first and the last five samples of one sequence are standards. Due to the memory effects the standard with the most similar isotope composition to the expected isotope composition of the samples is positioned prior to and after the samples. Also the standard with most similar isotope composition is used, if a standard is put additionally between the samples.

The data can be received as delta ratio to the reference standard V-SMOW as usually done (IAEA, 2009). An advantage of Picarro is the possibility of measuring small sample volumes. Furthermore, it is relatively small and immune against changing external conditions. Therefore it can be used in the field. On the other hand Picarro is very susceptible to memory effects and so far a higher precision than that of the mass spectrometer is not achieved.

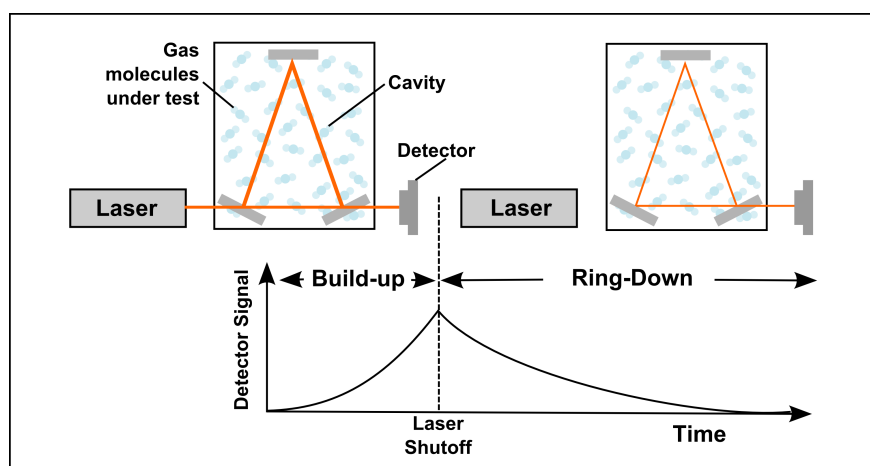


Fig. 4: Schematic illustration of the ring down measurement with a Picarro CRDS analyzer.

(modified according to Picarro, 2014, b).

4. Methods

4.1. Field work

4.1.1. Selection of an ice-wedge polygon

The selected ice-wedge polygon (Fig. 2) is located at the 1st Lena river terrace. It is hexagonal shaped, 20.6 m in diameter, located near the old weather and soil station of Samoylov Island and shows a low inclination towards north east (Meyer, 2002, a). It is a mature polygon type (Meyer, 2002, a). These polygons are quite common for the 1st Lena river terrace and usually show the occurrence of recent frost cracking and ice wedge growth (Meyer, 2002, a). It is characterized by clearly visible frost cracks and a well-developed relief between polygon wall and polygon center of about 0.5 m (Meyer, 2002, a). The center of the polygon was moist but did not show open water. The troughs above the ice wedge were up to 10 cm wide and 20 cm deep. There were no signs of degradation like pond water in the troughs above the frost cracks. At the beginning of the experiment the site showed good frost cracking conditions due to low isolation from the overlying soil, vegetation or snow (Meyer, 2002, a). A thin snow cover is likely since the snow may easily drift away by wind due to the elevated position of the ice-wedge polygon on the island (Meyer, 2002, a). Snow depth has been monitored by a snow depth sensor (*Campbell Scientific Sonic Ranging Sensor SR50*) (Meyer, 2002, a). The AL above the permafrost was measured to be between 0.2 m and 0.6 m thick.

The location near the old weather and soil station on Samoylov Island and a newly installed soil and weather station directly at the research polygon gives the ideal opportunity to compare climate data with isotope compositions of the ice wedges (Meyer, 2002, a). Furthermore, the meteorological stations at Tiksi and Stolb were used to fill any data gaps during recording of meteorological data on Samoylov Island.

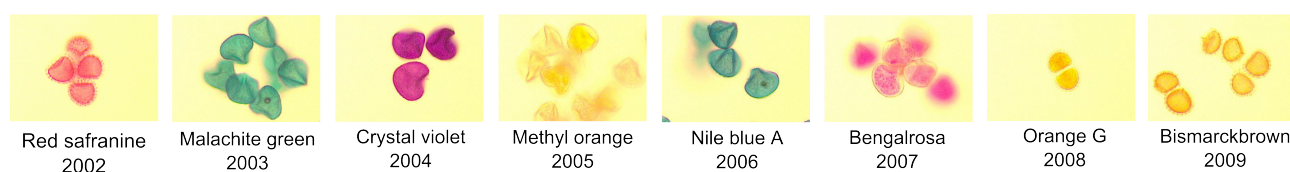


Fig. 5: *Lycopodium* spore tracers .

Type 1: red safranine, orange G, bismarckbrown; Type 2: malachite green, crystal violet, methyl orange, Nile blue A, bengalrosa

4.1.2. Spore (tracer) experiment

The aim of this experiment is to assign recently forming ground ice to the year of its formation and relate the isotope composition of the ice formed in a particular year with the corresponding temperature to calibrate a isotope thermometer. Therefore colored *Lycopodium* spores with a size ranging from 11 μm to 45 μm were applied as tracers to the selected ice-wedge polygon. There are two different types of *Lycopodium Clavatum* spores. The first type has little hairs whereas the surface of the second type is rather even (Fig. 5). Over an 8-year-period every year in August/-September spores with a different color were applied to the polygon. The color identifies the respective year (I. e. 2002 = red safranin) (Fig. 5). In the years 2002/03, 2008/09 and 2009/10 the spores were mainly of type 1 whereas in the other years they were of type 2.

The experiment started in 2002 and ended in 2010. The spores are assumed to behave like sediment particles. They are easily recognizable under the microscope and relatively resistant against weathering which makes them suitable tracers. They were disseminated around the frost cracks and were expected to penetrate into the cracks by the melt water and snow which may contribute to the growth of the ice wedge (Fig. 6). This way it should be possible to identify all types of ground ice, formed in a specific year by the color of the spores contained within. Before using the spores in the field it was successfully tested if it is possible to detect them in the sediment.

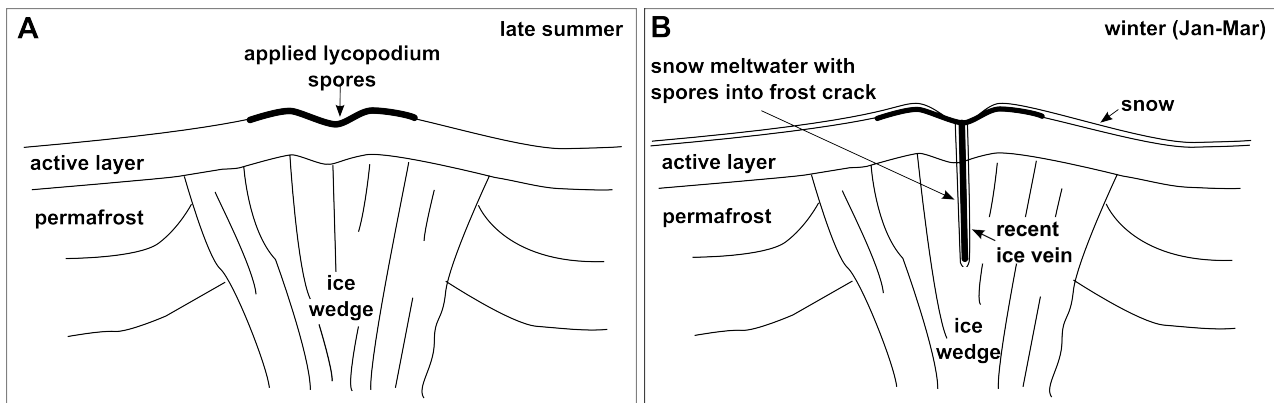


Fig. 6: Scheme of the tracer experiment (Meyer, 2002, a).

A: Scheme *Lycopodium* spores application on an ice wedge. **B:** Scheme of penetrating lycopodium spores into a frost crack.

4.1.3. Sampling (Ice wedge drilling)

In order to find spores back in the studied polygon, 13 ice cores were taken with a *Kovacs Mark II 9 cm Ice Coring System* in 2010 (Fig. 2). The ice cores are termed *LD10 BH-1* to *-13* where *LD10* is the short form for expedition *Lena Delta 2010* and *BH* stands for borehole. Only the ice which formed in 10 years was needed for this experiment. All drilling holes are located in the frost crack area in order to obtain the ice formed in the last few years.

The ice quality depends on a variety of factors such as the moisture standing in the troughs above the frost cracks. In consequence the quality of the ice cores differs (App. 1). Only the cores with sufficiently high quality (*BH2, 3, 4, 5, 8, 10, 11, 12, 13*) were used for the experiment. Due to the high moisture content no drilling was possible in the southern part of the polygon (Fig. 2).

4.1.4. Frost cracking experiment

A frost cracking experiment was carried out in 2002 to 2007 parallel to the tracer experiments in order to determine whether and when frost cracking occurs at the selected ice-wedge polygon. This experiment should reveal the frequency and the timing of frost cracking. (Meyer, 2002, a)

For the frost cracking experiments two 1 m long steel poles which were inserted as deep as possible into the permafrost on both sides of a frost crack and were connected with a copper wire (Fig. 7). Copper was chosen for its high linear extension coefficient of $16.1 \cdot 10^{-6} \text{ K}^{-1}$. It was intended that copper resist temperature fluctuations but breaks when sudden ruptures caused by frost cracking occur.

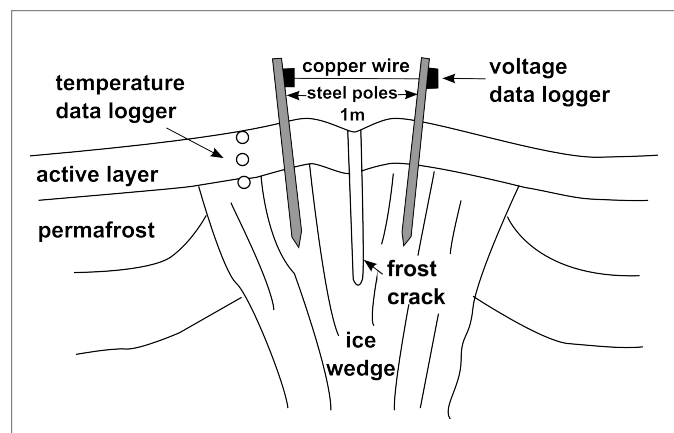


Fig. 7: Scheme of frost cracking experimental set up.
(Meyer, 2002, a).

In the first year (2002/03) experiments with different copper wires (0.5 mm, two-wire braid (HO3VH-H, 2x0.75 mm), single-wire braid (HO3VH-H, 1x0.75 mm)) were carried out in order to detect which wire works best. Finally, it has been decided to use the two-wire braid Cu wire for the following years. The test has shown that this wire responded well to sudden ruptures and stands temperature fluctuations more reliable than the others due to its composition of many individual wires. In order to protect the wire from animals Tabasco was used.

Six frost crack detecting wires were implemented at the ice-wedge polygon in the first year. In the following year the experimental setup got increased to 10 and since 2004/05 there are 11 frost crack detecting wires installed (Fig. 2). The last experimental setup differs from the others. The copper wire does not run between two steel poles above the ground but underground directly through the ice of the wedge. It was suspected to freeze into the ice and break when the ice cracks.

The first ten experiments were termed cracking experiment 1 to 10. The latest one was termed cracking experiment 20. The southern rim of the polygon was used for other research projects and therefore no cracking experiments were carried out in this area.

Six out of the ten experiments and the cracking experiment 20 were equipped with voltage data loggers (*type ESIS Minidan Volt*). Those loggers, were connected to the breaking cables sending signals every 20 minutes. In case of a breaking wire the circuit is interrupted and the measurement stops. Thereby the precise moment, position in the polygon and frequency of frost cracking can be detected. (Meyer, 2002, a). Furthermore, temperature loggers were installed in intervals of 15 cm at depths of 0.05 m, 0.20 m 0.35 m and 0.50 m into the ground (Fig. 2, 7). They allow to record the temperature gradient at the moment of thermal-contraction cracking. (Meyer, 2002, a)

4.2. Laboratory work

4.2.1. Subsampling of the ice cores in the cold-laboratory

The frozen ice cores were brought into the cold laboratory (GFZ, Potsdam, Germany), where they were cut for stable isotope analysis and spore detection. The cores were divided lengthwise in two halves. The first half was taken for archiving and the second one was cut into 5 cm slices for a better overview. The obtained 5 cm slices were termed i.e. *LD10-BH3-2 40-45 cm*. *LD10* denotes the Expedition, *BH3* marks the borehole, the next counter denotes the precise ice block when the material of one borehole is divided into several parts (for example if the drilling took place in several steps) and the last numbers give information about the original depth.

The most promising, undisturbed slices with clearly visible ice veins that seemed to contain spores were selected for further preparation. Once thawed parts were carefully removed with a band saw or the microtome before dividing the sample into three to six pieces. The pieces were numbered from right to left with A1 to A6. The focus was to obtain homogenous, single ice veins but not every ice segment contained an ice vein and not all ice veins could be separated precisely, for instance if two veins cross each other or an ice vein is absent. The ice vein samples were marked with a plus (+) and samples containing two ice veins with double pluses (++).

In total 108 samples were received (App. 2), 68 of which contained visible ice veins.

4.2.2. High-resolution experiment

A particular ice slice with clearly visible ice veins (Fig. 9) was selected for an additional experiment to yield information whether Michel's (1982) assumption of no fractionation occurring during refreezing of ice veins is correct. This is important for this bachelor thesis because single recent ice veins are difficult to subsample within the sawing process and external parts with potentially different isotope composition might be removed.

For this high-resolution experiment the selected ice slice was divided lengthwise into 2 mm to 5 mm wide sections with a microtome (Fig. 9). The sections were melted and the isotope composition of every single section was measured. As a consequence, several isotope data for one ice vein were obtained. If a fractionation during freezing occurred, the isotope compositions of these samples should differ over the ice vein. The last frozen, inner samples should display a more negative isotope composition than the first frozen, outer samples. Due to the small sample volume the stable isotope measurements were carried out with the *Picarro L2120-i Isotopic H₂O*.

4.2.3. Spore analysis

The 108 samples, archived in the ice laboratory, were melted and investigated for spores and their isotope composition. First, a rapid test was carried out to get an overview about the spore content. For this purpose, the water samples were shaken until all particles moved into suspension. A drop of water was subsequently pipetted from the sample and applied to a microscope slide. The pipette was exchanged after every sample. The microscope slides were dried and covered with a cover plate. To fix the cover plate glycerin was used first. But its low melting point of about 18 °C never really fixed the cover plate and made it necessary to use nail polish instead. The prepared

microscope slides were analyzed for spores with a Zeiss-Axioskop-Microscope. The spores of a sample were counted and the respective colors were noted (App. 3).

The remaining sample was filtered using filtration units and 0.45 µm cellulose acetate membrane filters in order to separate the water from the sediment. The filters with the sediment were archived in plastic containers. The water was bottled for isotope analyzes.

To verify the results of the first pipette test, a second test was done with the sediment samples. For this purpose, one third of the filters containing sediment was used. The sediment was removed from the filter by soaking it with distilled water only. Other substances like KOH or HCl were tested, but found inappropriate because KOH reduce the color of the spores and HCl did not substantially improve the visibility of the spores by removing carbonate components from the sample.

The remaining sediment was finally rinsed from the filter with distilled water and the filter was checked under the microscope to make sure that no sediment was left on the surface. The dissolved samples were sieved with a mesh size of 63 µm to remove greater particles to increase the recognizability of the spores. After every sample the sieve was thoroughly cleaned to prevent contamination.

Furthermore, a contamination test was carried out. For this purpose the sample containing the highest number of spores (*LD10-BH8-1/2 55-60 cm A2*) was sieved and afterwards the cleaned sieve was rinsed again with distilled water. The distilled water was applied to a microscope slide and analyzed for spores. The whole test was repeated three times (App. 5).

The sieved samples were filled into 50 ml bottles where they were concentrated by removing surplus water with an pipette once the sediment with spores moved to the ground. The remaining water that could not be discarded by pipette without removing sediment was evaporated in the oven at 50 °C until approximately 5 mm of water remained in the bottles. To ensure that no spores were lost during the concentration random samples of the removed water were applied to an microscope slide and examined under the microscope for spores.

The concentrated sediment samples were applied to microscope slides in the same way like for the quick test and analyzed for spores under the Zeiss-Axioskop-Microscope. Samples that showed a clear result in the quick test were not tested again (App. 4). This concerns all samples where more than four spores of only one color were found.

Statistical methods like PCA (Principal Component Analysis) and cluster analyzes were used to simplify the data and to assign the samples to specific years of formation.

4.2.4. Temperature data

To compare the isotope composition of ice-wedge samples with the average temperatures from Samoylov station, correlation matrices were calculated and the isotope composition (δD , $\delta^{18}O$) plotted as a function of the temperature.

In these correlation matrices, the monthly average temperatures from November to May, the average winter temperatures (December to February) (T_{winter}), the average spring temperatures (March to May) (T_{spring}) and the average temperatures of the cold season (November to May) ($T_{\text{cold season}}$) from 2002 to 2010 were considered.

The temperature data of the old and new climate station on Samoylov Island are combined in one dataset (Boike et al., 2008). Due to several gaps in the temperature measurements of Samoylov Island the temperatures from Tiksi and Stolb were proved on comparability to fill the gaps.

5. Results

5.1. Comparison of Picarro and mass spectrometer measurements

Despite different methodical approaches (*Finnigan MAT Delta-S mass spectrometer*, *Picarro L2120-i*) there are only small differences in the measured isotope composition of one sample (Fig. 8). For $\delta^{18}\text{O}$ the average deviation is 0.14 ‰ and for δD it is 1.1 ‰ between the measurements with the mass spectrometer and the Picarro (App. 6). Only one sample (*BH3-1 50-51 cm A3+*; number 2 in Fig. 8) shows relatively high deviations of 0.54 ‰ in $\delta^{18}\text{O}$ and 5.4 ‰ in δD . Considering the small sample volume, which might have been too small for the mass spectrometer, a correlation developed by Meyer et al., (2000) exists. Unfortunately, the exact sample volume, which is needed for the correlation, was not noted. Therefore no exact correction can be carried out. Nevertheless, the correction would approach the isotope compositions. For example a assumed sample volume of 0.5 ml leads to a δD of -162.5 ‰. With a δD of -164.6 measured at Picarro, the deviation between the data is only 2.1 ‰.

The standard deviation (SD) of the $\delta^{18}\text{O}$ measurements is slightly better for the *Finnigan MAT Delta-S mass spectrometer* ($\delta^{18}\text{O} = 0.09$ ‰) than for *Picarro L2120-i* ($\delta^{18}\text{O} = 0.11$ ‰). For the δD measurements it is the contrary, the maximal standard deviation is better for *Picarro L2120-i* ($\delta\text{D} = 0.2$ ‰) than for the mass spectrometer ($\delta\text{D} = 0.7$ ‰). This trend is also confirmed by the average of the standard deviation (App. 6).

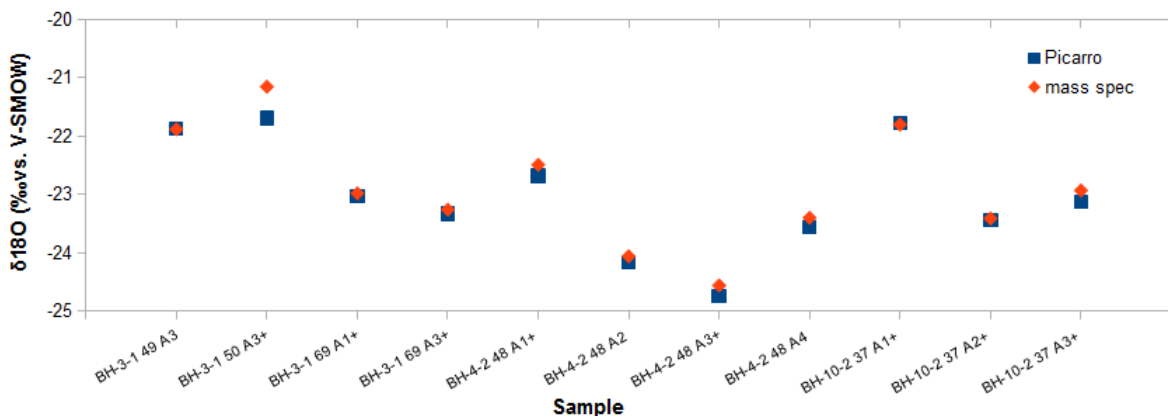


Fig. 8: Comparison of $\delta^{18}\text{O}$ results of *Finnigan MAT Delta-S mass spectrometer* and *Picarro L2120-i*.

5.2. High-resolution experiment

The high resolution experiment shows different isotope compositions for every sample of an ice block of 45 mm subsampled into 10 samples. The isotopic composition varies from -24.98 ‰ to 22.12 ‰. The isotope variations between the samples are quite low in the central area of the ice block and becomes higher towards the rim (Fig. 9).

Sample 9, 3 and sample 5 to 7 are single ice veins. In samples 5 to 7, located in the central section of the ice block, it was possible to take three samples within one ice vein. Here the isotope variations are quite small. The $\delta^{18}\text{O}$ values at the rims (5, 7) are slightly higher than in the center (6). The fluctuation of the isotope values in the vein between the highest (5) and the lowest (6) value is 0.32 ‰ for $\delta^{18}\text{O}$ and 1.1 ‰ for δD . Between part 6 and 7 the difference is only ± 0.2 ‰ and ± 0.9 ‰ for $\delta^{18}\text{O}$ and δD , respectively. The course of the d-excess values within the ice vein is contrary to the $\delta^{18}\text{O}$ variations.

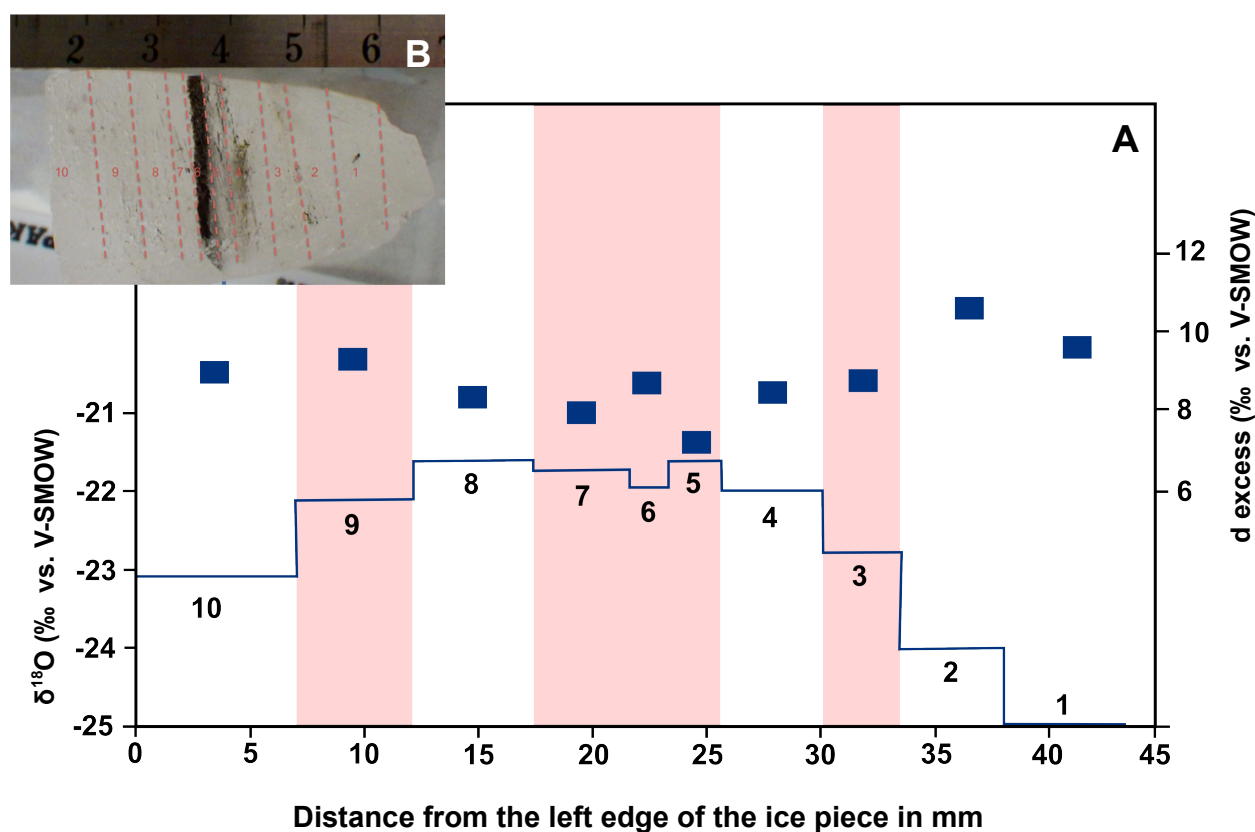


Fig. 9: $\delta^{18}\text{O}$ and d-excess measurement results of the High resolution experiment

A: $\delta^{18}\text{O}$ and d-excess values of the ice samples displayed in the original position in the ice piece (in mm from the left rim). Single ice veins are red highlighted. **B:** Photo of the selected ice piece for the high-resolution experiment with marked separation lines

5.3. Frost-cracking experiment

In order to understand how frost cracking influence the tracer experiment rate, time and location of observed cracking events has been evaluated as well as the conditions leading to frost cracking.

All cracking events occurred between 16 Nov and 06 Feb. The main number of thermal-contraction cracking is detected in December (N = 5) followed by November (N = 3) (Fig. 10). In January (N = 1) and February (N = 2) cracking events were only detected in 2003/04.

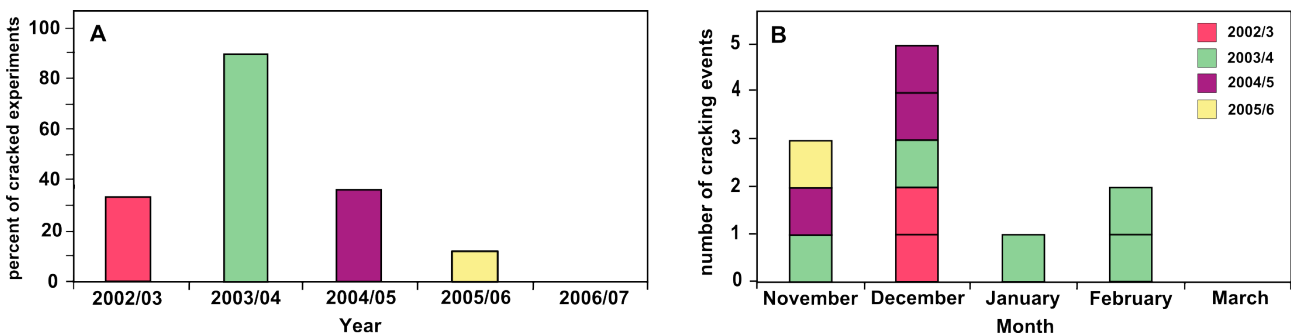


Fig. 10: Number of detected frost-cracking events

A: Detected cracking events in percent of installed experiments. **B:** Number of cracking events grouped in monthly occurrence. (The cracking event in November 2003/04 is later identified as outlier).

In 2002/03, in 33 % of the experiments frost cracking was detected. In the following year 2003/04 nearly every experiment cracked (90 %). Afterwards the rate of detected cracking events decreased (Fig. 10). Only 36 % of the experiments cracked in 2004/05 and just 12 % in 2005/06. Finally, in 2006/07 no cracking events could be observed (App. 7). Except from 2002/03 to 2003/04 the frost-cracking experiments detect a decreasing trend of cracking events

To determine if the decreasing number of detected cracking events are correlated to the snow depth, the data from the snow-depth sensor (Kattenstroth, 2009) and the number of cracking events were compared (Fig. 11). However the snow-depth data are from the polygon center not from the polygon rim, where the frost cracking occurs. In general the snow cover is much higher in the center than at the rim. Nevertheless the data show the approximate variation of snow depth.

The snow depth in the polygon center varies between 10 cm to 25 cm in the years 2003 to 2008 (Fig. 11). In 2003/04, the snow cover was highest with a max. snow depth of 56 cm. The highest measured snow cover at the rim of the polygon was 17 cm (Kattenstroth, 2009). When correlating monthly snow depth with the frost-cracking events, no relevant correlation could be found (0.03).

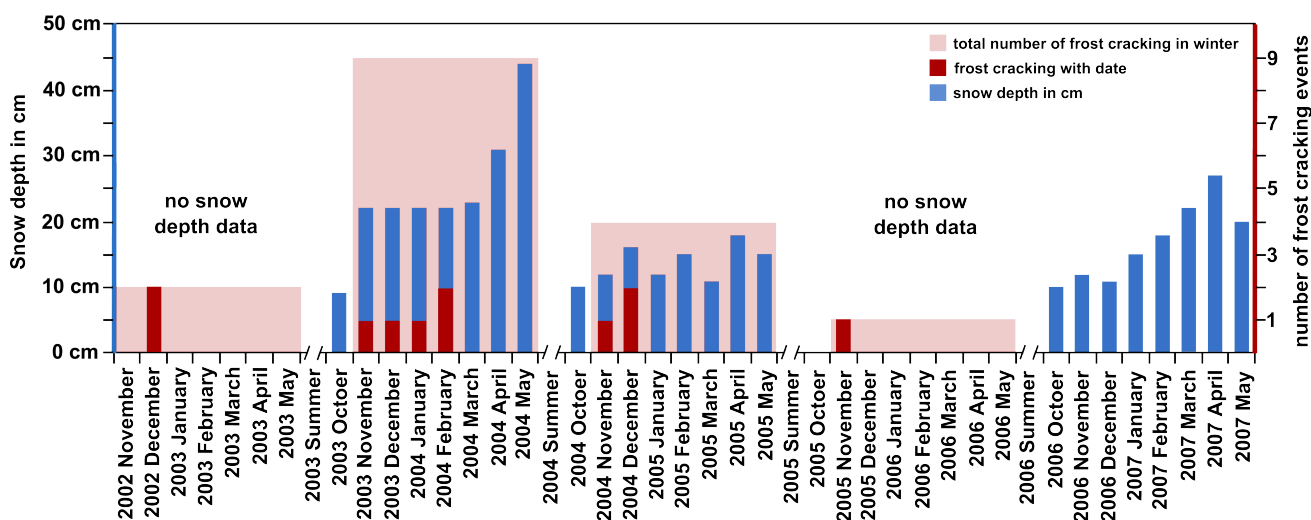


Fig. 11: Comparison of snow depth and number cracking events

Monthly frost cracking events with known date of occurrence are summed up in red bars and monthly snow depth by blue bars (Kattenstroth, 2009). The total number of cracking events detected in one winter is highlighted with red boxes.

An other factor, that might have influence on the frost-cracking events are the T_{winter} . The correlation between average T_{winter} and the total number of frost crackings detected in one winter is -0.93. Hence the colder the winter was the more cracking events could be observed.

The data of the installed temperature logger show that the strongest cooling events in the soil occur in November and December. The cooling rates increases to $-1.2\text{ }^{\circ}\text{C}/\text{day}$ in the soil layer above the permafrost in 40 cm depth (Fig. 12). The average cooling rates in these months were $-0.3\text{ }^{\circ}\text{C}/\text{day}$ in 2002/03 and 2003/04. The temperature variations in the upper soil layers show the same trends but they are much higher. In 5 cm depth, the highest cooling rate is $-6.6\text{ }^{\circ}\text{C}/\text{day}$ in 2002/03 and $-3.3\text{ }^{\circ}\text{C}/\text{day}$ in 2003/04. The average cooling rate in both years in November and December are $-0.3\text{ }^{\circ}\text{C}/\text{day}$ (App. 8).

Due to the fact that this soil station only measured from 2002 to early 2004, the data were complemented with data from a second soil station in the southern area of the investigated polygon. The data from the years 2002 to 2004 show that the measured temperature trends of both stations are quite the same (Fig. 12)

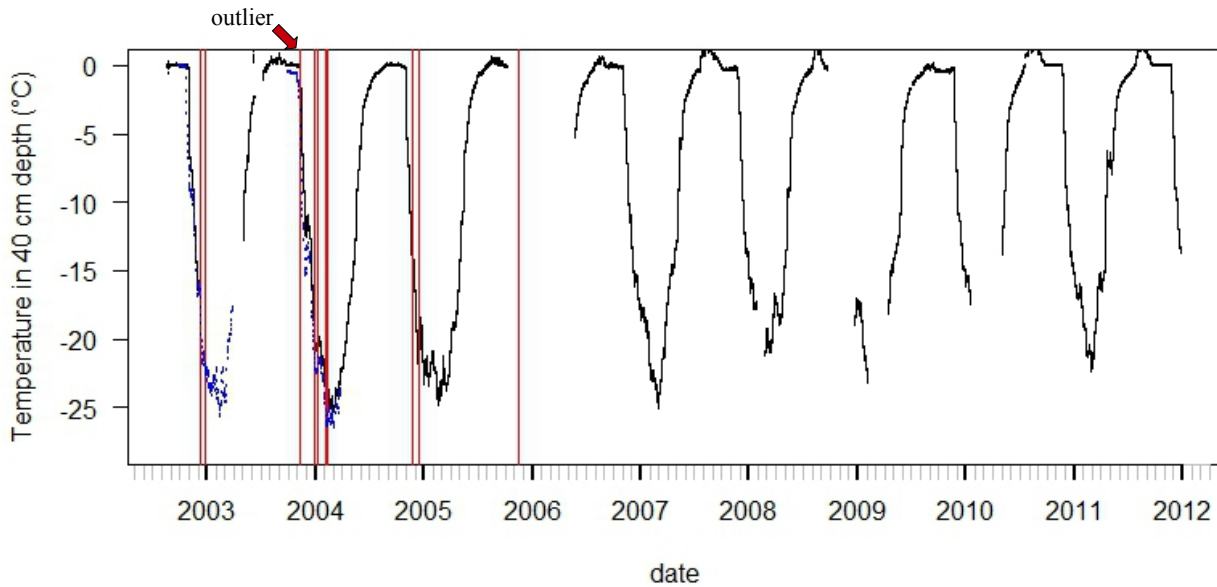


Fig. 12: Ice-wedge-polygon-soil temperatures

Soil temperature measured in 40 cm depth at the first soil station at the investigated polygon (blue) and a the second soil station in the south of the polygon (black) with marked data of frost-cracking events (vertical red lines).

In general, frost cracking often occurs at the end of strong cooling phases, right before the minimal temperatures are reached (Fig. 12). There is one exception where frost cracking was detected at an early cooling stage at 08 Nov 2003 occurring at around 0 °C right before the temperature starts to drop. Therefore it might have been caused by other effects and is discarded as outlier.

The cooling trend at 40 cm depth preceding the rupture of the breaking cable shows in average temperature decrease of about -0.5 °C/day over 13 days (App. 09), when leaving out the outlier.

Tab. III: Overview of cracking experiments

(X = detected cracking event; gray = no cracking experiment installed; - = no cracking observed;

(X) = outlier, No. = total number of observed cracking events; E = east; N = north; W = west)

Cracking experiment	No.	1	2	3	4	5	6	7	8	9	10	20
Location in the polygon	/	E	E	E	E	N	N	N	W	W	W	W
2002/03	2	X	-	X	-	-	-					
2003/04	9	X	X	X	X	X	-	X	X	X	X	
2004/05	4	-	X	-	-	-	X	X	-	-	(X)	-
2005/06	1	-	-	-	-	-	-	-	-	-	-	X
2006/07	0	-	-	-	-	-	-	-	-	-	-	-

For the location of the crackings events in the studied polygon no clear orientation can be observed

(Tab. III). Thermal-contraction cracking seems to occur all over the polygon. There might be a slight trend from east to west during the years, but due to the decreasing rate of events and the different number of cracking experiments this observation is indistinct.

5.4. Comparison of temperature data of Samoylov to other measuring stations

The correlation of the temperatures from Samoylov Island, Stolb (6 km NE) and Tiksi (120 km SE) (Fig. 13) should show which data are suitable to fill the data gaps in the Samoylov temperature data. In winter and spring the temperature variations of Samoylov and near station Stolb are quite similar with a maximum difference of 1 °C (average spring temperature 2006/07 and average winter temperature 2008/09). The only exception is in 2010, where average spring temperature from Samoylov Island differs by almost 3 °C from the temperatures measured at Tiksi and Stolb. Most likely the Samoylov Island temperatures are erroneous in this year.

The temperature from Tiksi is about 1 °C higher than on Samoylov Island in winter. In spring the temperatures of Samoylov and Tiksi are more similar and do not differ by more than by 1 °C.

The coldest winter was in 2003/04, followed by 2008/09. The winters in 2002/03, 2004/05, 2007/08 and 2009/10 were also quite cold. The warmest winters were in 2005/06 and 2006/07. For spring temperatures the two coldest years were in 2004 and 2006.

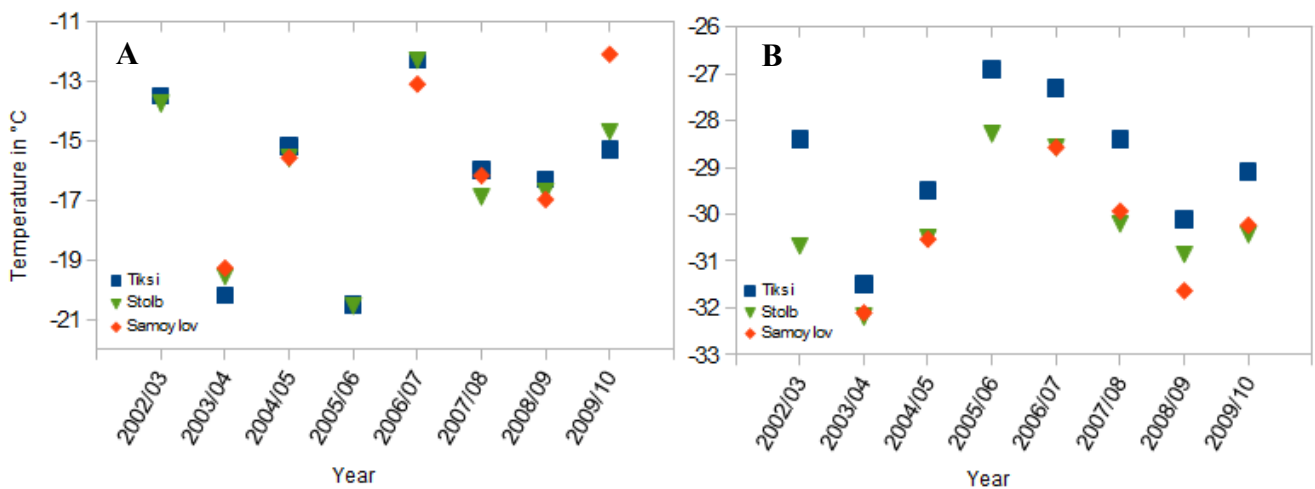


Fig 13: Comparison of average temperatures from Samoylov Island, Stolb and Tiksi
A: average spring temperatures B: average winter temperatures

5.5. Spore (tracer) experiment

5.5.1. Discovered spores

Different colored spores were used to assign single ice veins to the year of their formation. It was not possible to recognize the spores on a macroscopic scale in the ice, except for the red safranin spores. Nevertheless many spore containing ice-vein samples were achieved. Furthermore, some cloud-like structures were discovered by dividing the ice cores. They might have been formed by snow, falling into a frost crack.

Most of the spores were clearly visible and easy to recognize in the ground ice sample under the microscope. Especially the red safranin and crystal violet ones were easily notable. Also malachite green and Nile blue were conspicuous but may be confused with each other. Bengal rose showed signs of discoloration but still could be recognized. However, some colorless spores were found, that may have once been of Bengal rose color. Methyl orange, orange G and Bismarck brown were difficult to recognize due to their similarity to the color of the sediment. The *Lycopodium Clavatum* spores of the hairy type 1 are far more easy to recognize than the spores of type 2 - even when colors are not clearly visible.

The results of test 1 (pipette method) and 2 (concentration method) confirm each other largely (Fig. 14). The main trends of number of spores found in both tests are the same. However, in test two the number of spores found is however higher. Also spores of colors that could not be found in the first test (methyl orange, Bengal rose, orange G and Bismarck brown) were found in the second one. Apparently, the removal of the large sediment and organic particles made it easier to recognize even colorless spores.

The highest number of spores was of red safranin color (N = 881), higher than the number of all other recovered spores (green: 366, violet: 196, orange: 21, blue: 43, rose: 1, orange G: 8, brown: 21). The number of spores found from the years 2002 to 2007 decreases with exception of a minimum in 2005. After 2007 the number of spores slightly increases again. In total 42 colorless spores were found. Many samples contained spores from two or more years within one sample.

The contamination test showed that the highest contamination is less than 0.2 % during filtration (App. 5). No spores could be found in the removed water which was investigated to examine spore loss during pipetting.

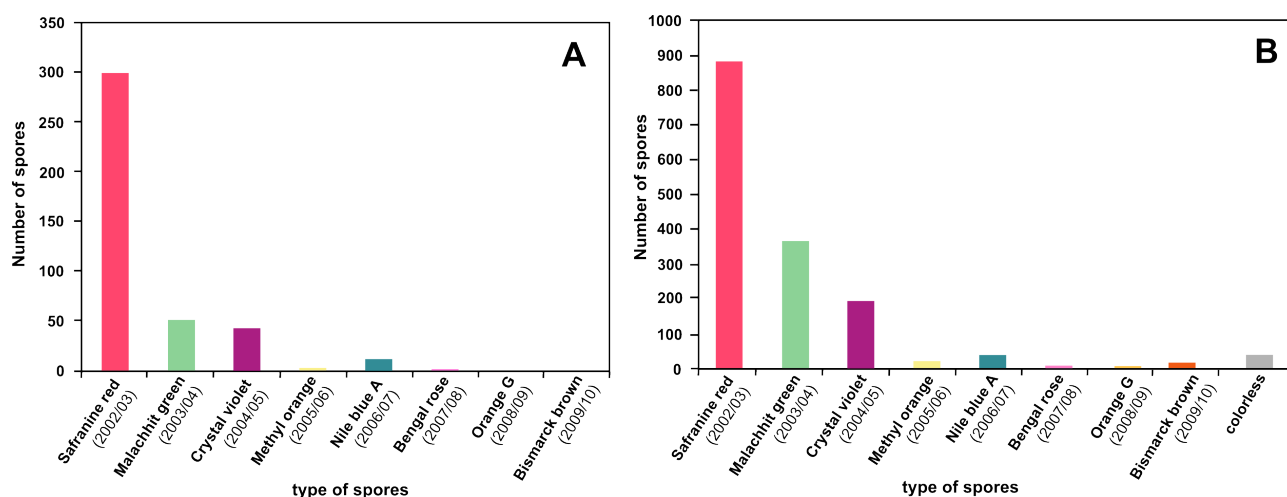


Fig 14: Quantitative results of the spore investigation tests 1 (A) and 2 (B)

5.5.2. Statistical classification of the samples

Apparently, red safranine spores (2002/03) had a much higher probability to penetrate into the ice wedge than spores of the following years. To correct this effect, the spore containing data were normalized, between 0 and 1 for the total number of spores of one color. Spores contained in one sample were given in percent to assess which color dominates in a discrete sample (App. 10). Samples with out spores were removed from the data set.

Afterwards, a cluster analysis and PCA (Principal Component Analysis) were carried out with the program R to assign the samples to specific years. The performed PCA is based on the euclidean distance and simplified the data to point out general similarity trends between the samples. The PCA result was plotted in a diagram where principal component one (PC1) was plotted against principal component two (PC2) (App. 11). The years 2002/03, 2003/04 and 2005/06 are clearly different from the other years. The differences decrease for the years 2004/05, 2006/07 and 2009/10 to almost none between 2007/08 and 2008/09.

The first cluster analysis was an euclidean cluster analysis. In this procedure the zero values are included in the similarity determination. For this cluster analysis the distance was calculated with a distance matrix computation and hierarchically clustered.

To verify if the zero values alter the results, a second cluster analysis (bray-curtis clustering) was carried out. This method does not include zero values but considers present spores only. Therefore the distance was calculated with the dissimilarity indices for community ecologists method and hierarchically clustered again.

To show the results of the cluster analyzes the euclidean clustered and bray curtis clustered data

were plotted as a cluster dendrogram (App. 12, 13). The attribution to the years of the different samples are the same in both cluster analyzes.

Because some samples ($N = 11$) could not be assigned with these methods, a k-means clustering was carried out. It was implied that eight clusters should be created. This corresponds to the number of years in the experiment. An ideal cluster is defined when all values of the sample are zero except for one spore color. For this spore color the value is set to one.

The k-means clustering classified all samples (App. 15). The new clusters contained the same samples as the previous clusters, with incorporation of these samples that could not be assigned to a discrete year before. With this procedure, all samples containing spores were attributed to the most probable year of formation.

5.5.3. Isotope variations over the years

The isotope compositions of all ice wedge samples can now be related to a specific year. Figs. 15 and 16 show the $\delta^{18}\text{O}$ values of the samples plotted against the probable year of formation. In Fig. 15 all samples are represented as single data points. There are quite a lot samples for the years 2002/03, 2003/04 and 2004/05. For 2005/06, 2006/07 and 2009/10 the number of samples decreases but still shows a usable amount. Only one sample could be assigned to 2007/08 and two to 2008/09. The isotope variations within one year are quite high, especially in 2004/05 where the $\delta^{18}\text{O}$ values vary by more than $\pm 6\text{‰}$.

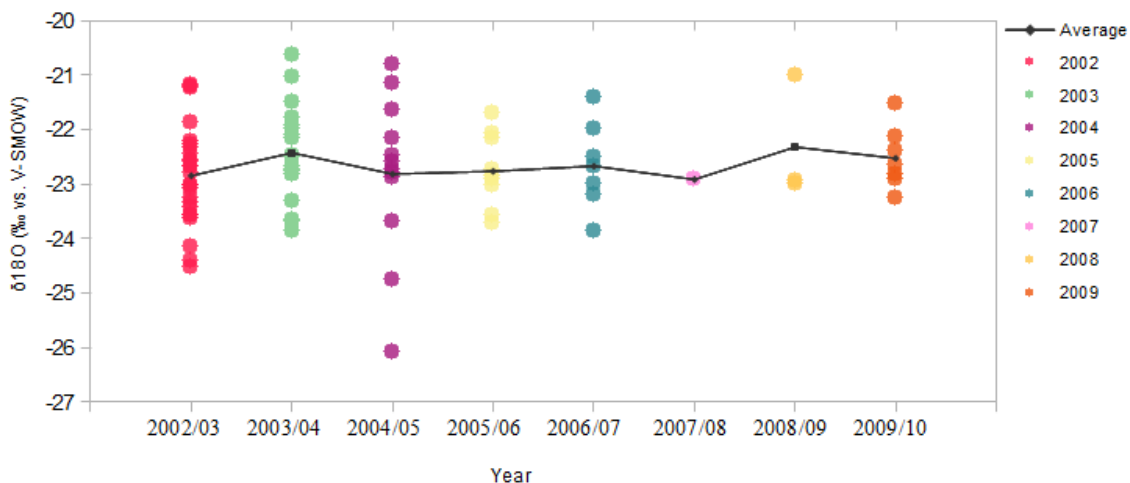


Fig. 15: $\delta^{18}\text{O}$ values of the samples assigned to the respective year (by k-clustering).

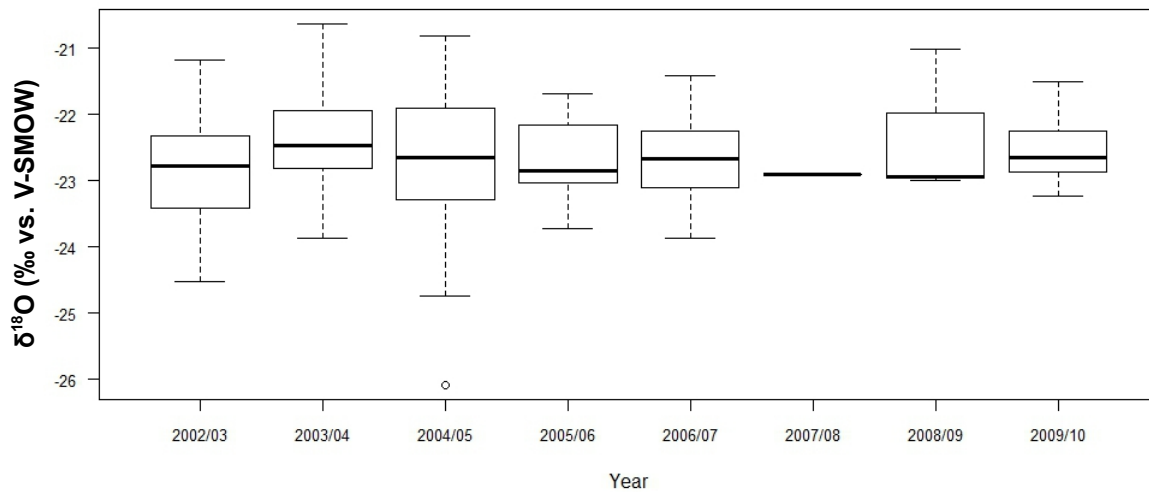


Fig. 16: Box plot of $\delta^{18}\text{O}$ values of the samples assigned to the respective year (by *k*-clustering).

Fig. 16 is a box and whiskers plot where the whiskers mark min. and max. values and are maximum 1.5 times of the length of the interquartile range (IQR) (Tukey, 1977). All boxes overlap in their ranges and there are only small differences between the median values. In 2004/05, one $\delta^{18}\text{O}$ value is outside the $1.5 \cdot \text{IQR}$. This could be indicative for an outlier, but since the data point is within the $3 \cdot \text{IQR}$ it not necessarily have to be one. Due to the fact that no further reasons which identify the value as an outlier could be found, the data point is not discharged from the data set.

5.5.4. Comparison of isotope compositions and temperatures

To compare the isotope composition of the ice-wedge samples to temperatures, median, maximum, minimum, and average isotope compositions were compared with the measured temperatures at Samoylov Island and Stolb.

The median was chosen for its robustness to outliers (like the one that might occur in 2004/05). Unfortunately, some of the data are unsuitable to calculate a median e.g. data from 2008/09, with only two values. Therefore the average isotope compositions were also correlated.

The gaps in the temperatures measured at Samoylov Island were filled with temperatures from Stolb. Furthermore, the spring temperatures from 2010, which were earlier found to be erroneous (see chapter. 5.4) were replaced by Stolb temperatures (App. 16). In order to compare the isotope data to a constantly measured data set, they were also correlated to Stolb temperatures. Due to the large distance and the differences between T_{winter} of Tiksi and Samoylov Island (Fig. 13), Tiksi temperatures are not considered here.

The average monthly temperatures from November to May as well as T_{winter} , T_{spring} and $T_{\text{cold season}}$ from 2002/03 to 2009/10 were correlated to the isotope compositions with a correlation matrix in R.

It is remarkable that the temperature variations between the different years are in general much higher than the isotope variations (App. 16, 20). This makes it difficult to recognize similarities and matching trends. Therefore the isotope and temperature values were normalized to values between zero and minus one and then also correlated (App. 17, 21).

5.5.4.1. Correlation of isotope and temperature data over all eight years

The correlation matrices over all eight years (Tab. IV) show the highest correlation in December and the second highest in April/May. The average isotope composition has a strong correlation coefficient with T_{December} . The median isotope composition shows a little weaker correlation with T_{December} , but higher correlations for T_{April} than the average isotope data (Tab. IV).

The temperature values from Samoylov Island and Stolb show quite similar correlation trends (Tab. IV). In December and April the correlation coefficients are slightly better for Samoylov Island than for Stolb, but in May it is the opposite (Tab. IV).

The correlations of the maximal Isotope data show the best correlation with April temperatures, while the minimal isotope compositions correlates best with December and January temperatures (Tab. IV).

Tab. IV: Correlation matrix of Stolb and Samoylov temperatures and $\delta^{18}\text{O}$ data over all eight years

(gray = negative correlation; yellow = positive correlation ; red = highest correlation in one column)

location	$\delta^{18}\text{O}$	Average temperature									
		Nov	Dec	Jan	Feb	Mar	Apr	May	Winter	Spring	Cold Season
Samoylov	Max.	0.12	-0.12	-0.22	-0.44	-0.42	0.35	-0.41	-0.50	-0.06	-0.27
	Min.	-0.30	0.14	0.23	-0.28	-0.16	-0.20	-0.00	0.03	-0.18	-0.18
	Average	-0.16	0.51	-0.29	-0.40	-0.36	0.03	0.01	-0.07	-0.12	-0.15
	Median	-0.24	0.32	-0.34	-0.42	-0.24	0.25	-0.01	-0.24	0.05	-0.10
Stolb	Max.	-0.10	-0.11	-0.12	-0.39	-0.27	0.38	-0.37	-0.42	0.01	-0.16
	Min.	-0.28	0.18	0.16	-0.22	-0.15	-0.18	-0.09	0.06	-0.18	-0.17
	Average	-0.23	0.47	-0.49	-0.37	-0.34	0.01	0.09	-0.210	-0.102	-0.20
	Median	-0.31	0.28	-0.47	-0.43	-0.22	0.23	0.08	-0.37	0.06	-0.13

5.5.4.2. Differentiation between ice-vein and no-ice-vein samples.

To verify whether there is a different in correlation when considering only clearly identifiable ice-vein samples or no-ice-vein samples, both sample types were compared to Samoyliv Island temperatures. The correlation matrix (App. 18) shows that the isotope composition of the ice-vein samples fit better than the non ice-vein samples. Conspicuous is that the highest correlation of average and median isotope compositions of the ice-vein samples is in April ($r_{\text{average}} = 0.44$; $r_{\text{median}} = 0.43$) followed by December ($r_{\text{average}} = 0.33$; $r_{\text{median}} = 0.20$). The isotope composition of the samples without ice veins fit best to May ($r_{\text{average}} = 0.22$; $r_{\text{median}} = 0.23$) and March ($r_{\text{average}} = 0.20$; $r_{\text{median}} = 0.21$) but show only weak correlations.

Correlating the isotope composition of the ice-vein samples with Stolb temperatures all correlations are weak. Best correlations for the average isotope composition are December and May ($r = 0.29$) followed by April ($r = 0.25$). When using median isotope compositions, May and April ($r = 0.22$) fit better than December ($r = 0.16$). The correlation of the non ice vein samples is far weaker. They are weakly correlate in March ($r = 0.09$), May ($r = 0.12$) and February ($r = 0.06$).

5.5.4.3. Correlation of isotope and temperature data over different time periods

To determine how correlations change over time, isotope composition and temperature data were additionally correlated in two- and four-year steps.

The correlations in two-year steps show an increasing number of positive correlation coefficients over the years (App. 19). In 2002/03 and 2003/04, only the winter months temperatures correlate with the $\delta^{18}\text{O}$ data. In the following years also the spring month temperatures show a correlation.

Tab. V: Correlation matrix of Samoylov temperatures and $\delta^{18}\text{O}$ data in four year steps

(gray = negative correlation; yellow = positive correlation ; red = highest correlation in one column)

$\delta^{18}\text{O}$	Years	Temperature									
		Nov	Dec	Jan	Feb	Mar	Apr	May	Winter	Spring	Cold Season
Average	2002-05	-0.80	0.60	-0.76	-0.92	-0.74	-0.20	-0.88	-0.57	-0.96	-0.57
	2004-07	0.44	0.74	0.651	-0.45	-0.40	0.45	0.24	0.68	0.26	0.66
	2006-09	0.96	0.42	0.41	0.18	0.25	0.47	0.88	0.65	0.79	0.74
Median	2002-05	-0.97	0.04	-0.53	-0.97	-0.47	0.37	-0.51	-0.68	-0.09	-0.68
	2004-07	0.03	-0.07	0.61	-0.57	-0.07	0.80	0.36	-0.16	0.60	0.63
	2006-09	0.99	0.57	0.54	0.06	0.24	0.62	0.87	0.69	0.90	0.84

When correlating temperatures and isotope composition in four-year steps the correlation coefficients increase over the years (Tab. V). In 2002-2005, the only positive correlations are in December and April. In 2004-2007, all month except February and March show moderate or strong correlation. Finally, in 2006-2009 all correlation coefficients are positive. In 2004-2007, the highest correlation for the average isotope data is in December, while the highest correlation for the median isotope data is in April. In 2006-2009, the correlations of both isotope data types are highest in November, but also the correlation of T_{spring} is very high (Tab. V).

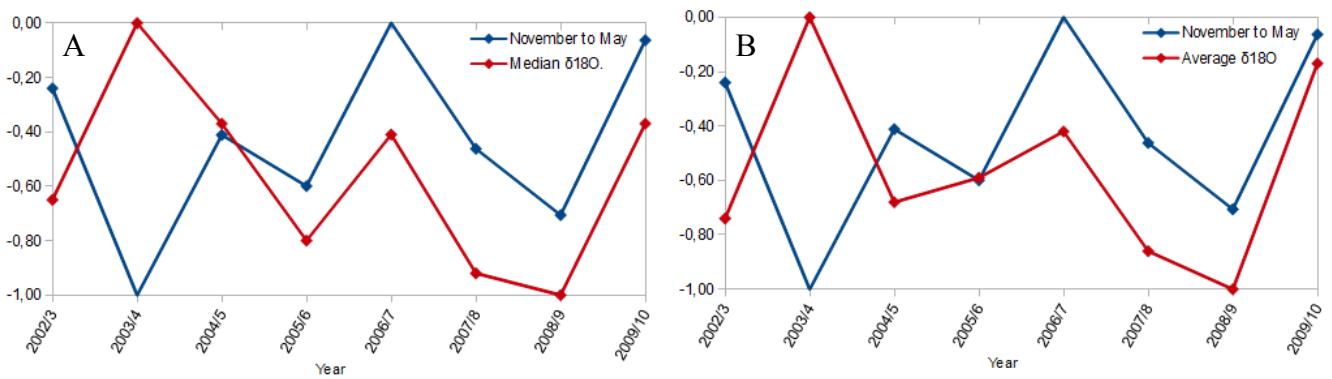


Fig. 17: Comparison of normalized $\delta^{18}O$ data and Samoylov temperatures

A: normalized median $\delta^{18}O$ data and normalized average Samoylov temperatures from November to May;

B: normalized median $\delta^{18}O$ data and normalized average Samoylov temperatures from November to May

The temporal course of the isotope curve in the first two years is always opposite to all average monthly temperatures (Fig. 17) except for December (Tab. IV). When leaving out the first two years (2002/03-2003/04) the correlation trend changes completely (Tab. VI) compared to the correlation over all eight years. Overall, the correlations are much stronger and reaching up to with no negative correlations anymore. The correlation coefficients with T_{spring} are higher than the correlation coefficients with T_{winter} . $T_{cold\ season}$ show the strongest correlations.

Tab. VI: Correlation matrix of Samoylov temperatures and $\delta^{18}O$ data from 2004 to 2010

(gray = negative correlation; yellow = positive correlation ; red = highest correlation in one column)

$\delta^{18}O$	Temperature									
	Nov	Dec	Jan	Feb	Mar	Apr	May	Spring	Spring	Cold Season
Median	0.28	0.15	0.30	0.00	0.29	0.52	0.67	0.23	0.60	0.75
Average	0.43	0.38	0.27	0.10	0.19	0.23	0.71	0.46	0.38	0.67

In summary, there are two correlation maxima between temperature and isotope composition: one in winter (December) related to the first years and one in spring (April) related to the later years. The highest correlation ($r = 0.51$) over the considered 8 years has been found between December temperatures and average $\delta^{18}\text{O}$. Leaving out the first two years the correlation for all average monthly temperatures improves.

5.5.5. Calibration of an stable-isotope thermometer for ice wedges

To calibrate a stable isotope thermometer a linear regression is calculated between temperature and isotope data (Fig.18). Depending on the data selected to set up this equation show different results. The three most important equations are given here exemplary more calculations can be found in the appendix (App. 22). For December temperatures from Samoylov Island and average $\delta^{18}\text{O}$ data (best correlation over all eight years) the linear regressions [Eq: 7] is as follows:

$$T = 7.17 * \delta^{18}\text{O} + 133.69 \quad R^2 = 0.26 \quad [\text{Eq: 7}]$$

When choose $T_{\text{cold season}}$ Samoylov Temperatures and average $\delta^{18}\text{O}$ data to consider the whole cold season variations over the eight years the equations [Eq: 8] is:

$$T = -1.09 * \delta^{18}\text{O} - 47.86 \quad R^2 = 0.02 \quad [\text{Eq: 8}]$$

Finally, when only take the last six years into account (best $T_{\text{cold season}}$ correlation) the linear regressions [Eq: 9] is as follows:

$$T = 4.40 * \delta^{18}\text{O} + 77.34 \quad R^2 = 0.45 \quad [\text{Eq: 9}]$$

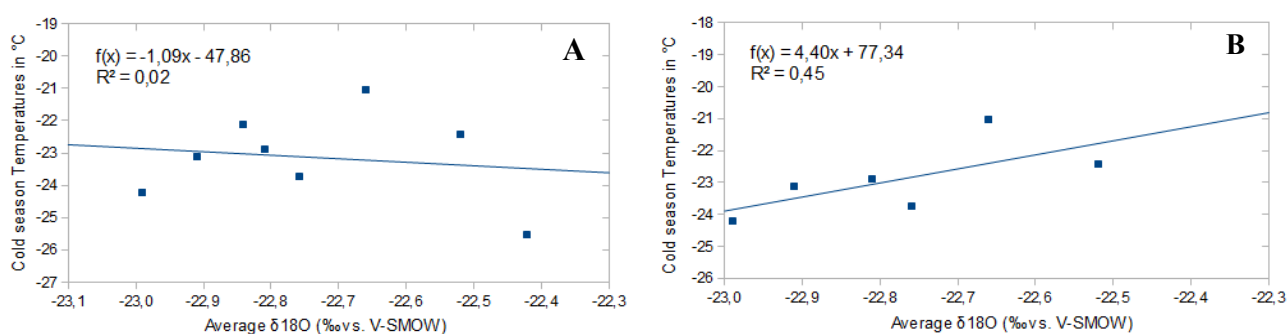


Fig.18: Linear regression between $T_{\text{cold season}}$ and average $\delta^{18}\text{O}$
A: considering all eight years. **B:** considering only the last six years.

6. Discussion

6.1. Methodical aspects

The comparison of the measurements with *Finnigan MAT Delta-S mass spectrometer* and with *Picarro L2120-i* showed identical values of individual samples for both methods. When considering the accepted precision of Picarro and the mass spectrometer (± 0.1 ‰ for $\delta^{18}\text{O}$ and ± 0.8 ‰ for δD) a difference of 0.2 ‰ and 1.6 ‰ can be explained for $\delta^{18}\text{O}$ and δD , respectively. Only two samples show higher differences: *BH3-1 50-51 cm A3+* with 0.54 ‰ difference in $\delta^{18}\text{O}$ and 5.4 ‰ in δD and *BH10-2 37-42 cm A3+* with a difference of 1.7 ‰ in δD . The deviation of the second sample only is 0.1 ‰ and therefore negligible. But the deviations in sample *BH3-1 50-51 cm A3+* are more than three times as high as the next highest deviation. This could be caused by the small sample volume which might not have been enough for the mass spectrometer measurement and did not allow for repeated measurement. When correct measured isotope composition with a correction for small sample volumes (Meyer 2000) the deviation gets smaller. However, this deviation is an exception. The comparison shows both methods provide useful isotope data and can be used for isotope analyzes. Except one all measured values of the Picarro and the mass spectrometer confirm each other. Consequently the measurements with the *Picarro L2120-i* can be used for this experiment despite the short experience time with the machine.

6.2. Interpretation of temperature differences between measuring stations

The comparison of the temperature data from Samoylov Island, Stolb and Tiksi shows suitable results, though there is a quite constant temperature offset of about 1 °C observed between Tiksi and Samoylov in winter (Fig. 13). The higher winter temperatures at Tiksi might be caused by the increased maritime influence to coastal Tiksi compared to Samoylov or Stolb. In spring, when river and sea are completely frozen the temperatures of Samoylov, Stolb and Tiksi differ less. Overall, the temperature curves have the same shape. Especially the temperatures from Stolb are suitable to fill the gaps in the Samoylov temperature data set. Only in spring 2010 a striking difference of the temperatures of Tiksi and Stolb compared to Samoylov Island is noticeable which is most likely an error in the Samoylov Island data set.

6.3. Evaluation of fractionation effects during refreezing

The high-resolution experiment allowed to separate one ice vein into three pieces (Fig. 9), sample 5 to 7). Isotope compositions for the different parts of that vein were obtained, with variations in this ice vein that are only slight. Except the $\delta^{18}\text{O}$ difference between part 5 and 6 all variations within the vein are low enough to be explained by the precision of *Picarro L2120-i Isotopic H₂O*. The $\delta^{18}\text{O}$ difference between part 5 and 6 is 0.12 ‰ to high to be explained by the highest certified 1σ deviation. Furthermore, the highest measured 1σ deviation in this sequence was 0.07 ‰ for $\delta^{18}\text{O}$ and 0.2 ‰ for δD . The doubled amount of this deviation got exceeded by all $\delta^{18}\text{O}$ and δD differences within the ice vein. Therefore a fractionation is possible.

If there was fractionation during refreezing in the ice vein the isotope composition at the rim of the ice vein should be higher than in the center because it freezes first. Such a trend can be observed in the measured isotope composition. Also the increases d-excess between part 5 and 7 and part 6 supports the theory of a fractionation (Fig. 9). This could indicate that contrary to Michels (1982) assumption there is fractionation in ice veins during refreezing, but only at a very small scale. For verification more measurements have to be carried out. Anyway, if there is fractionation occurring it seems to be of negligible influence for climate interpretation. Therefore preparation inaccuracies at the rim of an ice vein do not affect the isotope composition and consequently are not taken into account for the spore experiment.

6.4. Assessment of frost-cracking experiments

Apart from the increasing number of cracking events between 2002/03 and 2003/04 the frost cracking experiment showed a decreasing frequency of cracking events. This trend indicates that the polygon was quite active when the experiment started but decreased progressively during the years. This can not be explained by variations in the snow depth which may isolate the soil and prevent frost cracking since there is no negative correlation between snow depth and the number of frost-cracking events ($r = 0.03$). The highest detected snow cover at the polygon rim was 17 cm (Kattenstroth, 2009). Mackay (1993) assumed that depths of more than 50 cm prevent frost cracking. Such values were not achieved and therefore the isolation was never high enough to completely prevent frost cracking. Consequently the snow cover does not seem to be the crucial factor for the decreasing trend of frost cracking.

When looking at T_{winter} at Samoylov Island with data gaps filled by Stolb temperatures there is a correlation of $r = 0.93$ between decreasing temperatures and increasing numbers of frost cracking. Likely changing winter temperatures are responsible for the decreasing number of frost cracking.

That would also fit to field observations, which indicate signs of degradation like ponding water in the troughs above ice wedges. Additionally the increasing moisture content in the soil can slacken steel poles and prevent the copper wire from breaking even when thermal-contraction cracking takes place. This could erroneously strengthen the observed decreasing trend in the detected frost cracking with duration of experiment. Nevertheless this trend suggests deteriorating conditions for the tracer experiment.

Except for one cracking event detected in early November, the most events occurred at the end of the cooling phase, close before the minimum temperature got reached (Fig. 12). The early event on the 08. November, 2003 occurred at zero degrees before the temperature dropped. Therefore it is unlikely that a frost-cracking event took place and rather other reasons i.e. animal bite has to be taken into account. The observation of cracking occurring at the end of the cooling phase matches the results from Christiansen (2005) according to which cracking occurs after surface ground temperatures in the polygon center drop below $-15\text{ }^{\circ}\text{C}$. But the main season for thermal-contraction cracking is detected in December. This is earlier than Mackay (1974) (between mid January and March at north Canada) and Christiansen (between February and July at Spitsbergen) observed. Probably the more continental climate at Samoylov is responsible for the differences. In general temperature variations are stronger as more continental the climate is (Clark & Fritz, 1997). Due to the observation of the earliest cracking season at the most continental location (Samoylov Island) and the latest cracking season to the most maritime influenced area (Spitsbergen) it seems that as more continental the climate as earlier frost cracking occurs.

The calculation of temperature conditions preceding frost cracking was done without the outlier (event from 8 Nov 2003) and leads to an average cooling rate of $0.5\text{ }^{\circ}\text{C/day}$ over a period of 13 days at 40 cm depth. This temperature drop is less than the $1.8\text{ }^{\circ}\text{C/day}$ French (1996) observed as best conditions for frost cracking. Due to the fact that French (1996) refers to air temperatures, which in general fluctuate far more than soil temperatures in 40 cm depth the values are not comparable. The average monthly air temperatures at Samoylov Island varies by approximately $50\text{ }^{\circ}\text{C}$ (Kattenstroth, 2009) over one year. The average monthly soil temperatures in 40 cm depth varies by about $25\text{ }^{\circ}\text{C}$, which is just half the amount. But even doubling the average cooling rate to $1\text{ }^{\circ}\text{C}$ it is still less than French (1996) calculated, on the other hand the determined time period of temperature drop is longer in this experiment.

6.5. Appraisal of the Spore experiment

The spores turned out as suitable tracers because they truly penetrated into the ice and could be recognized under the microscope. Only bengal rose seems to discolor which may explain the small recovery rate of those spores. Methyl orange, orange G and Bismarck brown were difficult to recognize due to their similarity with the color of the sediment but still could be identified. For future experiments it would be advantageous to use more striking colors and avoid the use of discoloring substances. Furthermore, the spores of *Lycopodium Clavatum* type 1 turned out as more suitable due to their easy recognizable shape.

Both spore analyzes tests confirm each other (App. 3, 4). Test 2 improves the results of test 1 with a higher total number of recovered spores and additional spore colors that could not be found in test 1. The higher sediment concentration and the removal of great sediment particles in test 2 significantly improve the experiment.

Both tests show a decreasing number of recovered spores from 2003/04 to 2007/08. This fits to the decreasing number of thermal-contraction cracking events detected in the cracking experiment. If there is less cracking, there are less possibilities for spores to penetrate into the ice-wedges. There were not as many cracking events observed in 2002/03 than in 2003/04 but this may be due to the smaller number of cracking experiments and the inconsistent experiment set-up in 2002/03. Even if there was roughly the same amount of cracking events in 2002/03 and 2003/04 this would not explain the predominance of red safranine spores and another explanation has to be found.

Furthermore, 85 samples with differently colored spores were recovered, 36 of them containing more than two different colors. This might be caused by two crossing ice veins which could not be separated in the cold laboratory. But there are only two (App. 2) such samples and even they only could explain two different colored spores in one sample. Contamination during sample preparation has to be taken into account, but as the contamination test shows (App. 5) this could explain only a negligible small number of spores. Although a contamination might take place during ice division but that was not examined. This could only explain few scattered spores and not the great amount of mixed colored spores observed in many samples. More likely is that there are internal processes in the polygon which generate this effect. Possibly there were spores of previous years trapped in the active layer when the new ones were applied to the polygon. Hence, a mixture of spores could penetrate into the ice. In this case the younger spores would be crucial for classification. This theory is supported by the red safranine spores which still could be found in the active layer of sediment

cores drilled in 2010. In this case, it should be expected that the amount of spores from the previous year is the most frequent in a sample. But this is not the case. The red safranine spores are generally the most frequent ones, followed by malachite green, crystal violet and Nile blue. The spores of the other four years are only present in very small numbers. Overall, it seems that the red safranine spores have a higher probability for penetrating into the ice independent from the number of cracking events. Consequently other variables have to be considered. The spores were applied to the polygon by different people. This might make a difference, but would not explain the clearly decreasing trend in the number of spores over the years. Possibly the conditions for penetration into the ice were better in 2002/03 than in all other years. As mentioned above, there were no signs of degradation at the polygon in the first years but in the later years. This degradation could have influenced the tracer experiment, and increased the likelihood to remove spores by wind or water before frost cracking takes place.

Another consideration could be an alteration in precipitation. If in the subsequent years there is more rain in the season after the spores are applied and before it is cold enough for snow the spores can be flushed away before any frost cracking takes place.

6.6. Comparison of the statistical methods

It is necessary to compensate the decreasing amount of spores, therefore the standardization was done as described above (see chapter 5.5.4.) to at least partially prevent an overestimation of the spores of the first years (i.e. red safranine). Due to the uncertainty in the predominating processes, which leads to the different amount of spores and the mixed spores, statistical methods like cluster analyzes were used for the assignment of the samples to the discrete years. The results of the two different cluster analyzes confirm each other. There are no differences in the results of the euclidean and the bray-curtis clustering and the k-means clustering further adds the samples that could not be assigned before. Nevertheless the clusters lead to a simplification. The clustering has some weaknesses of the algorithm, for example samples could not be assigned to two years in case they contain spores of both years. Furthermore, logical connections, like a sample that contains the same amount of spores from two years probably belongs to the second year, are not considered. There are other statistical algorithms which offer the opportunity to assign one sample to different years. For future studies this might be a chance to even improve the results. But for now the results of the k-cluster analyze seems to provide best approximation.

6.7. Evaluation of the ice-wedge isotope thermometer calibration

The variation of average $\delta^{18}\text{O}$ values between 2002/03 and 2009/10 is very low and varies between -22.95 and -22.32 also illustrated in the overlapping ranges of the box plot (Fig. 16). The similarity is particularly striking when comparing the isotope compositions of the different years to the related temperatures (App. 20). Ideally both curves should have the same shape and an isotope variation of 0.7‰ per 1 °C mean annual air temperature variation would be expected (Dansgaard, 1964).

The isotope variations observed in this experiment seems much lower. Likely this low variation is caused by the large time period of ice wedge growth which might smooth the differences between the arithmetical mean and median $\delta^{18}\text{O}$ compositions of the different years. To prove this assumption the time period of ice wedge growth has to be determined. The correlation coefficients between temperature and $\delta^{18}\text{O}$ are highest in December and April/May, likely indicating two main penetration events. The first in December is probably related to thermal-contraction cracking takes place and snow fall into the crack. This theory is supported by the highest number of observed frost cracking events in December, as well as by cloud-like structures found in the ice of the ice cores during preparation, which might have formed rather by solid snow entering a frost crack than by snow melt water. This snow is presumably fresh and not compressed so far. It seems that snow and hoarfrost afterwards seals the crack (Christiansen, 2005) until spring when snow begins to melt and rain and snow melt water from the surface penetrates into the crack. Due to the fact that the AL is still frozen in spring no melt water from the AL can alter this signal. The relatively low correlations between the $\delta^{18}\text{O}$ data and the February and March temperatures might represent the time period when the frost cracks are sealed by hoarfrost and snow.

It seems that the isotope signal assigned to a specific year can represent both T_{winter} as well as T_{spring} . This is further supported by the highest correlation of the maximal $\delta^{18}\text{O}$ values with the April temperatures and the minimal $\delta^{18}\text{O}$ values with the December and January temperatures. Furthermore, it explains the high variation within the $\delta^{18}\text{O}$ values of the samples assigned to one year (Fig. 15). This high variation could smooth the differences between the mean and median isotope data of the different years like described before. Though this effect should be compensated when comparing the isotope variations with the temperatures from the whole growth phase ($T_{\text{cold season}}$). But still the interannual variation of $T_{\text{cold season}}$ (4.51 °C) is more than seven times higher than the variation of the ice-wedge isotope compositions (0.6‰) with 0.13‰ per 1 °C .

Hence, the processes responsible for ice-wedges growth have to be considered. Assuming that the

main dates for penetration are (1) the moment of frost cracking and (2) the opening of the frost crack during the early thawing period the temperatures in this phases might be quite similar. As introduced above (see chapter 5.3) the frost-cracking experiment showed that most cracking events appeared just before the minimal temperature was reached. The thawing period starts when the temperature rises at the surface above 0 °C and large amounts of snow melt water are generated. Hence the temperatures in the time period of ice-wedge growth might be quite similar in the different years and therefore the isotope compositions.

To calibrate a stable-isotope thermometer it has to be considered which temperature and isotope data are appropriate. The Samoylov temperatures are most suitable temperature data for correlation, since they display the temperatures directly from the investigation area and - as mentioned above - for data gaps and the outlier temperatures might be complemented with Stolb data (see chapter 6.2). For the isotope data the median seems to provide more suitable data for the first five years (Fig. 17). Unfortunately, no median can be calculated for the data from 2008/09 (Fig. 15). Hence the average isotope data were used for the calibration.

The only month which shows a strong correlation over all eight years is December ($r_{\text{average}} = 0,51$). But the reason for the high correlation with December temperatures and the low correlation with all other months is based on the first two years (Fig. 17).

The correlation over smaller time periods could indicate if there is a shift in seasonality of the processes involved (i.e. frost cracking, snow fall, crack infill). The correlation shows only coincidences with December between 2002 to 2005 ($R = 0.60$). From 2004 to 2007 also a strong correlation with January ($r = 0.65$) is calculated and moderate correlation coefficients for T_{November} ($r = 0.44$), T_{April} ($r = 0.45$) and T_{May} ($r = 0.24$) were found. The T_{December} correlation still is the strongest ($r = 0.74$). When consider longer temperature time seasons the correlations for T_{winter} ($r = 0.68$) and $T_{\text{cold season}}$ ($r = 0.66$) are both strong. In the last four years, T_{November} shows the highest correlation ($r = 0.96$) followed by T_{May} ($r = 0.88$). Also T_{April} ($r = 0.47$), T_{December} ($r = 0.42$) and T_{January} ($r = 0.41$) show moderate correlations. The correlation with T_{spring} ($r = 0.79$) is now stronger than the one with T_{winter} ($r = 0.65$). The correlation of $T_{\text{cold season}}$ is also strong ($r = 0.74$). This indicates a seasonality shift from a more winter temperature to a more spring temperature influenced isotope signal. Except for February all average months temperatures show at least moderate correlations in different time periods and likely all have an effect on the isotope composition. Consequently, the $T_{\text{cold season}}$ have to be selected for the isotope thermometer, especially when considering longer time intervals (i.e. a decade or more).

Unfortunately, the correlation coefficient between $T_{\text{cold season}}$ and average isotope composition data is not even moderate ($r = -0.15$). As mentioned before this relies on the first two years.

The correlation for 2004-2010 shows much higher correlation coefficients with all temperatures (Tab. VI) and has the strongest correlation with $T_{\text{cold season}}$ ($r = 0.67$). This could indicate a higher influence of December precipitation on the isotope signal in the first two years than in the following six years. When choosing the last six years for the calibration of an isotope thermometer the equation would be as follows:

$$T = 4.40 * \delta^{18}\text{O} + 77.34 \qquad R^2 = 0.45 \qquad [\text{Eq. 9}]$$

Consequently the $\delta^{18}\text{O}$ data variation is 0.1 ‰ per 1°C. But in Eq. 9 the years with the best database were left out. Furthermore, if the assumption is right that there was a shift from a December-influenced isotope signal to a more spring-influenced isotope signal a thermometer calibrated with this data would only represent an isotope temperature correlation for a ice wedges influenced by spring temperatures.

Due to the alteration of the polygon and the changes of associated processes during the experiment the data are not enough to obtain a suitable calculation. For significant results the experimental setup has to be extended.

7. Conclusions

This study aims to improve temperature reconstructions from ice wedges by means of a tracer experiment, carried out at Samoylov Island, Northern Siberia. The experiment compares stable-isotope data from ice-wedge ice to the respective temperatures of the year of ground-ice formation. This way a calibration of a stable isotope thermometer for ice wedges was carried out. Furthermore different environmental factors which might influence the isotope composition of the ice wedge were examined.

The comparison of temperature data from three Russian meteorological stations revealed that in winter there is a temperature shift of about one centigrade at Tiksi compared to Samoylov Island and Stolb, likely caused by a greater maritime influence in Tiksi. All other temperatures differ by less than one degree and all temperature curves have the same shape. Consequently, the temperatures from Stolb can be used to fill the gaps in the Samoylov temperature dataset.

A high-resolution stable isotope experiment shows that there could be a very small fractionation in ice veins during refreezing of snow melt water, but for verification more measurements are needed. If fractionation takes place, this only slightly above the methodological error and therefore should have no significant effect on the isotope composition of long-term climate reconstruction with ice wedges

Frost-cracking experiments reveal that most cracking events occurred at the end of a several-day cooling period, shortly before the winter minimum temperatures are reached. The main season for frost cracking at Samoylov Island is in December, but lasts from mid November to mid February. In 40 cm depth the conditions preceding frost-cracking events show average cooling rates of 0.5 °C/day over a period of about 13 days. A decreasing number of frost cracking events between 2003/04 to 2007/08 indicates deteriorating conditions in the ice-wedge polygon for the tracer experiment, further confirmed by water standing in the apexes above ice wedges at the end of the experiment.

Lycopodium spores turned out to be suitable tracers, which could be easily recognized under the microscope, especially spores of *Lycopodium Clavatum* type 1 due to their easily recognizable shape. Only bengal rose spores lost color and should therefore not be used again.

During the first years of the experiment, the spores had apparently better conditions to penetrate into the frost cracks than the spores of the later years. Reasons for this might be either the degradation of the polygon or changes in precipitation seasonality. Nevertheless statistical methods

made it possible to assign the samples to the discrete year of ground-ice formation. Spores of all colors (thus all years) were found again, which allowed to relate and statistically evaluate the ice-wedge isotope data to the meteorological conditions of the discrete period of formation.

The comparison of *Finnigan MAT Delta-S mass spectrometer* and *Picarro L2120-i* shows that the Picarro provides reliable data even for small sample volumes.

The correlation of temperature and isotope data indicates that there are two main ice-wedge penetration periods: one in December when thermal-contraction cracking takes place and another one in April/May when the snow begins to melt and may trickle into open cracks. This finding is further supported by the highest correlation of maximum $\delta^{18}\text{O}$ data to April temperatures and minimum $\delta^{18}\text{O}$ data to December/January temperatures as well as by cloud-like structures found in the ice wedges during preparation, which might be indicative rather for solid snow entering a frost crack than for snow melt water. The lowest correlation always occurs in February, were the cracks are probably sealed by snow and hoar frost. Due to the different penetration periods the isotope composition of recent ice wedges varies greatly within one year. However, the variability of the average isotope composition in the different considered years is low and show much lower variation (0.13 ‰ per 1 °C) as Dansgaard (1964) predicted for mean annual air temperatures (0.7 ‰ per 1 °C). This is likely due to the processes leading to ice-wedge growth i.e. frost-crack infill occurring after strong cooling in winter and at temperatures slightly $> 0^{\circ}\text{C}$ in spring. This restricts the seasonality of the considered precipitation period in this kind of short-term monitoring program and further might be accompanied by homogenization of the isotope signal in snow.

Considering the variation over longer timescales (2002-2010), the $\delta^{18}\text{O}$ data in the first two years only correlate with the winter months. In the following years there are also accordances with the spring temperatures indicating a shift in seasonality of ground-ice formation. All average monthly temperatures between November and May except February show at least moderate correlations with the isotope composition between 2004 and 2010. Consequently, all temperatures of the cold season (Nov-May) have to be considered to calibrate the isotope thermometer. Due to changing processes in the polygon and due to the observed seasonality shift after the first two years the most reliable equation of $T = 4.40 * \delta^{18}\text{O} + 77.34$ ($R^2 = 0.45$) was obtained for the last six years (2004-10).

In this thesis, a detailed study of the Siberian frost-cracking processes has been carried out to successfully attribute recent ground ice (i.e. ice wedges) to their year of formation. For the first time, statistical evidence indicating that ice-wedge processes have both a spring and winter component, which has to be taken into account for further climate reconstruction.

8. Outlook

With respect to the great number of recovered spores the tracer experiment generally worked fine, but could be improved in further investigations. As tracers, rather spores of *Lycopodium Clavatum* Type 1 should be chosen due to their distinctive shape. Furthermore, more durable colors have to be used to dye spores to prevent decoloration as it was observed for bengal rose spores and additionally striking colors are advisable.

In order to prevent interfering processes like the alteration of the ice-wedge polygon which is potentially responsible for the decreasing recovery rate of the spores over the years, the experiment has to be expanded to several polygons. Furthermore the experiment should be extended over a longer time period to determine whether the stable isotope maximum in 2003/04 is an outlier.

To assign the samples to specific years, an improved statistical algorithm would offer the opportunity to assign one sample to different years, especially when comparable amounts of differently colored spores are detected within one sample. Further logical considerations at samples with spores of several years could be done to assign them to the year which fits best i.e. latest spores being indicative for cracking activity.

Additionally, the high-resolution experiment should be repeated to confirm the results of the first one. The sampling resolution should be increased to more than three samples within one ice vein.

References

- Akhmadeeva, I., Becker, H., Friedrich K., Wagener, D., Pfeiffer, E. M. D., Quass, W., Zhurbenko, M., Zollner E., Boike, J. (1999): Modern Processes in Permafrost Affected soil, in: Expeditions in Siberia 1998, edited by: Rachold, V. and Grigoriev, M. N., Reports on Polar Research, 31, 19-80
- Boike J., Wille C. and Abnizova A. (2008): Climatology and summer energy and water balance of polygonal tundra in the Lena River Delta, Siberia, *Journal of Geophysical Research*, VOL. 113, G03025
- Boike, J., Langer, M., Lantuit, H., Muster, S., Roth, K., Sachs, T., Overduin, P., Westermann, S., McGuire, A. D. (2012): Permafrost-Physical Aspects, Carbon Cycling, Databases and Uncertainties. In *Recarbonization of the Biosphere* (pp. 159-185). Springer Netherlands
- Boike, J., Kattenstroth, B., Abramova, K., Bornemann, N., Chetverova, A., Fedorova, I., Fröb, K., Grigoriev, M., Grüber, M., Kutzbach, L., Langer, M., Minke, M., Muster, S., Piel, K., Pfeiffer, E. M., Stoof, G., Westermann, S., Wischniewski, K., Wille, C. and Hubberten, H. W. (2013): Baseline characteristics of climate, permafrost and land cover from a new permafrost observatory in the Lena River Delta, Siberia (1998-2011). *Biogeosciences*, 10(3), 2105-2128.
- Christiansen, H. H., (2005): Thermal Regime of Ice-wedge Cracking in Adventdalen, Svalbard. *Permafrost and Periglac. Process.* 16: 87-98.
- Clark I.D. And Fritz P. (1997): *Environmental Isotopes in Hydrology*.- Lewis Publishers. Boca Raton: pp. 328
- Craig, H. (1961): Isotopic variations in meteoric waters. *Science* 133: 1702–1703.
- Dansgaard W. (1964): Stable isotopes in precipitation. *Tellus* 16: 436-468
- French, H. M. (1996): *The periglacial environment*.- 2nd Ed. London, Longman: pp.341
- Gilg, O., Sané, R., Solovieva, D. V., Pozdnyakov, V. I., Sabard, B., Tsanos, D., Zöckler, C., Lappo, E. G., Syroechkovski, E.E., Eichhorn, G. (2000). Birds and mammals of the Lena Delta nature reserve, Siberia. *Arctic*, 118-133.
- Gkinis, V., Popp, J. T., Johnsen, S. T., Blunier, T. (2010) A continuous stream flash evaporator for the calibration of an IR cavity ring-down spectrometer for the isotopic analysis of water, *Isot. Environ. Health. S.*, 46, 463-475.
- Greene G. W. (1966): "Contraction theory of ice-wedge polygons: A qualitative discussion." *Permafrost international conference: proceedings* 11-15 November 1963 Lafayette, Indiana. No. 1287. National Academies
- Hoefs, J. (1997): *Stable Isotope Geochemistry*. Springer-Verlag Berlin Heidelberg
- International Permafrost Association (1998): *Multi-Language Glossary of Permafrost and Related Ground-Ice Terms*.- In: R. O. Van Everdingen (ed.), *The Arctic Institution of North America*, Calgary, Canada: 78
- International Atomic Energy Agency (IAEA) (2009): *Laser Spectroscopic Analysis of Liquid Water Samples for Stable Hydrogen and Oxygen Isotopes*. Vienna. Training course series No.35
- Kattenstroth, B. (2009): Master thesis: Long term climate, water balance and energy partitioning characteristics of a tundra site in the Lena River Delta, Siberia
- Jouzel, J., Alley, R. B., Cuffey, K. M., Dansgaard, W., Grootes, P., Hoffmann, G., Johnsen, S. J., Koster, R. D., Peel, D., Shuman, C. A., Stievenard, M., Stuiver, M., White, J. (1997): Validity of the temperature reconstruction from water isotopes in ice cores.- *J. Geophys. Res.* 102 (C12): 26471-26487.
- Polyakov, I. V., Drobot, S., Emery, W., Barry, R. (2003): Long-Term Ice Variability in Arctic Marginal Seas. *Journal of Climate*, Volume 16, S. 2078 – 2084

- Lachenbruch, AH. (1962): Mechanics of thermal construction cracks and ice wedge polygons in permafrost. Geological Society of America. Special Paper 70.
- Lemke, P. et al. (2007): Observations: Changes in snow, ice and frozen ground. In *Climate Change 2007: The Physical Science Basis. Contribution of Working Group I to the Fourth Assessment Report of the Intergovernmental Panel on Climate Change*, Solomon S et al.. Cambridge University Press: Cambridge and New York; 337-383
- Mackay, JR. (1974): Ice-wedges cracks, Garry Island, Northwest Territories. *Canadian Journal of Earth Sciences* 11: 1366-1383
- Mackay, JR. (1983): Oxygen isotope variations in permafrost, Tuktoyaktuk Peninsula area, Northwest Territories. *Current Research, Part B, Geological Survey of Canada Paper 83- 1B: 67-74*
- Mackay, JR. (1992): The frequency of ice-wedge cracking (1967-1987) at Garry Island, western Arctic coast, Canada. *Canadian Journal of Earth Sciences* 29: 236-248
- Mackay, JR. (1993): "Air temperature, snow cover, creep of frozen ground, and the time of ice-wedge cracking, western Arctic coast." *Canadian Journal of Earth Sciences* 30.8 (1993): 1720-1729.
- Merlivat L. & Jouzel J. (1979): Global climatic interpretation of the deuterium-oxygen 18 relationship for precipitation, *J. Geophys. Res.*, 84, 5029-5033,
- Meyer, H., Schönicke, L., Wand, U. (2000): Isotope studies of Hydrogen and oxygen in ground ice – experiences with the equilibration technique, *Isotopes Environ. Health Stud.*, Vol. 36, pp. 133-49
- Meyer H. (2002): The Expedition LENA 2002/03 Ecological Studies on Permafrost Soils and Landscapes; 3.4 Studies on recent cryogenesis (a)
- Meyer, H., Siegert, C., Dereviagin, A., Schirrmeister, L., Hubberten, H. W. (2002): Palaeoclimate Reconstruction on Big Lyakhovsky Island, North Siberia—Hydrogen and Oxygen Isotopes in Ice Wedges; *Permafrost Periglac. Process.* 13: 91–105 (b)
- Meyer, H., Dereviagin, A. Yu., Siegert, C. Hubberten, H. W. (2002): Paleoclimate Studies on Bykovsky Peninsula, North Siberia – Hydrogen and Oxygen Isotopes in Ground Ice, *Polarforschung* 70: 37 (c)
- Meyer, H., Schirrmeister, L., Yoshikawa, K., Opel, T., Wetterich, S., Hubberten, H. W., Brown, J. (2010): Permafrost evidence for severe winter cooling during the Younger Dryas in northern Alaska; *GEOPHYSICAL RESEARCH LETTERS*, VOL. 37, L03501
- Michel, FA. (1982): Isotope investigations of permafrost waters in northern Canada. PhD thesis, Department of Earth Sciences, University of Waterloo, Canada.
- Nikolayev, VI. and Mikhalev, DV. (1995): An oxygen-isotope paleothermometer from ice in Siberian permafrost. *Quaternary Research* 43 (1): 14-21.
- North Greenland Ice Core Project (NorthGRIP) Members. (2004): High-resolution record of northern Hemisphere climate extending into the last interglacial period. *Nature* 431 (7005): 147-151.
- Opel, T., Dereviagin, A. Yu., Meyer, H., Schirrmeister, L., Wetterich, S. (2010): Palaeoclimatic Information from Stable Water Isotopes of Holocene Ice Wedges on the Dmitrii Laptev Strait, Northeast Siberia, Russia., *Permafrost and Periglacial Processes*, Published online in Wiley InterScience
- Osterkamp, TE. (2005): Characteristics of the recent warming of permafrost in Alaska. *Journal of Geophysical Research*, VOL. 112, Published online in Wiley InterScience
- Péwé, T. L. (1966): Ice-wedge in Alaska: Classification, distribution and climatic significance. In *Proceedings, First International Permafrost Conference, National Academy of Sciences-National Research Council, Washington, D.C.*, publication on 1287, pp. 76-81.
- Picarro (2014): www.picarro.com/products_solutions/isotope_analyzers/ih2o_solids_liquids_and_vapor (a)

Picarro (2014): www.picarro.com/technology/cravity_ring_down_spectroscopy (b)

Romanovsky, V. E., Sazonovaa, T. S., Balobaevb, V. T., Shenderb, N. I., Sergueevc, D.O. 2007, Past and recent changes in air and permafrost temperature in eastern Siberia, *Global Planet. Change*, 56, 399-413

Shur, Y., Hinkel K M., and Nelson, F. E. (2005): "The transient layer: implications for geocryology and climate-change science." *Permafrost and Periglacial Processes* 16.1: 5-17.

Sachs, T., Wille, C., Boike, J., Kutzbach, L. (2008): "Environmental controls on ecosystem-scale CH₄ emission from polygonal tundra in the Lena River Delta, Siberia." *Journal of Geophysical Research: Biogeosciences* (2005–2012) 113.G3.

Tukey, J. W. (1977): "Exploratory data analysis."

Urey, H. C. (1947): The thermodynamic properties of isotopic substances: *Chemical Society (London) Journal*, p. 562-581.

Vaikmäe, R. (1989): "Oxygen isotopes in permafrost and ground ice: A new tool for paleoclimatic investigations." 5th Working Meeting Isotopes in Nature, Proceedings, Leipzig.

Vasil'chuk, YuK. (1991): Reconstruction of the palaeoclimate of the late Pleistocene and Holocene on the basis of isotope studies of subsurface ice and waters of the permafrost zone. *Water Resurces* 17(6): 640-674

Vasil'chuk, YuK. (1992): Oxygen Isotope Composition of Ground Ice. Application to Paleogeocryological Reconstructions. Geological Faculty of Moscow State University, Russian Academy of Sciences: Moscow; (in Russian).

Vasil'chuk, YuK. and Vasil'chuk, AC. (1998): Oxygen isotope and C¹⁴ data association with Late Pleistocene syngenetic ice-wedges in mountains of Magadan region, Siberia. *Permafrost and Periglacial Process.* 9: 177-183

Rachold, V. and Grigoriev, M. N. (1999): "Russian-German Cooperation SYSTEM LAPTEV SEA 2000: The Lena Delta 1998 Expedition." *Berichte zur Polarforschung (Reports on Polar Research)* 315.

Zhang, T., Barry, R. G., Knowles, K., Heginbottom, J. A., Brown, J. (1999): "Statistics and characteristics of permafrost and ground-ice distribution in the Northern Hemisphere 1." *Polar Geography* 23.2: 132-154.

Index of Appendices

Appendix	1: Overview boreholes	X
Appendix	2: Received samples	XI
Appendix	3: Results spore analyze test 1	XII
Appendix	4: Results spore analyze test 2	XIV
Appendix	5: Results contamination test	XVI
	Number of spores found in the original sample	
	Number of spores found in the distilled water sample	
	Contamination in %	
Appendix	6: Comparison of Picarro and mass spectrometer	XVII
	Measurement results Picarro and mass spectrometer	
	Comparison of measurement results	
Appendix	7: Overview results frost-cracking experiments	XVII
Appendix	8: Soil temperature data from the investigated polygon in 5 cm and 40 cm depth	XVIII
	Soil temperature data from 2002/03	
	Soil temperature data from 2003/04	
Appendix	9: Temperature conditions in 40 cm soil depth preceding a frost-cracking event	XIX
Appendix	10: Normalized spore numbers over rows and columns	XX
Appendix	11: Results of the PCA with PC1 plotted against PC2	XXII
Appendix	12: Cluster dendrogram of the euclidean clustering	XXIII
Appendix	13: Cluster dendrogram of the bray-curtis clustering	XXIV
Appendix	14: Table of attribution numbers	XXV
Appendix	15: Results k-clustering	XXVI
Appendix	16: Initial values for the correlation of temperature and $\delta^{18}\text{O}$ data	XXVII
Appendix	17: Normalized initial values for the correlation of temperature and $\delta^{18}\text{O}$ data	XXVII
Appendix	18: Correlation matrix of ice-vein and non ice-vein samples	XXVIII
Appendix	19: Correlation matrix with Samoylov temperatures in two year steps	XXVIII
Appendix	20: Visual comparison of $\delta^{18}\text{O}$ and temperature data	XXIX
	Average $\delta^{18}\text{O}$ and season temperature data	
	Average $\delta^{18}\text{O}$ and monthly spring temperature data	
	Average $\delta^{18}\text{O}$ and monthly winter temperature data	
	Median $\delta^{18}\text{O}$ and season temperature data	
	Median $\delta^{18}\text{O}$ and monthly spring temperature data	
	Median $\delta^{18}\text{O}$ and monthly winter temperature data	
Appendix	21: Visual comparison of normalized $\delta^{18}\text{O}$ and temperature data	XXX
	Average $\delta^{18}\text{O}$ and season temperature data	
	Average $\delta^{18}\text{O}$ and monthly spring temperature data	
	Average $\delta^{18}\text{O}$ and monthly winter temperature data	
	Median $\delta^{18}\text{O}$ and season temperature data	
	Median $\delta^{18}\text{O}$ and monthly spring temperature data	

Median $\delta^{18}\text{O}$ and monthly winter temperature data

Appendix

22: Linear regression equation of $\delta^{18}\text{O}$ and temperature data

XXXI

.....From 2002 to 2010

From 2004 to 2010

App. 1: Overview boreholes

Borehole	Part	AL	Ice	Spores	note	Number of 5 cm slices	Parts selected for further preparation
BH1	1	0-40 cm	40-46 cm	-	-	1	-
BH2	1	0-40 cm	40-56 cm	-	-	3	46-51 cm
BH3	1	0-38/40 cm	40-85 cm	maybe orange	muddy, moist bit in the ice ok, clear ice veins	9	48-49 cm 49-50 cm 50-51 cm 51-54 cm 69-71 cm
BH4	1	0-38 cm	38-48 cm	red in AL	very moist,	2	-
	2		48-58 cm	-	-	2	48-53 cm
BH5	1	0-40/42 cm	-	-	nice core	-	-
	2	-	40-84 cm	-	-	9	50-55 cm 70-75 cm 80-84 cm
	3	-	84-94 cm	-	-	2	90-94 cm
BH6	1	-	-	-	only mud no ice	-	-
BH7	1	-	-	-	only mud no ice	-	-
BH8	1	0-35 cm	35-40 cm	red	Moist, ice fragments	1	35-40 cm
	2	-	45-90 cm	red	In three parts	9	55-60 cm 60-65 cm 80-85 cm 87-90 cm
	3	-	90-100 cm	green	-	2	90-100 cm
BH9	1	-	-	-	Smal ice fragments	-	-
BH10	1	0-37 cm	-	-	-	-	-
	2	-	37-73 cm	maybe brown	-	7	37-42 cm
BH11	1	0-40 cm	40-94 cm	-	-	11	55-58 cm 84-94 cm
BH12	1	0-37 cm	37-101 cm	-	-	17	37-45 cm 96-101 cm
BH13	1	0-34 cm	34-85 cm	-	-	10	66-71 cm 76-81 cm
	2A	-	85-100 cm	-	-	3	-
	2B	-	-	-	-	-	-
	2C	-	-	-	-	-	-

App. 2: Received samples

	Received samples		
1	LD10-BH2-1	46-51 cm	A1
2	LD10-BH2-1	46-51 cm	A2+
3	LD10-BH2-1	46-51 cm	A3+
4	LD10-BH2-1	46-51 cm	A4
5	LD10-BH3-1	48-49 cm	A1+
6	LD10-BH3-1	48-49 cm	A2+
7	LD10-BH3-1	48-49 cm	A3
8	LD10-BH3-1	49-50 cm	A1+
9	LD10-BH3-1	49-50 cm	A2
10	LD10-BH3-1	49-50 cm	A3
11	LD10-BH3-1	50-51 cm	A1
12	LD10-BH3-1	50-51 cm	A2+
13	LD10-BH3-1	50-51 cm	A3+
14	LD10-BH3-1	50-51 cm	A4+
15	LD10-BH3-1	50-51 cm	A5
16	LD10-BH3-1	51-54 cm	A1
17	LD10-BH3-1	51-54 cm	A2(+)
18	LD10-BH3-1	51-54 cm	A3+
19	LD10-BH3-1	51-54 cm	A4+
20	LD10-BH3-1	51-54 cm	A5
21	LD10-BH3-1	69-71 cm	A1+
22	LD10-BH3-1	69-71 cm	A2
23	LD10-BH3-1	69-71 cm	A3+
24	LD10-BH3-1	69-71 cm	A4
25	LD10-BH4-2	48-53 cm	A1+
26	LD10-BH4-2	48-53 cm	A2
27	LD10-BH4-2	48-53 cm	A3+
28	LD10-BH4-2	48-53 cm	A4
29	LD10-BH4-2	48-53 cm	A5
30	LD10-BH5-2-2	50-55 cm	A1
31	LD10-BH5-2-2	50-55 cm	A2+
32	LD10-BH5-2-2	50-55 cm	A3+
33	LD10-BH5-2-2	50-55 cm	A4
34	LD10-BH5-2-3	70-75 cm	A1+
35	LD10-BH5-2-3	70-75 cm	A2++
36	LD10-BH5-2-3	70-75 cm	A3+
37	LD10-BH5-2-3	70-75 cm	A4
38	LD10-BH5-2-3	80-84 cm	A1
39	LD10-BH5-2-3	80-84 cm	A2+
40	LD10-BH5-2-3	80-84 cm	A3+
41	LD10-BH5-2-3	80-84 cm	A4+
42	LD10-BH5-2-3	80-84 cm	A5+
43	LD10-BH5-2-3	80-84 cm	A6+
44	LD10-BH5-3	88-94 cm	A1
45	LD10-BH5-3	88-94 cm	A2+
46	LD10-BH5-3	88-94 cm	A3
47	LD10-BH8-2-1/2	55-57 cm	A1+
48	LD10-BH8-2-1/2	55-57 cm	A2
49	LD10-BH8-2-1/2	55-57 cm	A3
50	LD10-BH8-2-1/2	55-57 cm	A4+
51	LD10-BH8-2-1/2	55-57 cm	A5+
52	LD10-BH8-2-1/2	55-57 cm	A6+
53	LD10-BH8-2-1/2	57-60 cm	A1+
54	LD10-BH8-2-1/2	57-60 cm	A5+
55	LD10-BH8-2-2	60-65 cm	A1+
56	LD10-BH8-2-2	60-65 cm	A2
57	LD10-BH8-2-2	60-65 cm	A3+
58	LD10-BH8-2-2	60-65 cm	A4+
59	LD10-BH8-2-2	60-65 cm	A5+
60	LD10-BH8-2-2	60-65 cm	A6
61	LD10-BH8-2-4	80-85 cm	A1
62	LD10-BH8-2-4	80-85 cm	A2

	Received samples		
63	LD10-BH8-2-4	80-85 cm	A3+
64	LD10-BH8-2-4	80-85 cm	A4+
65	LD10-BH8-2-4	80-85 cm	A5
66	LD10-BH8-2-6	87-90 cm	A1+
67	LD10-BH8-2-6	87-90 cm	A2
68	LD10-BH8-2-6	87-90 cm	A3+
69	LD10-BH8-2-6	87-90 cm	A4+
70	LD10-BH8-2-6	87-90 cm	A5+
71	LD10-BH8-3	90-95 cm	A1+
72	LD10-BH8-3	90-95 cm	A2+
73	LD10-BH8-3	90-95 cm	A3+
74	LD10-BH8-3	95-100 cm	A1+
75	LD10-BH8-3	95-100 cm	A2+
76	LD10-BH8-3	95-100 cm	A3+
77	LD10-BH10-2	37-42 cm	A1+
78	LD10-BH10-2	37-42 cm	A2+
79	LD10-BH10-2	37-42 cm	A3+
80	LD10-BH10-2	37-42 cm	A4
81	LD10-BH11-1-2	55-57 cm	A1
82	LD10-BH11-1-2	55-57 cm	A2++
83	LD10-BH11-1-2	55-57 cm	A3
84	LD10-BH11-1-2	57-59 cm	A1+
85	LD10-BH11-1-4	84-89 cm	A1
86	LD10-BH11-1-4	84-89 cm	A2+
87	LD10-BH11-1-4	84-89 cm	A3+
88	LD10-BH11-1-4	84-89 cm	A4
89	LD10-BH11-1-4	90-94 cm	A1+
90	LD10-BH12-1-1	37-45 cm	A1
91	LD10-BH12-1-1	37-45 cm	A2+
92	LD10-BH12-1-1	37-45 cm	A3+
93	LD10-BH12-1-5	96-98 cm	A2+
94	LD10-BH12-1-5	96-98 cm	A3
95	LD10-BH12-1-5	96-98 cm	A4+
96	LD10-BH12-1-5	96-98 cm	A5+
97	LD10-BH12-1-5	98-101 cm	A2+
98	LD10-BH12-1-5	98-101 cm	A3+
99	LD10-BH12-1-5	98-101 cm	A4(+)
100	LD10-BH13-1-2	66-69 cm	A1+
101	LD10-BH13-1-2	66-69 cm	A2
102	LD10-BH13-1-2	66-69 cm	A3
103	LD10-BH13-1-2	69-71 cm	A1+
104	LD10-BH13-1-2	76-81 cm	A1
105	LD10-BH13-1-2	76-81 cm	A2+
106	LD10-BH13-1-2	76-81 cm	A3(+)
107	LD10-BH13-1-2	76-81 cm	A4+
108	LD10-BH13-1-2	76-81 cm	A5

App. 3: Results spore analysis test 1

Sample	Red safranine 2002	Mmalachit green 2003	Crystal violet 2004	Methyl orange 2005	Nile blue 2006	Bengal rose 2007	Orange G 2008	Bismarck brown 2009
LD10-BH2-1 46-51 cm A1	-	-	-	-	-	-	-	-
LD10-BH2-1 46-51 cm A2+	1	1	1	-	-	-	-	-
LD10-BH2-1 46-51 cm A3+	-	-	1	-	1	-	-	-
LD10-BH2-1 46-51 cm A4	1	1	-	-	1	-	-	-
LD10-BH3-1 48-49 cm A1+	1	-	-	-	1	-	-	-
LD10-BH3-1 48-49 cm A2+	-	-	-	-	-	-	-	-
LD10-BH3-1 48-49 cm A3	-	-	-	-	-	-	-	-
LD10-BH3-1 49-50 cm A1+	1	2	-	-	-	-	-	-
LD10-BH3-1 49-50 cm A2	1	-	-	-	-	-	-	-
LD10-BH3-1 49-50 cm A3	-	-	-	-	-	-	-	-
LD10-BH3-1 50-51 cm A1	1	-	-	-	-	-	-	-
LD10-BH3-1 50-51 cm A2+	-	-	-	-	-	-	-	-
LD10-BH3-1 50-51 cm A3+	-	-	-	-	-	-	-	-
LD10-BH3-1 50-51 cm A4+	-	-	-	-	-	-	-	-
LD10-BH3-1 50-51 cm A5	-	-	-	-	-	-	-	-
LD10-BH3-1 51-54 cm A1	-	1	-	-	-	-	-	-
LD10-BH3-1 51-54 cm A2(+)	-	-	-	-	-	-	-	-
LD10-BH3-1 51-54 cm A3+	2	-	-	-	-	-	-	-
LD10-BH3-1 51-54 cm A4+	-	-	-	-	-	-	-	-
LD10-BH3-1 51-54 cm A5	-	-	-	-	-	-	-	-
LD10-BH3-1 69-71 cm A1+	-	-	-	-	-	-	-	-
LD10-BH3-1 69-71 cm A2	-	-	-	-	-	-	-	-
LD10-BH3-1 69-71 cm A3+	-	-	-	-	-	-	-	-
LD10-BH3-1 69-71 cm A4	-	-	-	-	-	-	-	-
LD10-BH4-2 48-53 cm A1+	4	-	-	-	-	-	-	-
LD10-BH4-2 48-53 cm A2	2	-	-	-	-	-	-	-
LD10-BH4-2 48-53 cm A3+	-	-	-	-	-	-	-	-
LD10-BH4-2 48-53 cm A4	-	-	-	-	-	-	-	-
LD10-BH4-2 48-53 cm A5	-	-	-	-	-	-	-	-
LD10-BH5-2-2 50-55 cm A1	1	-	1	-	-	-	-	-
LD10-BH5-2-2 50-55 cm A2+	1	-	-	-	-	-	-	-
LD10-BH5-2-2 50-55 cm A3+	1	-	-	1?	-	-	-	-
LD10-BH5-2-2 50-55 cm A4	3	-	-	-	? 1	-	-	-
LD10-BH5-2-3 70-75 cm A1+	-	-	-	-	-	-	-	-
LD10-BH5-2-3 70-75 cm A2++	-	-	-	-	-	-	-	-
LD10-BH5-2-3 70-75 cm A3+	1	-	-	-	-	-	-	-
LD10-BH5-2-3 70-75 cm A4	24	-	-	-	-	-	-	-
LD10-BH5-2-3 80-84 A1	9	-	-	-	-	-	-	-
LD10-BH5-2-3 80-84 A2+	-	-	-	-	-	-	-	-
LD10-BH5-2-3 80-84 A3+	1	-	-	-	-	-	-	-
LD10-BH5-2-3 80-84 A4+	-	-	-	-	-	-	-	-
LD10-BH5-2-3 80-84 A5+	5	-	-	-	-	-	-	-
LD10-BH5-2-3 80-84 A6+	15	1	-	-	-	-	-	-
LD10-BH5-3 88-94 cm A1	-	-	-	-	-	-	-	-
LD10-BH5-3 88-94 cm A2+	-	-	-	-	-	-	-	-
LD10-BH5-3 88-94 cm A3	-	-	-	-	1	-	-	-
LD10-BH8-1 35-40 cm A1/2+	> 30	-	-	-	-	-	-	-
LD10-BH8-2-1/2 55-57 cm A1+	> 30	1	4	-	-	-	-	-
LD10-BH8-2-1/2 55-57 cm A2	> 15	> 15	3	-	2	-	-	-
LD10-BH8-2-1/2 55-57 cm A3	2	1	-	-	-	-	-	-
LD10-BH8-2-1/2 55-57 cm A4+	5	-	-	-	-	-	-	-
LD10-BH8-2-1/2 55-57 cm A5+	2	1	-	-	-	-	-	-
LD10-BH8-2-1/2 55-57 cm A6+	3	2	2	-	-	-	-	-
LD10-BH8-2-1/2 57-60 cm A1+	> 30	1	4	-	-	-	-	-
LD10-BH8-2-1/2 57-60 cm A5+	1	1	-	-	-	-	-	-
LD10-BH8-2-2 60-65 cm A1+	> 30	3	13	-	-	-	-	-
LD10-BH8-2-2 60-65 cm A2	-	-	-	-	-	-	-	-
LD10-BH8-2-2 60-65 cm A3+	7	-	1	-	1	-	-	-
LD10-BH8-2-2 60-65 cm A4+	2	2	-	-	-	-	-	-
LD10-BH8-2-2 60-65 cm A5+	2	1	1	-	-	-	-	-
LD10-BH8-2-2 60-65 cm A6	-	-	-	-	-	-	-	-
LD10-BH8-2-4 80-85 cm A1	> 15	3	2	-	1	-	-	-
LD10-BH8-2-4 80-85 cm A2	-	-	-	-	-	-	-	-
LD10-BH8-2-4 80-85 cm A3+	> 15	1	1	-	-	2	-	-
LD10-BH8-2-4 80-85 cm A4+	1	2	-	-	-	-	-	-
LD10-BH8-2-4 80-85 cm A5	-	-	-	-	-	-	-	-
LD10-BH8-2-6 87-90 cm A1+	-	-	-	-	-	-	-	-
LD10-BH8-2-6 87-90 cm A2	-	-	-	-	-	-	-	-
LD10-BH8-2-6 87-90 cm A3+	1	-	-	-	-	-	-	-
LD10-BH8-2-6 87-90 cm A4+	-	-	-	-	1.?	-	-	-
LD10-BH8-2-6 87-90 cm A5+	-	-	-	-	-	-	-	-
LD10-BH8-3 90-95 cm A1+	> 15	4	1	-	-	-	-	-
LD10-BH8-3 90-95 cm A2+	-	-	-	-	-	-	-	-
LD10-BH8-3 90-95 cm A3+	-	2	-	-	-	-	-	-
LD10-BH8-3 95-100 cm A1+	> 15	-	-	-	-	-	-	-
LD10-BH8-3 95-100 cm A2+	-	-	-	-	-	-	-	-
LD10-BH8-3 95-100 cm A3+	-	-	-	-	-	-	-	-
LD10-BH10-2 37-42 cm A1+	-	-	-	-	-	-	-	-

Sample	Red safranin 2002	Mmalachit green 2003	Crystal violet 2004	Methyl orange 2005	Nile blue 2006	Bengal rose 2007	Orange G 2008	Bismarck brown 2009
LD10-BH10-2 37-42 cm A2+	-	1	-	-	-	-	-	-
LD10-BH10-2 37-42 cm A3+	5	-	-	-	-	-	-	-
LD10-BH10-2 37-42 cm A4	-	-	-	-	-	-	-	-
LD10-BH11-1-2 55-57 cm A1	-	-	-	-	-	-	-	-
LD10-BH11-1-2 55-57 cm A2++	-	-	-	-	-	-	-	-
LD10-BH11-1-2 55-57 cm A3	-	-	-	-	-	-	-	-
LD10-BH11-1-2 57-59 cm A1+	-	-	-	-	-	-	-	-
LD10-BH11-1-4 84-89 cm A1	-	-	-	-	-	-	-	-
LD10-BH11-1-4 84-89 cm A2+	-	-	-	-	-	-	-	-
LD10-BH11-1-4 84-89 cm A3+	-	-	-	-	-	-	-	-
LD10-BH11-1-4 84-89 cm A4	-	-	-	-	-	-	-	-
LD10-BH11-1-4 90-94 cm A1+	-	-	-	-	-	-	-	-
LD10-BH12-1-1 37-45 cm A1	7	-	-	-	-	-	-	-
LD10-BH12-1-1 37-45 cm A2+	-	1	-	-	-	-	-	-
LD10-BH12-1-1 37-45 cm A3+	7	1	2	-	-	-	-	-
LD10-BH12-1-5 96-98 cm A2+	1	-	-	-	-	-	-	-
LD10-BH12-1-5 96-98 cm A3	1	-	-	-	-	-	-	-
LD10-BH12-1-5 96-98 cm A4+	-	-	-	-	-	-	-	-
LD10-BH12-1-5 96-98 cm A5+	-	-	-	-	-	-	-	-
LD10-BH12-1-5 98-101 cm A2+	-	-	-	-	-	-	-	-
LD10-BH12-1-5 98-101 cm A3+	-	-	-	-	-	-	-	-
LD10-BH12-1-5 98-101 cm A4(+)	-	-	-	-	-	-	-	-
LD10-BH13-1-2 66-69 cm A1+	-	-	-	-	-	-	-	-
LD10-BH13-1-2 66-69 cm A2	-	-	-	-	-	-	-	-
LD10-BH13-1-2 66-69 cm A3	-	-	-	-	-	-	-	-
LD10-BH13-1-2 69-71 cm A1+	-	-	-	-	-	-	-	-
LD10-BH13-1-2 76-81 cm A1	-	-	-	-	-	-	-	-
LD10-BH13-1-2 76-81 cm A2+	-	-	-	-	-	-	-	-
LD10-BH13-1-2 76-81 cm A3(+)	-	-	-	-	-	-	-	-
LD10-BH13-1-2 76-81 cm A4+	-	-	-	-	-	-	-	-
LD10-BH13-1-2 76-81 cm A5	2	9	4	-	-	-	-	-

App. 4: Results spore analysis test 2

(grey = clear results in test one)

Sample	Red safranin	Mmalachit green	Crystal violet	Methyl orange	Nile blue	Bengal rose	Orange G	Bismarck brown	colorless
LD10-BH2-1 46-51 cm A1	-	-	1	-	2	-	-	-	-
LD10-BH2-1 46-51 cm A2+	3	2	1	-	-	-	-	-	-
LD10-BH2-1 46-51 cm A3+	3	-	2	-	-	-	-	-	-
LD10-BH2-1 46-51 cm A4	3	9	4	1	-	-	-	-	-
LD10-BH3-1 48-49 cm A1+	-	-	-	-	-	-	-	-	-
LD10-BH3-1 48-49 cm A2+	-	-	-	-	1	-	-	-	-
LD10-BH3-1 48-49 cm A3	-	-	-	-	-	-	-	-	-
LD10-BH3-1 49-50 cm A1+	2	-	-	-	-	-	-	-	-
LD10-BH3-1 49-50 cm A2	2	1	-	-	-	-	-	-	1
LD10-BH3-1 49-50 cm A3	1	-	-	-	-	-	-	-	-
LD10-BH3-1 50-51 cm A1	2	-	-	-	-	-	-	-	-
LD10-BH3-1 50-51 cm A2+	-	-	-	-	-	-	-	-	-
LD10-BH3-1 50-51 cm A3+	-	-	-	2	-	-	-	-	2
LD10-BH3-1 50-51 cm A4+	-	-	-	-	-	-	-	-	-
LD10-BH3-1 50-51 cm A5	1	-	-	2	-	-	-	-	3
LD10-BH3-1 51-54 cm A1	-	1	-	-	-	-	-	-	-
LD10-BH3-1 51-54 cm A2(+)	-	-	-	-	-	-	-	-	1
LD10-BH3-1 51-54 cm A3+	8	-	-	-	-	-	-	-	-
LD10-BH3-1 51-54 cm A4+	-	-	-	-	-	-	-	-	-
LD10-BH3-1 51-54 cm A5	1	-	-	-	-	-	-	1	-
LD10-BH3-1 69-71 cm A1+	-	-	-	1	-	-	-	-	-
LD10-BH3-1 69-71 cm A2	-	-	-	-	-	-	-	-	-
LD10-BH3-1 69-71 cm A3+	-	-	-	-	-	-	-	-	-
LD10-BH3-1 69-71 cm A4	-	-	-	-	-	-	-	-	-
LD10-BH4-2 48-53 cm A1+	-	-	-	-	-	-	-	-	-
LD10-BH4-2 48-53 cm A2	10	-	-	-	-	-	-	-	-
LD10-BH4-2 48-53 cm A3+	12	-	1	-	-	-	-	-	1
LD10-BH4-2 48-53 cm A4	5	-	-	-	-	-	-	-	-
LD10-BH4-2 48-53 cm A5	6	-	-	2	-	-	-	-	-
LD10-BH5-2-2 50-55 cm A1	3	-	-	-	1	-	-	-	-
LD10-BH5-2-2 50-55 cm A2+	1	-	-	-	3	-	-	-	3
LD10-BH5-2-2 50-55 cm A3+	-	-	-	-	-	-	-	-	-
LD10-BH5-2-2 50-55 cm A4	4	-	-	-	3	-	-	2	6
LD10-BH5-2-3 70-75 cm A1+	-	-	-	-	-	-	-	-	-
LD10-BH5-2-3 70-75 cm A2++	1	-	-	-	-	-	-	-	-
LD10-BH5-2-3 70-75 cm A3+	1	-	-	-	1	-	-	1	1
LD10-BH5-2-3 70-75 cm A4	-	-	-	-	-	-	-	-	-
LD10-BH5-2-3 80-84 A1	-	-	-	-	-	-	-	-	-
LD10-BH5-2-3 80-84 A2+	-	-	-	-	-	-	-	-	-
LD10-BH5-2-3 80-84 A3+	-	-	-	1	-	-	-	-	-
LD10-BH5-2-3 80-84 A4+	-	-	-	1	-	-	-	-	-
LD10-BH5-2-3 80-84 A5+	-	-	-	-	-	-	-	-	-
LD10-BH5-2-3 80-84 A6+	4	-	-	-	-	-	-	-	-
LD10-BH5-3 88-94 cm A1	52	-	-	-	-	-	-	-	-
LD10-BH5-3 88-94 cm A2+	4	-	-	-	-	-	-	-	-
LD10-BH5-3 88-94 cm A3	-	-	-	-	-	-	-	-	-
LD10-BH8-1 35-40 cm A1/2+	-	-	-	-	-	-	-	-	-
LD10-BH8-2-1/2 55-57 cm A1+	-	-	-	-	-	-	-	-	-
LD10-BH8-2-1/2 55-57 cm A2	297	180	59	-	18	-	-	-	10
LD10-BH8-2-1/2 55-57 cm A3	15	3	6	-	-	-	-	2	3
LD10-BH8-2-1/2 55-57 cm A4+	3	-	-	-	1	-	-	-	-
LD10-BH8-2-1/2 55-57 cm A5+	12	1	-	-	-	-	-	-	-
LD10-BH8-2-1/2 55-57 cm A6+	23	10	6	-	-	-	-	-	3
LD10-BH8-2-1/2 57-60 cm A1+	-	-	-	-	-	-	-	-	-
LD10-BH8-2-1/2 57-60 cm A5+	27	18	5	1	1	-	-	-	3
LD10-BH8-2-2 60-65 cm A1+	-	-	-	-	-	-	-	-	-
LD10-BH8-2-2 60-65 cm A2	61	30	20	-	4	-	3	-	9
LD10-BH8-2-2 60-65 cm A3+	32	15	14	1	-	-	-	1	7
LD10-BH8-2-2 60-65 cm A4+	3	1	-	-	-	-	-	-	2
LD10-BH8-2-2 60-65 cm A5+	-	-	-	-	-	-	-	-	-
LD10-BH8-2-2 60-65 cm A6	42	6	9	-	1	-	-	-	3
LD10-BH8-2-4 80-85 cm A1	-	-	-	-	-	-	-	-	-
LD10-BH8-2-4 80-85 cm A2	25	15	2	-	-	-	-	-	1
LD10-BH8-2-4 80-85 cm A3+	-	-	-	-	-	-	-	-	-
LD10-BH8-2-4 80-85 cm A4+	17	17	5	-	-	-	-	-	1
LD10-BH8-2-4 80-85 cm A5	4	7	4	-	-	-	-	-	1
LD10-BH8-2-6 87-90 cm A1+	1	-	2	-	-	-	-	-	-
LD10-BH8-2-6 87-90 cm A2	-	-	-	-	-	-	-	-	-
LD10-BH8-2-6 87-90 cm A3+	-	-	-	-	-	-	-	-	-
LD10-BH8-2-6 87-90 cm A4+	3	2	-	-	-	-	-	-	-
LD10-BH8-2-6 87-90 cm A5+	1	-	2	-	-	-	-	-	-
LD10-BH8-3 90-95 cm A1+	3	-	-	-	-	-	-	2	-
LD10-BH8-3 90-95 cm A2+	-	-	-	-	-	-	-	-	-
LD10-BH8-3 90-95 cm A3+	1	2	1	-	-	-	-	-	-
LD10-BH8-3 95-100 cm A1+	2	-	1	-	-	-	-	-	-
LD10-BH8-3 95-100 cm A2+	5	1	-	-	-	-	-	-	1
LD10-BH8-3 95-100 cm A3+	2	-	-	-	-	-	-	-	-
LD10-BH10-2 37-42 cm A1+	3	-	-	-	-	-	-	-	-

Sample	Red safranin 2002	Mmalachit green 2003	Crystal violet 2004	Methyl orange 2005	Nile blue 2006	Bengal rose 2007	Orange G 2008	Bismarck brown 2009	colorless
LD10-BH10-2 37-42 cm A2+	10	-	-	-	-	-	-	-	-
LD10-BH10-2 37-42 cm A3+									
LD10-BH10-2 37-42 cm A4	12	3	-	-	-	-	-	-	-
LD10-BH11-1-2 55-57 cm A1	-	-	-	-	-	-	-	-	-
LD10-BH11-1-2 55-57 cm A2++	-	-	-	-	-	-	-	-	-
LD10-BH11-1-2 55-57 cm A3	-	-	-	-	-	-	-	-	-
LD10-BH11-1-2 57-59 cm A1+	-	-	-	1	-	-	-	-	-
LD10-BH11-1-4 84-94 cm A1	-	-	-	-	-	-	-	-	-
LD10-BH11-1-4 84-94 cm A2+	-	-	-	-	-	-	-	-	-
LD10-BH11-1-4 84-94 cm A3+	-	-	-	-	-	-	-	-	1
LD10-BH11-1-4 84-94 cm A4	-	-	-	-	-	-	-	1	-
LD10-BH12-1-1 37-45 cm A1									
LD10-BH12-1-1 37-45 cm A2+	32	8	2	-	-	-	-	-	-
LD10-BH12-1-1 37-45 cm A3+	68	6	22	-	-	-	-	-	-
LD10-BH12-1-5 96-98 cm A2+	1	-	-	2	-	-	-	-	-
LD10-BH12-1-5 96-98 cm A3	2	-	-	-	-	-	-	-	-
LD10-BH12-1-5 96-98 cm A4+	3	-	-	-	-	-	-	-	-
LD10-BH12-1-5 96-98 cm A5+	8	2	16	-	-	-	-	-	-
LD10-BH12-1-5 98-101 cm A2+	1	-	-	-	-	-	-	-	-
LD10-BH12-1-5 98-101 cm A3+	3	1	-	1	-	-	1	-	-
LD10-BH12-1-5 98-101 cm A4(+)	-	2	-	-	-	-	-	-	-
LD10-BH13-1-2 66-69 cm A1+	-	-	-	-	-	-	-	-	-
LD10-BH13-1-2 66-69 cm A2	1	1	-	-	-	-	-	-	1
LD10-BH13-1-2 66-69 cm A3	1	1	-	-	-	-	-	-	-
LD10-BH13-1-2 69-71 cm A1+	1	-	-	-	-	-	-	-	-
LD10-BH13-1-2 76-81 cm A1	4	1	-	-	-	-	-	3	-
LD10-BH13-1-2 76-81 cm A2+	-	-	-	-	-	-	-	-	-
LD10-BH13-1-2 76-81 cm A3(+)	6	-	-	-	2	-	-	-	-
LD10-BH13-1-2 76-81 cm A4+	-	-	-	1	-	-	-	-	-
LD10-BH13-1-2 76-81 cm A5	17	20	11	4	5	-	4	8	-

App. 5: Results contamination test

Number of spores found in the original sample

	Red safranine	Malachite green	Crystal violet	Methyl orange	Nile blue	Bengalrosa	Orange G	Bismarck brown	colorless	Sum
Test 1	279	152	44	2	24	1	9	9	26	546
Test 2	405	190	76	4	26	7	16	11	34	769
Test 3	297	180	59	1	18	1	2	2	10	570

Number of spores found in the distilled water sample

	Red safranine	Malachite green	Crystal violet	Methyl orange	Nile blue	Bengalrosa	Orange G	Bismarck brown	colorless	Sum
Test 1	1	-	-	-	-	-	-	-	-	-
Test 2	-	-	-	-	-	-	-	-	-	-
Test 3	-	1	-	-	-	-	-	-	-	-

Contamination in %

	Test 1	Test 2	Test 3	Total number
Sample	546	769	570	1885
DW	1	-	1	2
Contamination in %	0,18	-	0,17	0,10
Highest contamination	~ 0,2 %			

App. 6: Comparison of Picarro and mass spectrometer

Measurement results Picarro and mass spectrometer

Sample	Picarro					Mass spectrometer				
	$\delta^{18}\text{O}$ [‰]	1 σ	δD [‰]	1 σ	d excess	$\delta^{18}\text{O}$ [‰]	1 σ	δD [‰]	1 σ	d excess
LD10-BH3-1 (49-50) A3	-21,94	0,02	-166,7	0,1	8,8	-21,88	0,0	-165,9	0,2	9,1
LD10-BH3-1 (50-51) A3+	-21,18	0,01	-159,1	0,1	10,4	-21,15	0,0	-159,2	0,7	10
LD10-BH3-1 (69-71) A3+	-23,03	0,01	-174,4	0,0	9,8	-22,98	0,0	-174,1	0,3	9,7
LD10-BH3-1 (69-71) A3+	-23,33	0,05	-177,6	0,2	9	-23,26	0,0	-177,1	0,5	8,9
LD10-BH4-2 (48-53) A1+	-22,68	0,03	-168,6	0,1	12,9	-22,49	0,02	-168,2	0,2	11,7
LD10-BH4-2 (48-53) A2	-24,16	0,07	-182,9	0,1	10,4	-24,06	0,02	-182,1	0,1	10,4
LD10-BH4-2 (48-53) A3+	-24,75	0,02	-187,5	0,1	10,6	-24,56	0,03	-186,9	0,2	9,6
LD10-BH4-2 (48-53) A4	-23,56	0,06	-178,4	0,1	10,1	-23,4	0,02	-177,5	0,3	9,7
LD10-BH10-2 (37-42) A1+	-21,77	0,11	-164,4	0,1	9,8	-21,8	0,06	-163,8	0,4	10,6
LD10-BH10-2 (37-42) A2+	-23,44	0,02	-176,4	0,2	11,0	-23,41	0,07	-175,2	0,3	12,1
LD10-BH10-2 (37-42) A3+	-23,13	0,03	-174,2	0,2	10,8	-22,93	0,09	-172,5	0,3	10,9
Minimum	-24,75	0,01	-187,5	0	8,8	-24,56	0	-186,9	0,1	8,9
Maximum	-21,18	0,11	-159,1	0,2	12,9	-21,15	0,09	-159,2	0,7	12,1
Average	-23,00	0,04	-173,65	0,12	10,33	-22,90	0,03	-172,95	0,32	10,25
Median	-23,13	0,03	-174,4	0,1	10,4	-22,98	0,02	-174,1	0,3	10

Comparison of measurement results

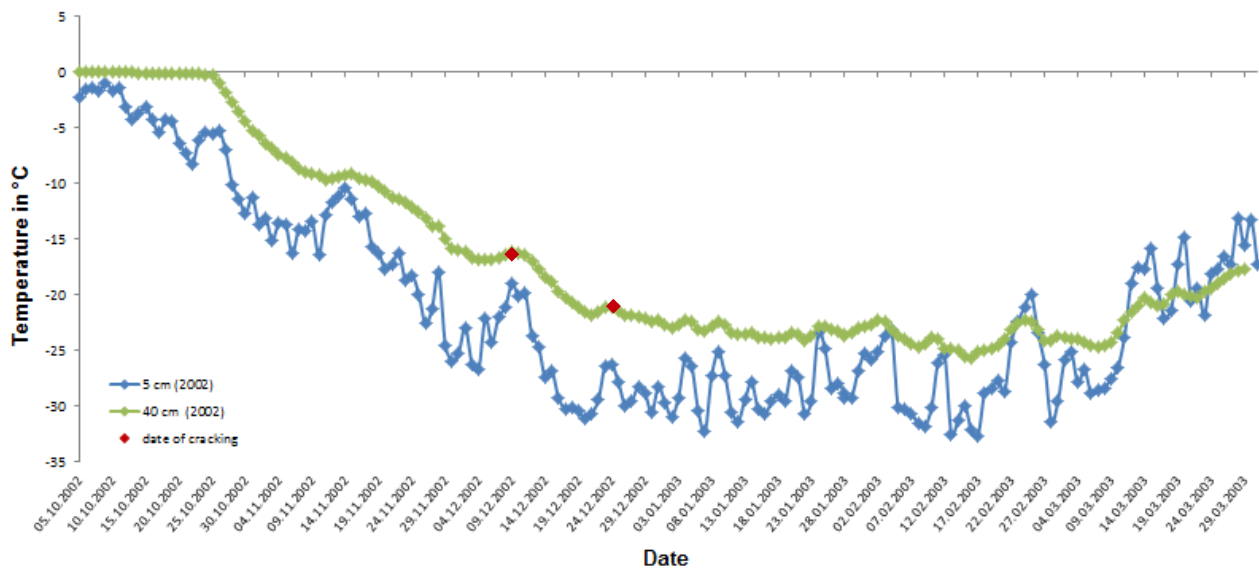
	Picarro		Mass spectrometer		Difference	
	$\delta^{18}\text{O}$ [‰]	δD [‰]	$\delta^{18}\text{O}$ [‰]	δD [‰]	Difference $\delta^{18}\text{O}$ [‰]	Difference δD [‰]
LD10-BH3-1 (49-50) A3	-21,88	-165,9	-21,88	-165,9	0	0
LD10-BH3-1 (50-51) A3+	-21,69	-164,6	-21,15	-159,2	-0,54	-5,4
LD10-BH3-1 (69-71) A3+	-23,03	-174,4	-22,98	-174,1	-0,05	-0,3
LD10-BH3-1 (69-71) A3+	-23,33	-177,6	-23,26	-177,1	-0,07	-0,5
LD10-BH4-2 (48-53) A1+	-22,68	-168,6	-22,49	-168,2	-0,19	-0,4
LD10-BH4-2 (48-53) A2	-24,16	-182,9	-24,06	-182,1	-0,1	-0,8
LD10-BH4-2 (48-53) A3+	-24,75	-187,5	-24,56	-186,9	-0,19	-0,6
LD10-BH4-2 (48-53) A4	-23,56	-178,4	-23,40	-177,5	-0,16	-0,9
LD10-BH10-2 (37-42) A1+	-21,77	-164,4	-21,8	-163,8	-0,03	-0,6
LD10-BH10-2 (37-42) A2+	-23,44	-176,4	-23,41	-175,2	-0,03	-1,2
LD10-BH10-2 (37-42) A3+	-23,13	-174,2	-22,93	-172,5	-0,2	-1,7
Maximum difference					0	0
Minimum difference					± 0,54	± 5,4
Average difference					± 0,142	± 1,127
Median difference					± 0,1	± 0,6

App. 7: Overview results frost-cracking experiments

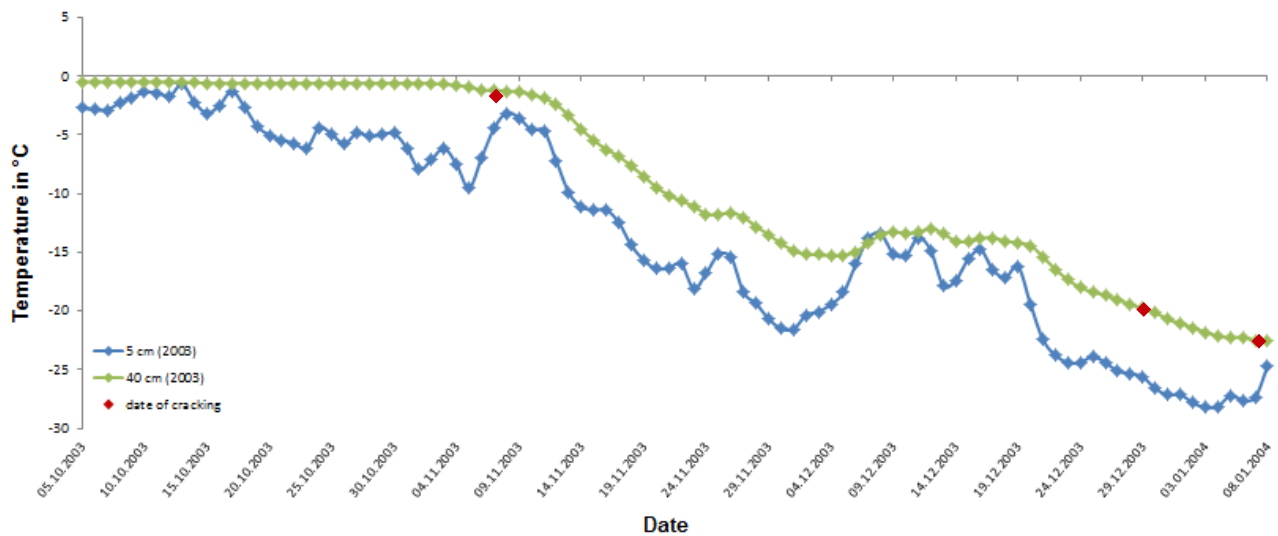
Year	Logger-Nr.	Frost cracking	Date	Note
2002/3	1	yes	26.12.2002	ripped, afterwards contacted by individual wires
	2	no	-	-
	3	yes	09.12.2002	-
	4	no	-	-
	5	no	-	-
	6	no	-	changing contact and no contact
2003/4	1	yes	Later 6.2.2004	-
	2	yes	-	-
	3	yes	-	contact still possible by individual wires
	4	yes	-	-
	5	yes	-	contact still possible by individual wires
	6	no	31.12.2003	bite marks
	7	yes	07.01.2004	-
	8	yes	10.02.2004	contact still possible by individual wires
	9	yes	08.11.2003	contact still possible by individual wires
	10	yes	-	-
2004/5	1	no	-	pole loose
	2	yes	17.12.2004	-
	3	not complete	-	pole very loose
	4	no	-	pole very loose
	5	not complete	-	still contact to about 10 fibers
	6	yes	22.11.2004	-
	7	yes	12.12.2004	-
	8	no	-	pole very loose
	9	no	-	pole loose
	10	yes	-	-
20	no	-	-	
2005/6	1	no	-	-
	2	no	-	-
	3	no	-	-
	4	no	-	-
	5	no	-	-
	6	no	-	-
	7	no	-	-
	8	no	-	-
	9	no	-	-
	10	no	-	-
20	yes	16.11.2006	-	
2006/7	1	no	-	-
	2	no	-	-
	3	no	-	-
	4	no	-	-
	5	no	-	-
	6	no	-	-
	7	no	-	-
	8	no	-	-
	9	no	-	-
	10	no	-	-
20	no	-	-	

App. 8: Soil temperature data from the investigated polygon in 5 cm and 40 cm depth

Soil temperature data from 2002/03



Soil temperature data from 2003/04



App. 9: Temperature conditions in 40 cm soil depth preceding a frost-cracking event

(red highlighted = cracking event found as outlier)

Date of cracking event	09.12.02	26.12.02	08.11.03	31.12.03	07.01.04	06.02.04	10.02.04	22.11.04	12.12.04	17.12.04	16.11.06
Temperature drop in °C/day before the event	-0.41	-0.55	-0.02	-0.50	-0.44	-0.33	-0.76	-0.57	-0.56	-0.50	-0.51
Number of days with temperature drop before the event	24	12	3	13	18	6	8	19	10	15	9

App. 10: Normalized spore numbers over rows and columns

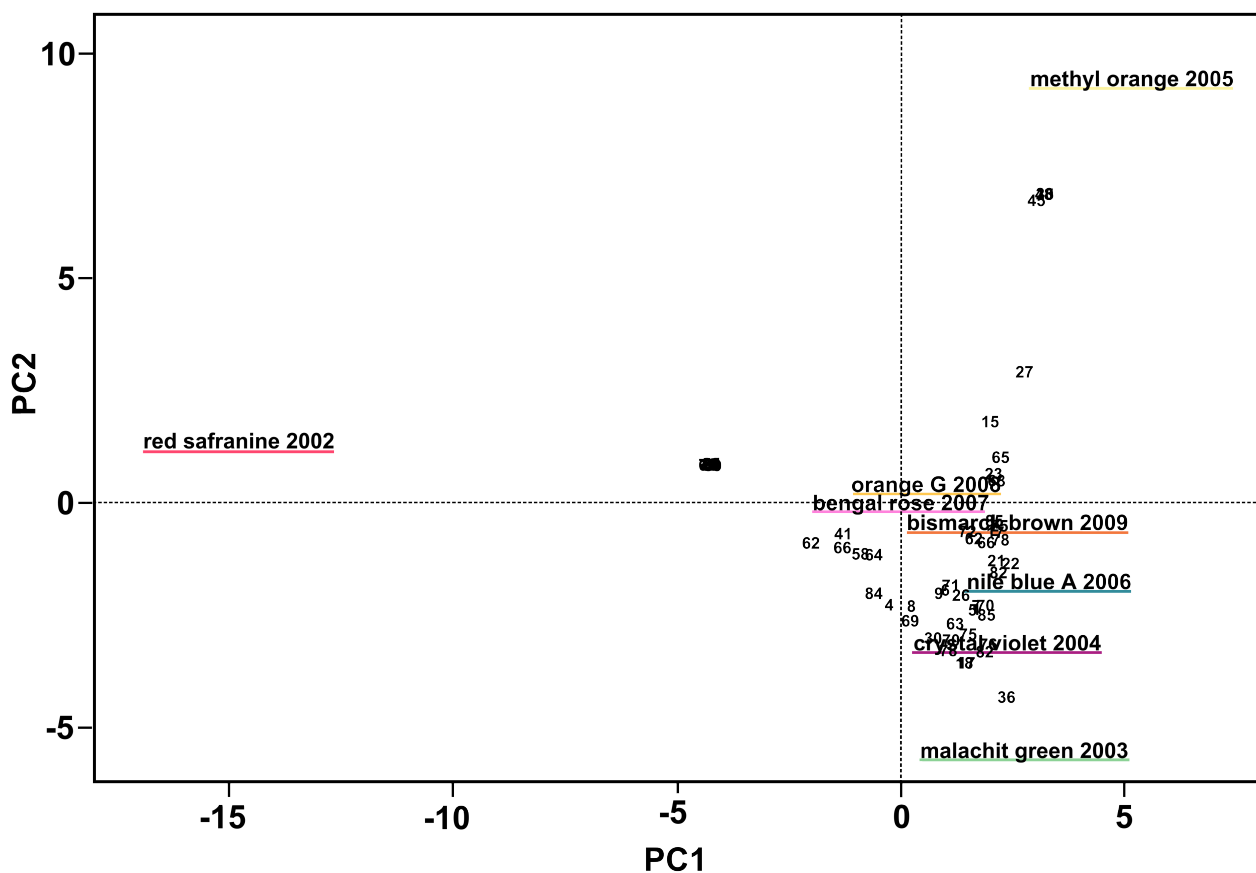
(Samples containing no spores were left out)

Sample	Synonym	Red safranin 2002	Mmalachit green 2003	Crystal violet 2004	Methyl orange 2005	Nile blue 2006	Bengal rose 2007	Orange G 2008	Bismarck brown 2009
LD10-BH10-2 37-42 cm A1+	1	100,00	0,00	0,00	0,00	0,00	0,00	0,00	0,00
LD10-BH10-2 37-42 cm A2+	2	100,00	0,00	0,00	0,00	0,00	0,00	0,00	0,00
LD10-BH10-2 37-42 cm A3+	3	100,00	0,00	0,00	0,00	0,00	0,00	0,00	0,00
LD10-BH10-2 37-42 cm A4	4	39,13	60,87	0,00	0,00	0,00	0,00	0,00	0,00
LD10-BH11-1-2 57-59 cm A1+	5	0,00	0,00	0,00	100,00	0,00	0,00	0,00	0,00
LD10-BH11-1-4 84-94 cm A4	6	0,00	0,00	0,00	0,00	0,00	0,00	0,00	100,00
LD10-BH12-1-1 37-45 cm A1	7	100,00	0,00	0,00	0,00	0,00	0,00	0,00	0,00
LD10-BH12-1-1 37-45 cm A2	8	31,29	48,67	20,04	0,00	0,00	0,00	0,00	0,00
LD10-BH12-1-1 37-45 cm A3	9	20,56	11,28	68,16	0,00	0,00	0,00	0,00	0,00
LD10-BH12-1-5 96-98 cm A2+	10	0,31	0,00	0,00	99,69	0,00	0,00	0,00	0,00
LD10-BH12-1-5 96-98 cm A3	11	100,00	0,00	0,00	0,00	0,00	0,00	0,00	0,00
LD10-BH12-1-5 96-98 cm A4+	12	100,00	0,00	0,00	0,00	0,00	0,00	0,00	0,00
LD10-BH12-1-5 96-98 cm A5+	13	4,34	6,75	88,91	0,00	0,00	0,00	0,00	0,00
LD10-BH12-1-5 98-101 cm A2+	14	100,00	0,00	0,00	0,00	0,00	0,00	0,00	0,00
LD10-BH12-1-5 98-101 cm A3+	15	0,51	1,06	0,00	27,15	0,00	0,00	71,27	0,00
LD10-BH12-1-5 98-101cm A4+	16	0,00	100,00	0,00	0,00	0,00	0,00	0,00	0,00
LD10-BH13-1-2 66-71 cm	17	13,85	86,15	0,00	0,00	0,00	0,00	0,00	0,00
LD10-BH13-1-2 66-71 cm	18	13,85	86,15	0,00	0,00	0,00	0,00	0,00	0,00
LD10-BH13-1-2 66-71 cm	19	100,00	0,00	0,00	0,00	0,00	0,00	0,00	0,00
LD10-BH13-1-2 76-81 cm	20	0,86	1,34	0,00	0,00	0,00	0,00	0,00	97,81
LD10-BH13-1-2 76-81 cm	21	4,38	0,00	0,00	0,00	95,62	0,00	0,00	0,00
LD10-BH13-1-2 76-81 cm	22	0,00	0,00	0,00	100,00	0,00	0,00	0,00	0,00
LD10-BH13-1-2 76-81 cm	23	0,41	3,03	2,75	15,51	7,98	0,00	40,71	29,61
LD10-BH2-1 46-51 cm A1	24	0,00	0,00	7,25	0,00	92,75	0,00	0,00	0,00
LD10-BH2-1 46-51 cm A2+	25	11,68	48,43	39,89	0,00	0,00	0,00	0,00	0,00
LD10-BH2-1 46-51 cm A3+	26	12,77	0,00	87,23	0,00	0,00	0,00	0,00	0,00
LD10-BH2-1 46-51 cm A4	27	1,16	21,61	15,82	61,41	0,00	0,00	0,00	0,00
LD10-BH3-1 48-49 cm A2+	28	0,00	0,00	0,00	0,00	100,00	0,00	0,00	0,00
LD10-BH3-1 49-50 cm A1+	29	100,00	0,00	0,00	0,00	0,00	0,00	0,00	0,00
LD10-BH3-1 49-50 cm A2	30	24,33	75,67	0,00	0,00	0,00	0,00	0,00	0,00
LD10-BH3-1 49-50 cm A3	31	100,00	0,00	0,00	0,00	0,00	0,00	0,00	0,00
LD10-BH3-1 50-51 cm A1	32	100,00	0,00	0,00	0,00	0,00	0,00	0,00	0,00
LD10-BH3-1 50-51 cm A3+	33	0,00	0,00	0,00	100,00	0,00	0,00	0,00	0,00
LD10-BH3-1 50-51 cm A5	34	0,31	0,00	0,00	99,69	0,00	0,00	0,00	0,00
LD10-BH3-1 51-54 cm A1	35	0,00	100,00	0,00	0,00	0,00	0,00	0,00	0,00
LD10-BH3-1 51-54 cm A3+	36	100,00	0,00	0,00	0,00	0,00	0,00	0,00	0,00
LD10-BH3-1 51-54 cm A5	37	0,65	0,00	0,00	0,00	0,00	0,00	0,00	99,35
LD10-BH3-1 69-71 cm A1+	38	0,00	0,00	0,00	100,00	0,00	0,00	0,00	0,00
LD10-BH4-2 48-53 cm A1+	39	100,00	0,00	0,00	0,00	0,00	0,00	0,00	0,00
LD10-BH4-2 48-53 cm A2	40	100,00	0,00	0,00	0,00	0,00	0,00	0,00	0,00
LD10-BH4-2 48-53 cm A3+	41	53,94	0,00	46,06	0,00	0,00	0,00	0,00	0,00
LD10-BH4-2 48-53 cm A4	42	100,00	0,00	0,00	0,00	0,00	0,00	0,00	0,00
LD10-BH4-2 48-53 cm A5	43	1,85	0,00	0,00	98,15	0,00	0,00	0,00	0,00
LD10-BH5-2-2 50-55 cm A1	44	4,38	0,00	0,00	0,00	95,62	0,00	0,00	0,00
LD10-BH5-2-2 50-55 cm A2+	45	0,51	0,00	0,00	0,00	99,49	0,00	0,00	0,00
LD10-BH5-2-2 50-55 cm A4	46	0,79	0,00	0,00	0,00	38,97	0,00	0,00	60,23
LD10-BH5-2-3 70-75 cm A2++	47	100,00	0,00	0,00	0,00	0,00	0,00	0,00	0,00
LD10-BH5-2-3 70-75 cm A3+	48	0,46	0,00	0,00	0,00	30,00	0,00	0,00	69,54
LD10-BH5-2-3 70-75 cm A4	49	100,00	0,00	0,00	0,00	0,00	0,00	0,00	0,00
LD10-BH5-2-3 80-84 A1	50	100,00	0,00	0,00	0,00	0,00	0,00	0,00	0,00
LD10-BH5-2-3 80-84 A3+	51	0,00	0,00	0,00	100,00	0,00	0,00	0,00	0,00
LD10-BH5-2-3 80-84 A4+	52	0,00	0,00	0,00	100,00	0,00	0,00	0,00	0,00
LD10-BH5-2-3 80-84 A5+	53	100,00	0,00	0,00	0,00	0,00	0,00	0,00	0,00
LD10-BH5-2-3 80-84 A6+	54	100,00	0,00	0,00	0,00	0,00	0,00	0,00	0,00
LD10-BH5-3 88-94 cm A1	55	100,00	0,00	0,00	0,00	0,00	0,00	0,00	0,00
LD10-BH5-3 88-94 cm A2+	56	100,00	0,00	0,00	0,00	0,00	0,00	0,00	0,00
LD10-BH8-1 35-40 cm A1/2+	57	100,00	0,00	0,00	0,00	0,00	0,00	0,00	0,00
LD10-BH8-2-1/2 55-57 cm A1+	58	48,51	15,69	35,80	0,00	0,00	0,00	0,00	0,00
LD10-BH8-2-1/2 55-57 cm A2	59	9,28	34,99	18,89	0,00	36,84	0,00	0,00	0,00
LD10-BH8-2-1/2 55-57 cm A3	60	3,76	4,68	15,42	0,00	0,00	0,00	0,00	76,14
LD10-BH8-2-1/2 55-57 cm A4+	61	4,38	0,00	0,00	0,00	95,62	0,00	0,00	0,00
LD10-BH8-2-1/2 55-57 cm A5+	62	65,86	34,14	0,00	0,00	0,00	0,00	0,00	0,00
LD10-BH8-2-1/2 55-57 cm A6+	63	15,68	42,41	41,91	0,00	0,00	0,00	0,00	0,00
LD10-BH8-2-1/2 57-60 cm A1+	64	43,93	14,38	31,59	0,00	10,10	0,00	0,00	0,00
LD10-BH8-2-1/2 57-60 cm A5+	65	6,51	27,00	12,35	38,35	15,79	0,00	0,00	0,00
LD10-BH8-2-2 60-65 cm A1+	66	54,07	16,18	29,75	0,00	0,00	0,00	0,00	0,00
LD10-BH8-2-2 60-65 cm A2	67	3,10	9,49	10,42	0,00	13,32	0,00	63,68	0,00

Sample	Synonym	Red safranin 2002	Mmalachit green 2003	Crystal violet 2004	Methyl orange 2005	Nile blue 2006	Bengal rose 2007	Orange G 2008	Bismarck brown 2009
LD10-BH8-2-2 60-65 cm A3+	68	5,52	16,10	24,75	27,44	0,00	0,00	0,00	26,19
LD10-BH8-2-2 60-65 cm A4+	69	32,53	67,47	0,00	0,00	0,00	0,00	0,00	0,00
LD10-BH8-2-2 60-65 cm A5+	70	10,68	56,48	32,84	0,00	0,00	0,00	0,00	0,00
LD10-BH8-2-2 60-65 cm A6	71	17,72	15,75	38,91	0,00	27,63	0,00	0,00	0,00
LD10-BH8-2-4 80-85 cm A1	72	2,64	7,99	6,24	0,00	4,43	75,29	0,00	3,42
LD10-BH8-2-4 80-85 cm A2	73	18,01	67,23	14,77	0,00	0,00	0,00	0,00	0,00
LD10-BH8-2-4 80-85 cm A3+	74	8,83	30,51	22,11	0,00	38,55	0,00	0,00	0,00
LD10-BH8-2-4 80-85 cm A4+	75	9,77	60,78	29,45	0,00	0,00	0,00	0,00	0,00
LD10-BH8-2-4 80-85 cm A5	76	4,52	49,19	46,30	0,00	0,00	0,00	0,00	0,00
LD10-BH8-2-6 87-90 cm A1+	77	4,65	0,00	95,35	0,00	0,00	0,00	0,00	0,00
LD10-BH8-2-6 87-90 cm A4+	78	19,43	80,57	0,00	0,00	0,00	0,00	0,00	0,00
LD10-BH8-2-6 87-90 cm A5+	79	4,65	0,00	95,35	0,00	0,00	0,00	0,00	0,00
LD10-BH8-3 90-95 cm A1+	80	0,98	0,00	0,00	0,00	0,00	0,00	0,00	99,02
LD10-BH8-3 90-95 cm A2+	81	4,01	8,33	0,00	0,00	87,66	0,00	0,00	0,00
LD10-BH8-3 90-95 cm A3+	82	4,22	52,52	43,26	0,00	0,00	0,00	0,00	0,00
LD10-BH8-3 95-100 cm A1+	83	16,33	0,00	83,67	0,00	0,00	0,00	0,00	0,00
LD10-BH8-3 95-100 cm A2+	84	44,56	55,44	0,00	0,00	0,00	0,00	0,00	0,00
LD10-BH8-3 95-100 cm A3+	85	100,00	0,00	0,00	0,00	0,00	0,00	0,00	0,00

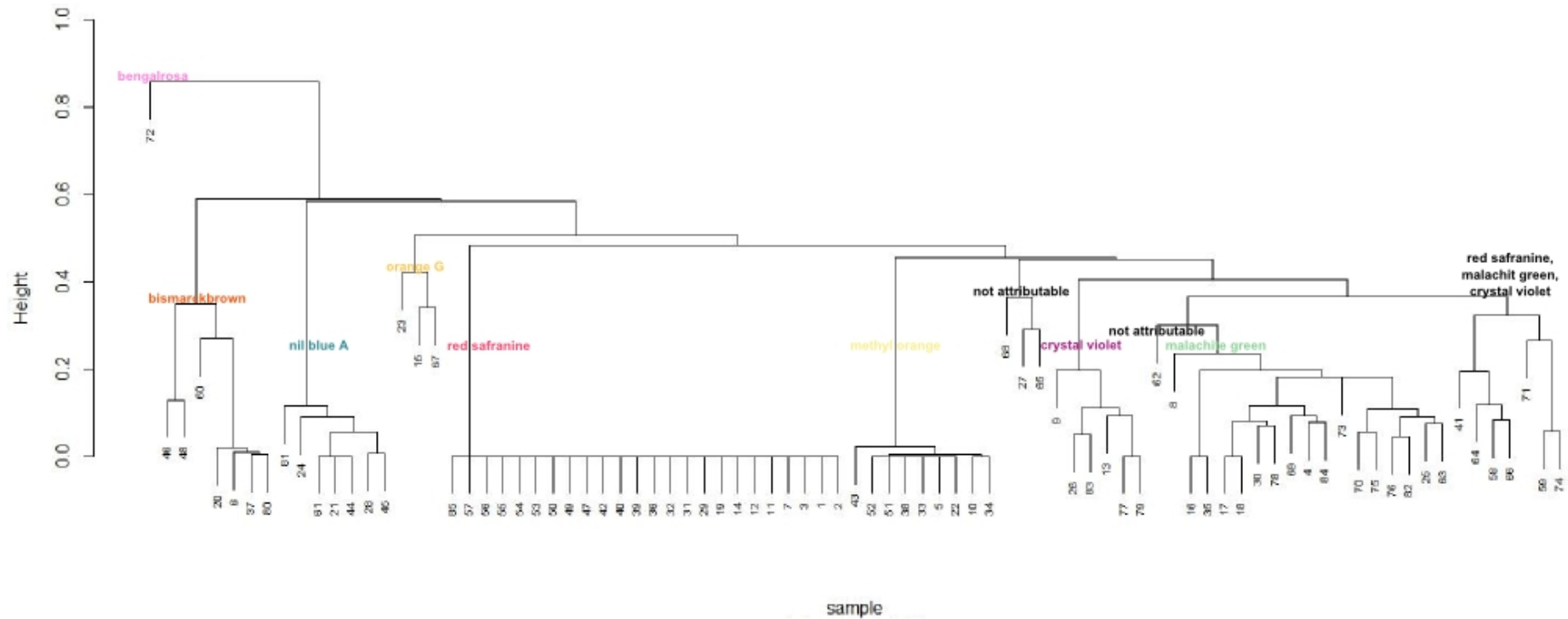
App. 11: Results of the PCA with PC1 plotted against PC2

(Table of attribution numbers see App. 14)



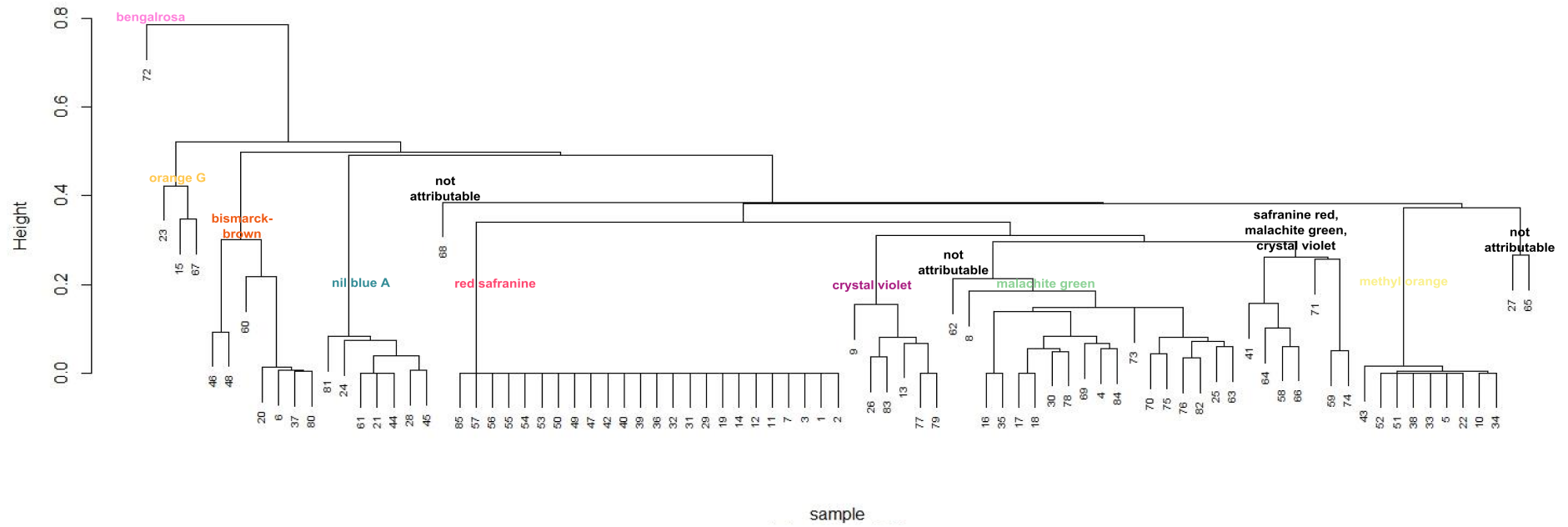
App. 12: Cluster dendrogram of the euclidean clustering

(Table of attribution numbers see App. 14)



App. 13: Cluster dendrogram of the bray-curtis clustering

(Table of attribution numbers see App. 14)



App. 14: Table of attribution numbers

Sample	Abbreviation
LD10-BH10-2 37-42 cm A1+	1
LD10-BH10-2 37-42 cm A2+	2
LD10-BH10-2 37-42 cm A3+	3
LD10-BH10-2 37-42 cm A4	4
LD10-BH11-1-2 57-59 cm A1+	5
LD10-BH11-1-4 84-89 cm A4	6
LD10-BH12-1-1 37-45 cm A1	7
LD10-BH12-1-1 37-45 cm A2+	8
LD10-BH12-1-1 37-45 cm A3+	9
LD10-BH12-1-5 96-98 cm A2+	10
LD10-BH12-1-5 96-98 cm A3	11
LD10-BH12-1-5 96-98 cm A4+	12
LD10-BH12-1-5 96-98 cm A5+	13
LD10-BH12-1-5 98-101 cm A2+	14
LD10-BH12-1-5 98-101 cm A3+	15
LD10-BH12-1-5 98-101 cm A4(+)	16
LD10-BH13-1-2 66-69 cm A2	17
LD10-BH13-1-2 66-69 cm A3	18
LD10-BH13-1-2 69-71 cm A1+	19
LD10-BH13-1-2 76-81 cm A1	20
LD10-BH13-1-2 76-81 cm A3 (+)	21
LD10-BH13-1-2 76-81 cm A4+	22
LD10-BH13-1-2 76-81 cm A5	23
LD10-BH2-1 46-51 cm A1	24
LD10-BH2-1 46-51 cm A2+	25
LD10-BH2-1 46-51 cm A3+	26
LD10-BH2-1 46-51 cm A4	27
LD10-BH3-1 48-49 cm A2+	28
LD10-BH3-1 49-50 cm A1+	29
LD10-BH3-1 49-50 cm A2	30
LD10-BH3-1 49-50 cm A3	31
LD10-BH3-1 50-51 cm A1	32
LD10-BH3-1 50-51 cm A3+	33
LD10-BH3-1 50-51 cm A5	34
LD10-BH3-1 51-54 cm A1	35
LD10-BH3-1 51-54 cm A3+	36
LD10-BH3-1 51-54 cm A5	37
LD10-BH3-1 69-71 cm A1+	38
LD10-BH4-2 48-53 cm A1+	39
LD10-BH4-2 48-53 cm A2	40
LD10-BH4-2 48-53 cm A3+	41
LD10-BH4-2 48-53 cm A4	42
LD10-BH4-2 48-53 cm A5	43

Sample	Abbreviation
LD10-BH5-2-2 50-55 cm A1	44
LD10-BH5-2-2 50-55 cm A2+	45
LD10-BH5-2-2 50-55 cm A4	46
LD10-BH5-2-3 70-75 cm A2++	47
LD10-BH5-2-3 70-75 cm A3+	48
LD10-BH5-2-3 70-75 cm A4	49
LD10-BH5-2-3 80-84 A1	50
LD10-BH5-2-3 80-84 A3+	51
LD10-BH5-2-3 80-84 A4+	52
LD10-BH5-2-3 80-84 A5+	53
LD10-BH5-2-3 80-84 A6+	54
LD10-BH5-3 88-94 cm A1	55
LD10-BH5-3 88-94 cm A2+	56
LD10-BH8-1 35-40 cm A1/2+	57
LD10-BH8-2-1/2 55-57 cm A1+	58
LD10-BH8-2-1/2 55-57 cm A2	59
LD10-BH8-2-1/2 55-57 cm A3	60
LD10-BH8-2-1/2 55-57 cm A4+	61
LD10-BH8-2-1/2 55-57 cm A5+	62
LD10-BH8-2-1/2 55-57 cm A6+	63
LD10-BH8-2-1/2 57-60 cm A1+	64
LD10-BH8-2-1/2 57-60 cm A5+	65
LD10-BH8-2-2 60-65 cm A1+	66
LD10-BH8-2-2 60-65 cm A2	67
LD10-BH8-2-2 60-65 cm A3+	68
LD10-BH8-2-2 60-65 cm A4+	69
LD10-BH8-2-2 60-65 cm A5+	70
LD10-BH8-2-2 60-65 cm A6	71
LD10-BH8-2-4 80-85 cm A1	72
LD10-BH8-2-4 80-85 cm A2	73
LD10-BH8-2-4 80-85 cm A3+	74
LD10-BH8-2-4 80-85 cm A4+	75
LD10-BH8-2-4 80-85 cm A5	76
LD10-BH8-2-6 87-90 cm A1+	77
LD10-BH8-2-6 87-90 cm A4+	78
LD10-BH8-2-6 87-90 cm A5+	79
LD10-BH8-3 90-95 cm A1+	80
LD10-BH8-3 90-95 cm A2+	81
LD10-BH8-3 90-95 cm A3+	82
LD10-BH8-3 95-100 cm A1+	83
LD10-BH8-3 95-100 cm A2+	84
LD10-BH8-3 95-100 cm A3	85

App. 15: Results k-clustering

Red safranine 2002	Malachite green 2003	Crystal violet 2004	Methyl orange 2005	Nile blue 2006	Bengalrosa 2007	Orange G 2008	Bismarck brown 2009
LD10-BH10-2 37-42 cm A1+	LD10-BH10-2 37-42 cm A4	LD10-BH12-1-1 37-45 cm A3+	LD10-BH11-1-2 57-59 cm A1+	LD10-BH13-1-2 76-81 cm A5	LD10-BH8-2-4 80-85 cm A1	LD10-BH12-1-5 98-101 cm A3+	LD10-BH11-1-4 84-94 cm A4
LD10-BH10-2 37-42 cm A2+	LD10-BH12-1-1 37-45 cm A2+	LD10-BH12-1-5 96-98 cm A5+	LD10-BH12-1-5 96-98 cm A2+	LD10-BH2-1 46-51 cm A1		LD10-BH13-1-2 76-81 cm A5	LD10-BH13-1-2 76-81 cm A1
LD10-BH10-2 37-42 cm A3+	LD10-BH12-1-5 98-101 cm A4(+)	LD10-BH2-1 46-51 cm A3+	LD10-BH13-1-2 76-81 cm A4+	LD10-BH3-1 48-49 cm A2+		LD10-BH8-2-2 60-65 cm A2	LD10-BH3-1 51-54 cm A5
LD10-BH12-1-1 37-45 cm A1	LD10-BH13-1-2 66-69 cm A2	LD10-BH4-2 48-53 cm A3+	LD10-BH2-1 46-51 cm A4	LD10-BH5-2-2 50-55 cm A1			LD10-BH5-2-2 50-55 cm A4
LD10-BH12-1-5 96-98 cm A3	LD10-BH13-1-2 66-69 cm A3	LD10-BH8-2-1/2 55-57 cm A1+	LD10-BH3-1 50-51 cm A3+	LD10-BH5-2-2 50-55 cm A2+			LD10-BH5-2-3 70-75 cm A3+
LD10-BH12-1-5 96-98 cm A4+	LD10-BH2-1 46-51 cm A2+	LD10-BH8-2-1/2 57-60 cm A1+	LD10-BH3-1 50-51 cm A5	LD10-BH8-2-1/2 55-60 cm A4+			LD10-BH8-2-1/2 55-60 cm A3
LD10-BH12-1-5 98-101 cm A2+	LD10-BH3-1 49-50 cm A2	LD10-BH8-2-2 60-65 cm A1+	LD10-BH3-1 69-71 cm A1+	LD10-BH8-3 90-100 cm A2+			LD10-BH8-3 90-100 cm A1+
LD10-BH13-1-2 69-71 cm A1+	LD10-BH3-1 51-54 cm A1	LD10-BH8-2-2 60-65 cm A3+	LD10-BH4-2 48-53 cm A5				
LD10-BH3-1 49-50 cm A1+	LD10-BH8-2/1 55-57 cm A2	LD10-BH8-2-2 60-65 cm A6	LD10-BH2-3 80-84 cm A3+				
LD10-BH3-1 49-50 cm A3	LD10-BH8-2/1 55-57 cm A6+	LD10-BH8-2-6 87-90 cm A1+	LD10-BH5-2-3 80-84 A4+				
LD10-BH3-1 50-51 cm A1	LD10-BH8-2/1 57-60 cm A5+	LD10-BH8-2-6 87-90 cm A5+					
LD10-BH3-1 51-54 cm A3+	LD10-BH8-2-2 60-65cm A4+	LD10-BH8-3 95-100 cm A1+					
LD10-BH4-2 48-53 cm A1+	LD10-BH8-2-2 60-65 cm A5+						
LD10-BH4-2 48-53 cm A2	LD10-BH8-2-4 80-85 cm A2						
LD10-BH4-2 48-53 cm A4	LD10-BH8-2-4 80-85 cm A3+						
LD10-BH5-2-3 70-75 cm A2++	LD10-BH8-2-4 80-85 cm A4+						
LD10-BH5-2-3 70-75 cm A4	LD10-BH8-2-4 80-85 cm A5						
LD10-BH5-2-3 80-84 A1	LD10-BH8-2-6 87-90 cm A4+						
LD10-BH5-2-3 80-84 A5+	LD10-BH8-3 90-95 cm A3+						
LD10-BH5-2-3 80-84 A6+	LD10-BH8-3 95- 100 cm A2+						
LD10-BH5-3 88-94 cm A1							
LD10-BH-3 88-94 cm A2+							
LD10-BH8-1 35-40 cm A1/2+							
LD10-BH8-2-1/2 55-57 cm A5+							
LD10-BH8-3 95-100 cm A3+							

App. 16: Initial values for the correlation of temperature and $\delta^{18}\text{O}$ data

	$\delta^{18}\text{O}$				Samoylov										Stolb											
	Max.	Min.	Average	Median	Nov	Dec	Jan	Feb	Mar	Apr	May	T _{winter}	T _{spring}	T _{cold season}	Nov	Dec	Jan	Feb	Mar	Apr	May	T _{winter}	T _{spring}	T _{cold season}		
2002/03	-21.18	-24.52	-22.84	-22.78	-21.5	-31.2	-31.2	-29.6	-20.6	-16.3	-4.5	-30.7	-13.8	-22.1	-21.5	-31.2	-31.2	-29.6	-20.6	-16.3	-3.5	-30.7	-13.8	-22.1		
2003/04	-20.64	-23.87	-22.42	-22.48	-24.7	-27.1	-32.7	-36.5	-29.9	-19.9	-8.0	-32.1	-19.2	-25.5	-24.7	-27.1	-32.7	-36.7	-30.2	-20.0	-8.4	-32.2	-19.6	-25.7		
2004/05	-20.81	-26.08	-22.81	-22.65	-21.7	-31.7	-28.9	-31.0	-25.7	-15.8	-5.2	-30.5	-15.6	-22.9	-21.9	-31.7	-28.9	-30.9	-25.8	-15.8	-5.2	-30.5	-15.6	-22.9		
2005/06	-21.69	-23.73	-22.76	-22.85	-19.7	-26.2	-29.9	-28.7	-28.3	-26.6	-6.8	-28.3	-20.5	-23.7	-19.7	-26.2	-29.9	-28.7	-28.3	-26.6	-6.8	-28.3	-20.5	-23.7		
2006/07	-21.42	-23.87	-22.66	-22.67	-22.2	-25.3	-26.5	-33.9	-24.7	-11.6	-3	-28.6	-13.1	-21.0	-22.2	-25.3	-26.6	-33.9	-22.3	-11.7	-2.3	-28.6	-12.3	-20.7		
2007/08	-22.91	-22.91	-22.91	-22.91	-23.5	-29.7	-29.1	-31.0	-23.1	-21.1	-4.3	-29.9	-16.2	-23.1	-23.5	-29.7	-29.5	-31.5	-24.4	-21.55	-4.7	-30.2	-16.9	-23.5		
2008/09	-21.01	-22.99	-22.99	-22.95	-23.7	-32.6	-27.2	-35.1	-28.4	-15.6	-6.9	-31.6	-17.0	-24.2	-23.2	-31.8	-26.5	-34.3	-27.2	-14.8	-8.1	-30.9	-16.7	-23.7		
2009/10	-21.51	-23.24	-22.52	-22.65	-22.2	-30.8	-27.4	-32.5	-25.6	-15.7	-2.8	-30.2	-12.1	-22.24	-22.2	-30.8	-29.5	-31.0	-25.6	-15.7	-2.8	-30.4	-14.7	-22.5		
Max.	-20.64	-22.91	-22.42	-22.42	-19.7	-25.3	-26.5	-28.7	-20.4	-11.4	-3.0	-28.3	-12.1	-21.3	-19.7	-25.3	-26.5	-28.7	-20.6	-11.7	-2.8	-28.3	-12.3	-20.7		
Min.	-22.91	-26.08	-22.99	-22.95	-24.7	-32.6	-32.7	-36.5	-29.9	-26.6	-8.0	-32.1	-20.5	-25.5	-24.7	-31.8	-32.7	-36.7	-30.2	-26.6	-8.4	-32.2	-20.5	-25.7		
Diff.	± 2.27	± 3.17	± 0.57	± 0.47	± 5.0	± 7.3	± 6.2	± 7.8	± 9.5	± 15.2	± 5.0	± 3.8	± 8.4	± 4.5	± 5.0	± 6.6	± 6.3	± 68.0	± 9.7	± 14.9	± 5.6	± 3.9	± 8.3	± 5.0		

App. 17: Normalized initial values for the correlation of temperature and $\delta^{18}\text{O}$ data

	$\delta^{18}\text{O}$				Samoylov temperatures										Stolb temperatures											
	Max	Min.	Average	Median	Nov	Dec	Jan	Feb	Mar	Apr	May	T _{winter}	T _{spring}	T _{cold season}	Nov	Dec	Jan	Feb	Mar	Apr	May	T _{winter}	T _{spring}	T _{cold season}		
2002/03	-0.24	-0.51	-0.74	-0.65	-0.36	-0.81	-0.76	-0.11	-0.02	-0.32	-0.29	-0.63	-0.20	-0.24	-0.35	-0.91	-0.76	-0.11	-0.00	-0.31	-0.29	-0.61	-0.18	-0.28		
2003/04	-0.00	-0.30	-0.00	-0.00	-1.00	-0.25	-1.00	-1.00	-1.00	-0.56	-1.00	-1.00	-0.85	-1.00	-1.00	-0.28	-1.00	-1.00	-1.00	-0.56	-1.00	-1.00	-0.88	-1.00		
2004/05	-0.07	-1.00	-0.68	-0.37	-0.44	-0.88	-0.39	-0.30	-0.56	-0.29	-0.44	-0.59	-0.41	-0.41	-0.43	-0.98	-0.39	-0.28	-0.54	-0.28	-0.42	-0.57	-0.40	-0.44		
2005/06	-0.46	-0.26	-0.59	-0.80	-0.00	-0.13	-0.55	-0.00	-0.83	-1.00	-0.77	-0.00	-1.00	-0.60	-0.00	-0.14	-0.55	-0.00	-0.80	-1.00	-0.72	-0.00	-1.00	-0.61		
2006/07	-0.34	-0.30	-0.42	-0.41	-0.50	-0.00	-0.00	-0.67	-0.45	-0.01	-0.00	-0.08	-0.12	-0.00	-0.50	-0.00	-0.01	-0.64	-0.18	-0.00	-0.03	-0.07	-0.00	-0.00		
2007/08	-1.00	-0.00	-0.86	-0.92	-0.76	-0.60	-0.42	-0.30	-0.28	-0.64	-0.26	-0.43	-0.48	-0.46	-0.75	-0.68	-0.48	-0.34	-0.40	-0.66	-0.33	-0.49	-0.56	-0.57		
2008/09	-0.16	-0.03	-1.00	-1.00	-0.80	-1.00	-0.11	-0.82	-0.84	-0.28	-0.78	-0.88	-0.58	-0.71	-0.71	-1.00	-0.00	-0.69	-0.69	-0.21	-0.94	-0.66	-0.53	-0.60		
2009/10	-0.38	-0.10	-0.17	-1.37	-0.50	-0.75	-0.15	-0.49	-0.00	-0.00	-0.30	-0.51	-0.00	-0.06	-0.50	-0.85	-0.28	-0.28	-0.52	-0.27	-0.00	-0.55	-0.29	-0.36		

App. 18: Correlation matrix of ice-vein and no-ice-vein samples

(gray = negative correlation; yellow = positive correlation ; red = highest correlation in one column)

	Samoylov temperatures				Stolb temperatures			
	$\delta^{18}\text{O}$ ice-vein samples		$\delta^{18}\text{O}$ no-ice-vein samples		$\delta^{18}\text{O}$ ice-vein samples		$\delta^{18}\text{O}$ no-ice-vein samples	
	Averages	Median	Averages	Median	Averages	Median	Averages	Median
November	-0,22	-0,28	-0,32	-0,31	-0.28	-0.33	-0.32	-0.32
December	0,33	0,19	-0,08	-0,09	0.29	0.16	-0.10	-0.10
January	0,07	0,03	0,01	0,02	-0.19	-0.24	-0.00	-0.00
February	-0,47	-0,48	0,15	0,15	-0.38	-0.38	0.06	0.07
March	0,08	0,07	0,20	0,21	-0.25	-0.32	0.12	0.13
April	0,44	0,43	-0,31	-0,30	0.25	0.22	-0.32	-0.31
May	0,05	-0,029	0,22	0,23	0.29	0.22	0.09	0.10
T _{winter}	-0,06	-0,17	0,06	0,06	-0.17	-0.29	-0.02	-0.02
T _{spring}	0,30	0,27	-0,05	-0,04	0.12	0.06	-0.12	-0.11
T _{cold season}	0,20	0,12	-0,07	-0,06	-0.00	-0.10	-0.15	-0.14
Max	0,44	0,43	0,22	0,23	0.29	0.22	0.12	0.13
Min	-0,47	-0,48	-0,32	-0,31	-0.38	-0.38	-0.32	-0.32

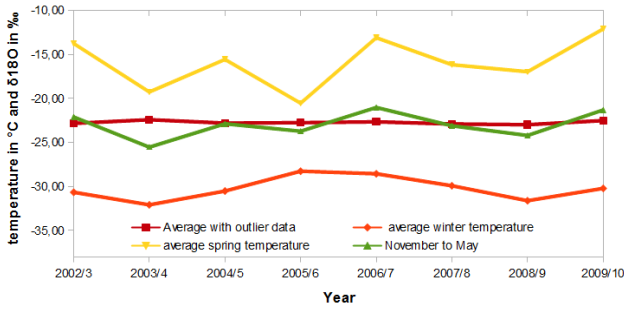
App. 19: Correlation matrix with Samoylov temperatures in two year stapes

(gray = negative correlation; yellow = positive correlation)

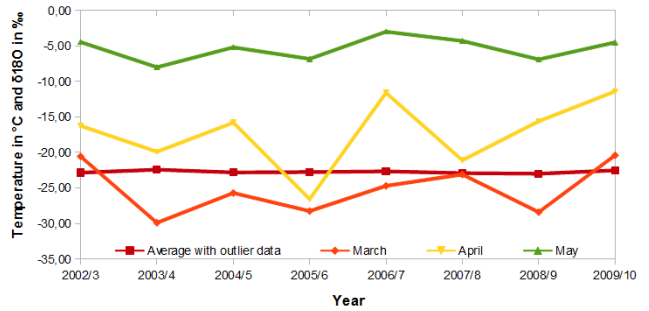
	Average $\delta^{18}\text{O}$				Median $\delta^{18}\text{O}$			
	2002 to 03	2004 to 05	2006 to 07	2008 to 09	2002 to 03	2004 to 05	2006 to 07	2008 to 09
November	-1	1	1	1	-1	-1	1	1
December	1	1	1	1	1	-1	1	1
January	-1	-1	1	-1	-1	1	1	-1
February	-1	1	-1	1	-1	-1	-1	1
March	-1	-1	-1	1	-1	1	-1	1
April	-1	-1	1	1	-1	1	1	1
May	-1	-1	1	1	-1	1	1	1

App. 20: Visual comparison of $\delta^{18}\text{O}$ and temperature data

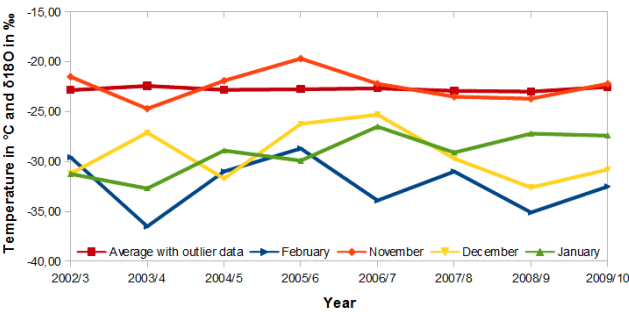
Average $\delta^{18}\text{O}$ and season temperature data



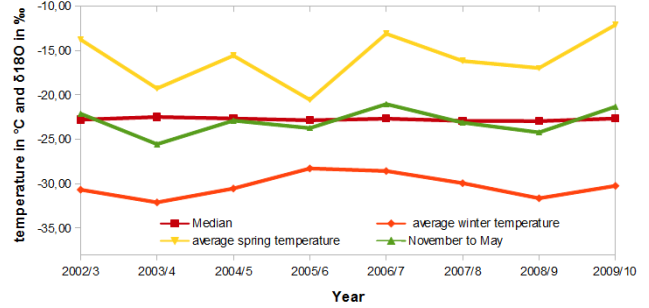
Average $\delta^{18}\text{O}$ and monthly spring temperature data



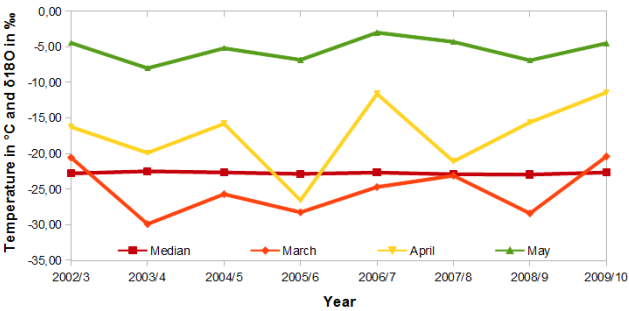
Average $\delta^{18}\text{O}$ and monthly winter temperature data



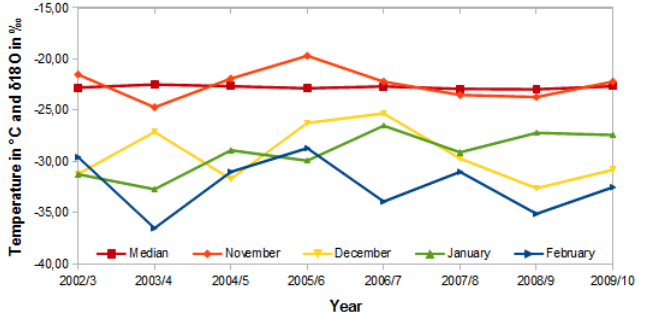
Median $\delta^{18}\text{O}$ and season temperature data



Median $\delta^{18}\text{O}$ and monthly spring temperature data



Median $\delta^{18}\text{O}$ and monthly winter temperature data

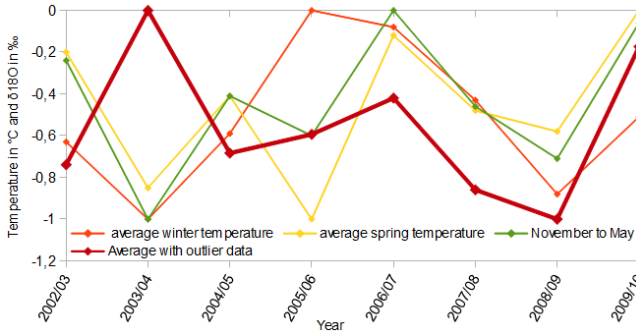


App. 21: Visual comparison of normalized

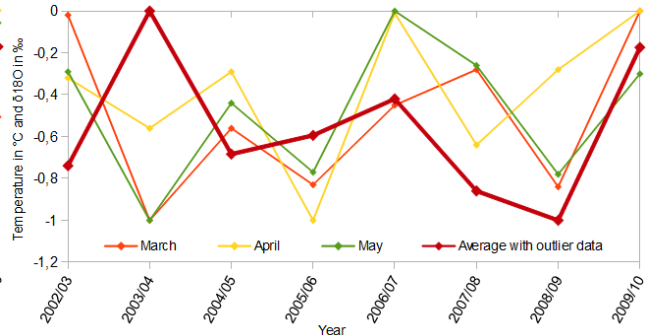
$\delta^{18}\text{O}$

and temperature data

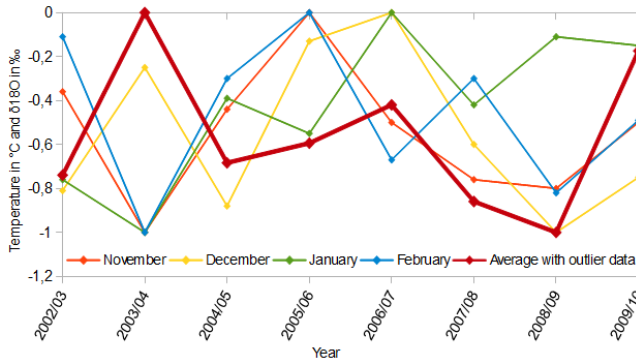
Average $\delta^{18}\text{O}$ and season temperature data



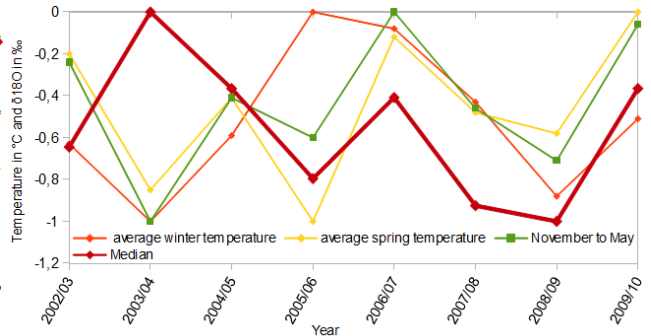
Average $\delta^{18}\text{O}$ and monthly spring temperature data



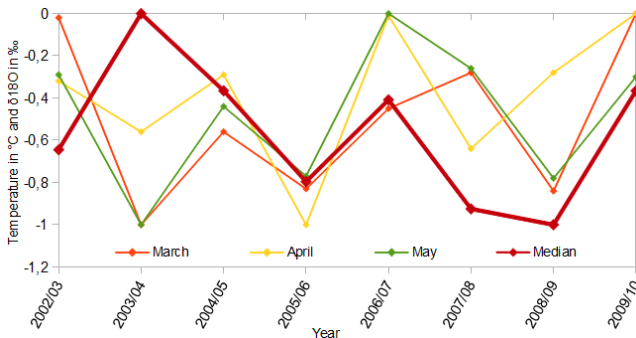
Average $\delta^{18}\text{O}$ and monthly winter temperature data



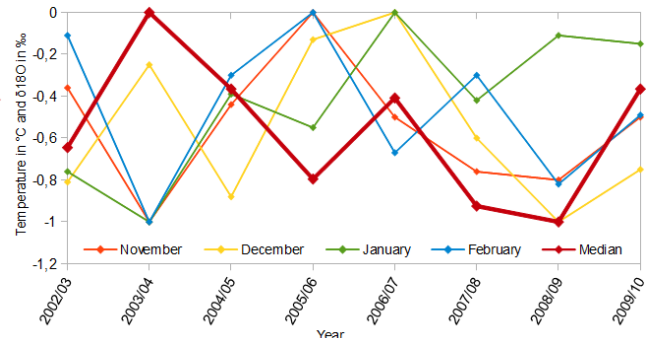
Median $\delta^{18}\text{O}$ and season temperature data



Median $\delta^{18}\text{O}$ and monthly spring temperature data



Median $\delta^{18}\text{O}$ and monthly winter temperature data



App. 22: Linear regression equation of $\delta^{18}\text{O}$ and temperature data

From 2002 to 2010

November		
Average $\delta^{18}\text{O}$:	$T = -1.3 * \delta^{18}\text{O} - 51.99$	$(R^2 = 0.027)$
Median $\delta^{18}\text{O}$:	$T = -2.262 * \delta^{18}\text{O} - 73.87$	$(R^2 = 0.05)$
December		
Average $\delta^{18}\text{O}$:	$T = 7.15 * \delta^{18}\text{O} + 133.18$	$(R^2 = 0.25)$
Median $\delta^{18}\text{O}$:	$T = 5.71 * \delta^{18}\text{O} + 100.43$	$(R^2 = 0.11)$
January		
Average $\delta^{18}\text{O}$:	$T = -3.14 * \delta^{18}\text{O} - 100.61$	$(R^2 = 0.08)$
Median $\delta^{18}\text{O}$:	$T = -4.61 * \delta^{18}\text{O} - 133.92$	$(R^2 = 0.18)$
February		
Average $\delta^{18}\text{O}$:	$T = -5.59 * \delta^{18}\text{O} - 159.33$	$(R^2 = 0.16)$
Median $\delta^{18}\text{O}$:	$T = -7.10 * \delta^{18}\text{O} - 193.67$	$(R^2 = 0.017)$
March		
Average $\delta^{18}\text{O}$:	$T = -5.56 * \delta^{18}\text{O} - 152.17$	$(R^2 = 0.12)$
Median $\delta^{18}\text{O}$:	$T = -4.64 * \delta^{18}\text{O} - 131.19$	$(R^2 = 0.06)$
April		
Average $\delta^{18}\text{O}$:	$T = -0.71 * \delta^{18}\text{O} - 1.71$	$(R^2 = 0.00)$
Median $\delta^{18}\text{O}$:	$T = 7.19 * \delta^{18}\text{O} + 145.65$	$(R^2 = 0.62)$
May		
Average $\delta^{18}\text{O}$:	$T = 0.13 * \delta^{18}\text{O} - 2.25$	$(R^2 = 0.00)$
Median $\delta^{18}\text{O}$:	$T = -0.03 * \delta^{18}\text{O} - 5.95$	$(R^2 = 0.00)$
Winter		
Average $\delta^{18}\text{O}$:	$T = -0.53 * \delta^{18}\text{O} - 42.35$	$(R^2 = 0.01)$
Median $\delta^{18}\text{O}$:	$T = -2.00 * \delta^{18}\text{O} - 75.79$	$(R^2 = 0.06)$
Spring		
Average $\delta^{18}\text{O}$:	$T = -1.58 * \delta^{18}\text{O} - 52.06$	$(R^2 = 0.01)$
Median $\delta^{18}\text{O}$:	$T = 0.84 * \delta^{18}\text{O} + 2.76$	$(R^2 = 0.00)$
Cold season		
Average $\delta^{18}\text{O}$:	$T = -1.088 * \delta^{18}\text{O} - 47.88$	$(R^2 = 0.02)$
Median $\delta^{18}\text{O}$:	$T = -0.83 * \delta^{18}\text{O} - 42.00$	$(R^2 = 0.01)$

From 2004 to 2010

November		
Average $\delta^{18}\text{O}$:	$T = 3.60 * \delta^{18}\text{O} + 60,80$	$(R^2 = 0.027)$
Median $\delta^{18}\text{O}$:	$T = 2.97 * \delta^{18}\text{O} + 45.39$	$(R^2 = 0.08)$
December		
Average $\delta^{18}\text{O}$:	$T = 6.74 * \delta^{18}\text{O} + 124.03$	$(R^2 = 0.15)$
Median $\delta^{18}\text{O}$:	$T = 3.43 * \delta^{18}\text{O} + 48.69$	$(R^2 = 0.03)$
January		
Average $\delta^{18}\text{O}$:	$T = 2.12 * \delta^{18}\text{O} + 20.00$	$(R^2 = 2.12)$
Median $\delta^{18}\text{O}$:	$T = 2.76 * \delta^{18}\text{O} + 34.72$	$(R^2 = 0.08)$
February		
Average $\delta^{18}\text{O}$:	$T = 1.39 * \delta^{18}\text{O} - 0.41$	$(R^2 = 0.01)$
Median $\delta^{18}\text{O}$:	$T = 0.22 * \delta^{18}\text{O} - 27.00$	$(R^2 = 0.00)$
March		
Average $\delta^{18}\text{O}$:	$T = 2.34 * \delta^{18}\text{O} - 27.27$	$(R^2 = 0.04)$
Median $\delta^{18}\text{O}$:	$T = 4.40 * \delta^{18}\text{O} + 74.29$	$(R^2 = 0.09)$
April		
Average $\delta^{18}\text{O}$:	$T = 7.15 * \delta^{18}\text{O} + 145.01$	$(R^2 = 0.05)$
Median $\delta^{18}\text{O}$:	$T = 19.54 * \delta^{18}\text{O} + 427.43$	$(R^2 = 0.26)$
May		
Average $\delta^{18}\text{O}$:	$T = 7.49 * \delta^{18}\text{O} + 165.71$	$(R^2 = 0.50)$
Median $\delta^{18}\text{O}$:	$T = 8.67 * \delta^{18}\text{O} + 192.66$	$(R^2 = 0.08)$
Winter		
Average $\delta^{18}\text{O}$:	$T = 3.41 * \delta^{18}\text{O} + 47.74$	$(R^2 = 0.21)$
Median $\delta^{18}\text{O}$:	$T = 2.13 * \delta^{18}\text{O} + 18.74$	$(R^2 = 0.18)$
Spring		
Average $\delta^{18}\text{O}$:	$T = 5.66 * \delta^{18}\text{O} + 112.73$	$(R^2 = 0.14)$
Median $\delta^{18}\text{O}$:	$T = 10.87 * \delta^{18}\text{O} + 231.44$	$(R^2 = 0.34)$
Cold season		
Average $\delta^{18}\text{O}$:	$T = 4.40 * \delta^{18}\text{O} + 77.37$	$(R^2 = 0.45)$
Median $\delta^{18}\text{O}$:	$T = 5.98 * \delta^{18}\text{O} + 113.29$	$(R^2 = 0.56)$

Acknowledgments

I would like to express my gratitude to Dr. Hanno Meyer, who supervised my work with a lot of dedication and tireless effort. Also I like to thank Prof. Dr. Ulrike Herzschuh for the useful suggestions for statistical evaluations. Furthermore, I would like to thank Dr. Prof Wolfgang Hubberten who aroused my interest for stable isotope geochemistry.

Special thanks to Victoria Viert and Stefan Lips for their support during the writing process and to my parents who always promoted me.

Affidavit

Eidesstattliche Erklärung zur Bachelorarbeit

Ich versichere, die Bachelorarbeit selbständig und lediglich unter Benutzung der angegebenen Quellen und Hilfsmittel verfasst zu haben. Alle Stellen, die wörtlich oder sinngemäß aus veröffentlichten oder noch nicht veröffentlichten Quellen entnommen sind, sind als solche kenntlich gemacht. Die Zeichnungen oder Abbildungen in dieser Arbeit sind von mir selbst erstellt worden oder mit einem entsprechenden Quellennachweis versehen.

Ich erkläre weiterhin, dass die vorliegende Arbeit noch nicht im Rahmen eines anderen Prüfungsverfahrens eingereicht wurde.

Potsdam, den _____